

CZECH TECHNICAL
UNIVERSITY
IN PRAGUE

FACULTY OF MECHANICAL
ENGINEERING



MASTER'S
THESIS

2020

Bc. Jan Syblík



**FACULTY
OF MECHANICAL
ENGINEERING
CTU IN PRAGUE**

CZECH TECHNICAL UNIVERSITY IN PRAGUE

MASTER'S THESIS

**Subchannel Analysis of VVER-440
Using SUBCHANFLOW**

Bc. Jan Syblík

supervised by

doc. Ing. Václav Dostál, Sc.D.

Master Study Programme
Nuclear Power Engineering Equipment

July 20, 2020

I. OSOBNÍ A STUDIJNÍ ÚDAJE

Příjmení: **Syblík** Jméno: **Jan** Osobní číslo: **410538**
Fakulta/ústav: **Fakulta strojní**
Zadávající katedra/ústav: **Ústav energetiky**
Studijní program: **Jaderná energetická zařízení**
Studijní obor: **Jaderná energetická zařízení**

II. ÚDAJE K DIPLOMOVÉ PRÁCI

Název diplomové práce:

Subkanálová analýza VVER-440 pomocí kódu Subchanflow

Název diplomové práce anglicky:

Subchannel Analysis of VVER-440 Using Subchanflow Code

Pokyny pro vypracování:

- 1) Vypracujte stručnou rešerši na téma VVER-440 (typ V-213), design, popis parametrů ustáleného stavu a přechodových stavů typu LOFA,
- 2) Popište charakteristiky subkanálových kódů s důrazem na kód Subchanflow
- 3) Proveďte detailní bezpečnostní analýzu ustáleného stavu a přechodových stavů typu LOFA pomocí kódu Subchanflow.

Seznam doporučené literatury:

- [1] TODREAS, Neil E. and Mujid S. KAZIMI. Nuclear systems II: Elements of Thermal Hydraulic Design. New York: Hemisphere Pub., c1990. ISBN 9781560320791.
- [2] U. Imke User manual for SUBCHANFLOW 3.5, Karlsruhe Institut of Technology, 2017.
- [3] Kanglong Zhang, Victor Hugo Sanchez-Espinoza, Optimization and verification of the coupled code TRACE/SubChanFlow using the VVER-1000 coolant mixing benchmark data, Nuclear Engineering and Design, Volume 353, 2019, 110238, ISSN 0029-5493
- [4] D.S. Rowe, COBRA IIIC: A Digital Computer Program for Steady-State and Transient Thermal Analysis of Rod Bundle Nuclear Fuel Elements, BNWL-1695, Pacific Northwest Laboratory (1973).
- [5] TODREAS, Neil E. and Mujid S. KAZIMI. Nuclear systems I: Thermal Hydraulic Fundamentals. 2nd ed. Boca Raton, 2012. ISBN 978-143-9808-870.

Jméno a pracoviště vedoucí(ho) diplomové práce:


doc. Ing. Václav Dostál, Ph.D., ústav energetiky FS


Jméno a pracoviště druhé(ho) vedoucí(ho) nebo konzultanta(ky) diplomové práce:

Datum zadání diplomové práce: **24.04.2020**

Termín odevzdání diplomové práce: **26.06.2020**

Platnost zadání diplomové práce: **31.12.2021**



doc. Ing. Václav Dostál, Ph.D.
podpis vedoucí(ho) práce


podpis vedoucí(ho) ústavu/katedry


prof. Ing. Michael Valášek, DrSc.
podpis děkana(ky)

III. PŘEVZETÍ ZADÁNÍ

Diplomant bere na vědomí, že je povinen vypracovat diplomovou práci samostatně, bez cizí pomoci, s výjimkou poskytnutých konzultací. Seznam použité literatury, jiných pramenů a jmen konzultantů je třeba uvést v diplomové práci.


Datum převzetí zadání


Podpis studenta

Statutory Declaration

I declare that I have developed and written the enclosed Master's Thesis completely by myself, and I have not used sources or means without declaration in the text.

Čestné prohlášení

Prohlašuji, že jsem diplomovou práci vypracoval samostatně a na základě literatury a pramenů uvedených v seznamu použité literatury.

V Praze dne

.....

Bc. Jan Syblík

Annotation sheet

Author's name	Bc. Jan Syblík
English title	Subchannel Analysis of VVER-440 Using SUBCHANFLOW
Czech title	Subkanálová analýza VVER-440 pomocí kódu SUBCHANFLOW
Academic year:	2019/2020
Field of study	Master study programme: Nuclear Power Engineering Equipment / Jaderná energetická zařízení
Department	Department of Energy Engineering / Ústav energetiky
Supervisor	doc. Ing. Václav Dostál, Sc.D.
Consultant	Ing. Alis Musa, Ph.D.
Bibliographic data	
Number of pages:	85
Number of figures:	51
Number of tables:	9
Number of appendices:	49

Abstract

This thesis focuses on modelling of specific transients using subchannel analysis of the VVER technology. The first chapter is dedicated to the subchannel analysis nowadays status. Besides other analyses, subchannel simulation is used worldwide for safety analyses and description of nuclear power plant's active zone thermal hydraulic behaviour. Furthermore, code-to-code benchmarks and coupling procedures are described. The following chapter presents the main VVER characteristics. Thereafter, the loss of flow accidents (LOFAs) phenomenology is described, followed by the subchannel analysis, its background, numerical approaches and the SUBCHANFLOW software structure. This chapter also includes a description of Python programmes created for post-processing, transient modelling processes and geometry implementation improvement used for SUBCHANFLOW. In the part of methodology are described operational conditions for VVER-440 along with calculation procedure. The last part presents the results from the steady-state analysis simulated by SUBCHANFLOW, LOFA transients results and comparison with the safety criteria, the four analysed scenarios are: 1/6 reactor coolant pump trip, 2/6, 3/6 and total LOFA (6/6 reactor coolant pumps trip).

Keywords

SUBCHANFLOW, subchannel analysis, LOFA, VVER-440;

Abstrakt

Tato práce se zabývá modelováním konkrétních přechodových jevů pomocí subkanálové analýzy technologie VVER. První kapitola je věnována současnému stavu subkanálové analýzy. Subkanálová analýza se používá v celosvětovém měřítku mimo jiné pro bezpečnostní analýzy a simulace termohydraulického chování aktivní zóny jaderných elektráren. Navíc jsou popsány code-to-code benchmarky a coupling. Další kapitola obsahuje popis hlavních charakteristik VVER. Následně je uvedena fenomenologie událostí se ztrátou chladiva (LOFA) a další část popisuje subkanálovou analýzu, historii, numerické přístupy a strukturu softwaru SUBCHANFLOW. Tato kapitola se také zabývá vytvořenými softwary v programovacím jazyce Python, které byly vytvořeny pro následné zpracování, procesy spojené s přechodovými analýzami a zlepšení procesu implementace geometrie do kódu SUBCHANFLOW. V části metodiky výpočtu jsou popsány provozní podmínky pro VVER-440 a postup výpočtu. Poslední část je založena na výsledcích analýzy ustáleného režimu simulovaného kódem SUBCHANFLOW, výsledcích přechodových stavů LOFA a porovnání výpočtu s bezpečnostními kritérii, kde konkrétními scénáři LOFA jsou: výpadek jednoho hlavního cirkulačního čerpadla ze šesti 1/6, 2/6, 3/6 a celková LOFA (výpadek všech hlavních cirkulačních čerpadel 6/6).

Czech Keywords

SUBCHANFLOW, subkanálová analýza, LOFA, VVER-440;

Acknowledgement

I would like to thank to the supervisor specialist of this thesis Ing. Alis Musa, Ph.D. for wise advices related to the investigated phenomenon and to Ing. Guido Mazzini, Ph.D. for consultations about implementation data from the programme TRACE. Also I would like to thank to my family for psychological support, my father for providing me computational time and Ing. Jan Štěpánek, Ph.D. for interesting remarks related to the topic of this thesis.

Poděkování

Své díky bych rád vyjádřil Ing. Alis Musa, Ph.D. za cenné připomínky při psaní této diplomové práce a Ing. Guido Mazzini, Ph.D. za odborné konzultace nad implementačními daty z programu TRACE. Dále bych rád poděkoval své rodině za psychickou podporu, svému otci za poskytnutí výpočetního času a také Ing. Janu Štěpánkovi, Ph.D. za zajímavé postřehy týkající se tématu této diplomové práce.

Contents

1	Introduction	1
1.1	Motivation	1
1.2	Organization of Thesis	2
2	State of the Art	3
2.1	Brief History of Subchannel Analysis	3
2.2	Nowadays Status of Subchannel Analysis	4
2.3	Code-to-Code Benchmark	4
2.3.1	Shin Kori 3&4	4
2.3.2	BWR	5
2.3.3	Turbine and Reactor Coolant Pump Trip	5
2.4	Coupling	5
2.4.1	TRIGA	6
2.4.2	REA	6
2.4.3	NURESIM	7
2.4.4	VVER	7
2.4.5	DYNSUB	8
2.4.6	RIA	8
2.5	Summary	9
3	VVER-440	10
3.1	Description	10
3.2	Operating Conditions	12
3.3	Material Properties	12
3.3.1	Cladding	13
3.3.2	Fuel	13
3.4	Summary	15
4	Phenomenology During Transients	16
4.1	Introduction	16
4.2	LOFA	17

4.2.1	Trip of Different Number of RCPs	18
4.2.2	Loss of Power Supply to all RCPs	19
4.2.3	Seizure of One RCP	19
4.2.4	Break of the One RCP Shaft	19
4.2.5	Inadvertent Closure of One Main Isolation (Shut-off) Valve	19
4.2.6	Partial Blockage of the Coolant Flow through a Fuel Cassette	20
4.3	Reactor Coolant Pumps Trip Scenarios	20
4.3.1	One of Six RCP Trip	21
4.3.2	Two of Six RCPs Trip	21
4.3.3	Three of Six RCPs Trip	21
4.3.4	Total LOFA (Six of Six RCPs Trip)	21
4.4	Summary	24
5	Subchannel Analysis	25
5.1	Introduction	25
5.2	Terminology	25
5.2.1	Geometry	25
5.2.2	Mass Flow Rate	27
5.2.3	Axial Mass Flow Rate	27
5.2.4	Momentum and Energy Transfer Rates	27
5.2.5	Transverse Mass Flow Rate per Unit Length	27
5.3	Conservation Equations	28
5.3.1	Geometric Relations	28
5.3.2	Continuity Equation	28
5.3.3	Energy Equation	28
5.3.4	Axial Linear Momentum Equation	29
5.4	Summary	29
6	SUBCHANFLOW	30
6.1	Subchannel Analysis Software	30
6.1.1	COBRA-IIIC	30
6.1.2	COBRA-IV-I	31
6.1.3	VIPRE-01	31
6.2	SUBCHANFLOW Code Description	31
6.3	Input Parameters	31
6.3.1	Properties	31
6.3.2	Correlations	32
6.3.3	Special Parameters	32
6.3.4	Axial Heat Flux	32

6.3.5	Rods and Channels Layout	33
6.3.6	Calculation Control	33
6.3.7	Grid Spacer Wire Wrap	33
6.3.8	Lateral Transport	34
6.3.9	Operating Conditions	34
6.3.10	Point Kinetics	34
6.4	Output	34
6.5	Geometry	34
6.6	Benchmark with TestCase	38
6.7	Summary	40
7	Methodology Description	41
7.1	Operational Conditions for VVER-440	41
7.2	Calculation Procedure	42
7.3	Python Software	44
7.4	Summary	44
8	Results	46
8.1	Steady-state	46
8.2	LOFA Calculation	46
8.3	One RCP trip	47
8.4	Two RCPs Trip	53
8.5	Three RCPs Trip	59
8.6	Total LOFA (Six RCPs Trip)	65
8.7	Final Outcome	70
8.8	Summary	71
9	Conclusion	72
	Author's References Not Related to the Study	79
10	Appendix	80
10.1	Mixing Coefficients in SCF	80
10.1.1	Constant Mixing Coefficient	80
10.1.2	Rogers & Tahir (Triangulars)	80
10.2	Friction Factors in SCF	81
10.2.1	Armand	81
10.2.2	Lockhart-Martinelli	82
10.2.3	Blasius	82
10.2.4	Rehme	83
10.2.5	Churchill	83

10.3 Critical Heat Flux in SCF	84
10.3.1 Biasi	84
10.3.2 OKB	84
10.3.3 W-3	84
10.3.4 Levitan	85
10.3.5 EPRI with Shape Function	85
10.3.6 Doroshchuk	85

List of Figures

3.1.1 3D figure of VVER-440 reactor primary circuit [19].	11
3.1.2 2D figure of VVER-440 reactor primary circuit [19].	11
4.2.1 Pool boiling curve for water at atmospheric pressure with boiling regimes [24].	18
5.1.1 Relation of subchannel control volume to the AZ [5].	26
5.2.1 Difference between two possible approaches in subchannels definition [5].	26
6.5.1 Rods positions in VVER-440.	36
6.5.2 Subchannels positions in VVER-440.	37
6.6.1 Edge numbering of the rods in TestCase.	38
6.6.2 Corner subchannels geometry generated by HEGGS (left) and geometry in TestCase.	39
6.6.3 Centered numbering of the rods done by HEGGS code.	39
6.6.4 Axial temperature on the HR outer cladding diameter.	40
7.1.1 The relative axial power profile vs. the relative axial location.	42
7.2.1 Calculation procedure scheme.	43
8.1.1 MDNBR and the HR position during steady-state.	47
8.3.1 Relative mass flow \dot{m}/\dot{m}_0 and relative power \dot{P}/\dot{P}_0	48
8.3.2 Bar chart of MDNBR rods occurrences between 31.5 s and 34.7 s.	48
8.3.3 MDNBR in FC during 1/6 RCP trip.	49
8.3.4 MDNBR of rods 105-108 and the remaining HRs between particular time period.	50
8.3.5 The HR 106 MDNBR.	51
8.3.6 The HR 106 maximum fuel center temperature.	51
8.3.7 The HR 106 fuel center temperature at t_1 , t_2 , t_3 and t_4	52
8.3.8 The HR 106 maximum cladding temperature.	52
8.3.9 The highest equilibrium quality x in the HC 176.	53
8.4.1 Relative mass flow \dot{m}/\dot{m}_0 and relative power \dot{P}/\dot{P}_0	54
8.4.2 Bar chart of MDNBR rods occurrences between 16.7 s and 35.1 s.	54

8.4.3 MDNBR in the whole FC.	55
8.4.4 Rods 104-107 and the remaining HRs MDNBR between particular time period.	56
8.4.5 The HR 106 MDNBR.	56
8.4.6 The HR 106 maximum fuel center temperature.	57
8.4.7 The HR 106 fuel center temperature at t_1, t_2, t_3 and t_4	58
8.4.8 The HR 106 maximum cladding temperature.	58
8.4.9 The highest equilibrium quality x in the HC 176.	59
8.5.1 Relative mass flow \dot{m}/\dot{m}_0 and relative power \dot{P}/\dot{P}_0	60
8.5.2 Bar chart of MDNBR rods occurrences between 12.4 s and 35.5 s.	60
8.5.3 MDNBR versus time t between seconds 10 and 37.	61
8.5.4 Rods 105-108 and the remaining HRs MDNBR between particular time period.	62
8.5.5 The HR 106 MDNBR.	62
8.5.6 The HR 106 maximum fuel center temperature.	63
8.5.7 The HR 106 fuel center temperature at t_1, t_2, t_3 and t_4	63
8.5.8 The HR 106 maximum cladding temperature.	64
8.5.9 The highest equilibrium quality x in the HC 176.	65
8.6.1 Relative mass flow \dot{m}/\dot{m}_0 and relative power \dot{P}/\dot{P}_0	66
8.6.2 Bar chart of MDNBR rods occurrences between 9.2 s and 11.9 s.	66
8.6.3 Minimum departure from nucleate boiling ratio against time t	67
8.6.4 The HR 95 MDNBR.	68
8.6.5 The HR 95 maximum fuel center temperature.	68
8.6.6 The HR 95 fuel center temperature at t_1, t_2, t_3 and t_4	69
8.6.7 The HR 95 maximum cladding temperature.	69
8.6.8 The highest equilibrium quality x in the HC 156.	70

List of Tables

3.3.1 Thermomechanical properties of cladding and fuel materials [21].	13
4.3.1 1/6 RCPs trip sequence simulated in TRACE.	21
4.3.2 2/6 RCPs trip sequence [21].	22
4.3.3 3/6 RCPs trip sequence [21].	23
4.3.4 6/6 RCPs trip sequence (Total LOFA) [21].	24
6.6.1 Physical values of benchmarking with TestCase.	38
6.6.2 Benchmarking results of HEGGS method with TestCase.	39
8.1.1 Steady-state parameters	46
8.7.1 Final results.	71

List of Symbols

Symbol	Unit	Description
A	[m ²]	Actual Channel Area (at Axial Cell Center)
c_p	[J/kg/K]	Specific Heat Capacity
d	[m]	Diameter
F	[N]	Force
g	[m]	Gap Between Subchannels
G	[kg/s/m ²]	Mass Flux
h	[J/kg]	Specific Enthalpy
\dot{m}	[kg/s]	Mass Flow
L	[m]	Length
p	[Pa]	Pressure
P	[W]	Power
PP	[m]	Pin Pitch
q	[W/m ²]	Heat Flux
Q	[J]	Heat
r	[m]	Perimeter
ra	[m]	Rod Surface Roughness
Re	[-]	Reynolds Number
s	[J/kg/K]	Specific Entropy
t	[s]	Time
T	[°C]	Temperature
u	[m/s]	Velocity
V	[m ³]	Volume
W	[kg/s]	Transverse Mass Flow Rate
x	[-]	Equilibrium Quality

List of Subscripts

Symbol	Description
av	Average
ax	Axial
cr	Critical
ex	Exit
f	Fluid
h	Heated
in	Inlet
l	Liquid
L	Laminar
lat	Lateral
s	Sum
t	Total
v	Vapour
w	Wetted

List of Superscripts

Symbol	Description
err	Error
D	Turbulent
H	Energy
M	Momentum

Greek Nomenclature

Symbol	Unit	Description
α	[-]	Void Fraction
α_T	[K ⁻¹]	Thermal Expansion Coefficient
γ	[-]	Volume Porosity
Γ	[-]	Gamma Function
λ	[W/m/K]	Specific Thermal Conductivity
μ	[Pa·s]	Dynamic Viscosity
ν	[m ² /s]	Kinematic Viscosity
φ	[-]	Two-phase Friction Multiplier
ρ	[kg/m ³]	Density

Latin Nomenclature of Parameters

Symbol	Unit	Description
a_{ch}	[-]	Parameter in Churchill's Correlation
b_{ch}	[-]	Parameter in Churchill's Correlation
b_{Lc}	[-]	Laminar Constant for Blasius Type Friction Model
b_{Lp}	[-]	Laminar Pre-factor for Blasius Type F. Model
b_{Lr}	[-]	Laminar Exponent for Blasius Type F. Model
b_{Tc}	[-]	Turbulent Constant for Blasius Type F. Model
b_{Tp}	[-]	Turbulent Pre-factor for Blasius Type F. Model
b_{Tr}	[-]	Turbulent Exponent for Blasius Type F. Model
c_{ch}	[-]	Parameter in Churchill's Correlation
c_{mix}	[-]	Mixing Coefficient
C	[-]	Chisholm Constant
f_f	[-]	Friction Coefficient of Mixture
Rh_t	[-]	Friction Calculation Parameter
w	[kg/s/m]	Channel Gap Mixing Flow Parameter
x_{tt}	[-]	Lockhart-Martinelli Parameter
X_m	[-]	Annular Zone Parameter

List of Abbreviations

Abbreviation	Meaning
AZ	Active Zone
BOC	Beginning of Cycle
BT	Bubbler Tank
BVA	Bypass Valve to Atmosphere
BVC	Bypass Valve to Condenser
BWR	Boiling Water Reactor
CFD	Computational Fluid Dynamics
CHF	Critical Heat Flux
COBRA	Coolant Boiling in Rod Arrays
CVR	Research Centre Řež
DBA	Design Basis Accident
DG	Diesel Generator
DNB	Departure from Nucleate Boiling
DNBR	Departure from Nucleate Boiling Ratio
ELS	Emergency Load Sequencer
EPRI	Electric Power Research Institute
FA	Fuel Assembly
FC	Fuel Cassette
FSAR	Final Safety Analysis Report
HC	Hot Channel
HEGGS	Hexagonal Geometry Generator Software
HR	Hot Rod
KIT	Karlsruher Institut für Technologie
LOCA	Loss of Coolant Accident
LOFA	Loss of Flow Accident
LOOBP	Loss of Operational and Backup Power Supply
LWR	Light Water Reactor
MCNP	Monte Carlo N-Particle Transport Code
MDNBR	Minimum Departure from Nucleate Boiling Ratio
NPP	Nuclear Power Plant
NRC	U.S. Nuclear Regulatory Commission
NURESIM	European Nuclear Reactor Simulation
P.C.	Primary Circuit
PH	Pressuriser Heaters

Abbreviation	Meaning
PP	Pin Pitch
PWR	Pressurized Water Reactor
RCP	Reactor Coolant Pump
RCS	Reactor Control System
RD	Rod Diameter
REA	Rod Ejection Accident
RIA	Reactivity Insertion Accident
RLS	Reactor Limitation System
RPV	Reactor Pressure Vessel
RTS	Reactor Trip System
S.C.	Secondary Circuit
SCF	SUBCHANFLOW
SCRAM	Emergency Shutdown of a Reactor
SG	Steam Generator
SMR	Small Modular Reactor
SPA	SUBCHANFLOW Post-processing Analysis
SSASA	Software for SUBCHANFLOW Automatic Sensitivity Analysis
SUBVID	SUBCHANFLOW Video Analysis
SURO	National Radiation Protection Institute
TE	Drainage of Coolant from P.C.
TK	Make-up and Boron Control System
TRACE	TRAC/RELAP Advanced Computational Engine
TRIGA	Training Research Isotope General Atomics
VIPRE	Versatile Internals and Component Program for Reactors: EPRI
VVER	Water-Water Power Reactor

Chapter 1

Introduction

Modern approach in electrical power engineering leads to emphasising on low carbon emission sources. In comparison with other green electric sources, nuclear power plants reach one of the best results in the field of safety, sustainability, low carbon emissions during the whole unit lifetime or amount of produced electricity by a power plant per square kilometre.

Even though nuclear power plants are often considered to be the proper option in order to lower carbon emissions, this type of power plant is still highly complex and complicated structure that involves various technical specializations (nuclear physics, chemistry, mechanical engineering, civil engineering etc.).

This complexity determines the requirement of high focus on safety issues, modern methods of studies and analysis of processes in the nuclear power plant and in the facilities connected to the nuclear research in general, e.g. supporting research facilities.

The scope of this thesis is to perform steady-state and transient analysis for VVER-440 type reactor using so called subchannel analysis which is nowadays a necessary safety approach for nuclear power and research reactors safety analyses.

1.1 Motivation

Subchannel analysis has capabilities of predicting key safety parameters such as margin to critical heat flux, fuel center temperature or cladding temperature.

Besides, the subchannel analysis calculates mixing of the flow between neighbouring subchannels, void fraction or equilibrium quality. These and other parameters are crucial indicators of a reactor safe operation.

The motivation for using subchannel analysis is safe operation during steady-state and various transient scenarios in the nuclear power plants.

One of the main benefits of this analysis is better understanding of the fuel assembly thermal hydraulic performance and its influence on operational conditions. Subchannel analysis results offer detailed local information of coolant medium thermal hydraulics

performance and materials thermomechanical behaviour in the active zone.

Due to the continuous improvement of material engineering, the structure of used components used in the nuclear power plants are enhanced. New structures of modern materials require more detailed safety analysis and methods have to be developed. E.g. considering nowadays approaches in the subchannel analysis it is possible to research new fuel with higher enrichment. This influences not only the active zone of the reactor itself but also spent fuel pools or spent fuel containers.

1.2 Organization of Thesis

This thesis focuses on the analysis of steady-state and transients of reactor VVER-440 V-213 from the subchannel analysis perspective. The main objective of this thesis is to develop models that simulate normal operating conditions and transients. From the results it is possible to evaluate the fulfilment of safety limits for a specific nuclear fuel.

The main VVER-440 characteristics are briefly described in the first part of this thesis followed by the description of normal, abnormal and accidental regimes. Then the topic of nowadays status in the field of subchannel analysis research is added. Furthermore, a subchannel methodology, its history, numerical methods and usable correlations are performed. In the following chapters, the analysis of steady-state and transient scenarios in subchannel code called SUBCHANFLOW is represented and based on the results the main conclusions were drawn.

In the Appendix are attached possible correlations that may be used for the calculation in SUBCHANFLOW. These correlations solve mixing coefficients, friction factors and critical heat flux.

Chapter 2

State of the Art

This chapter describes nowadays use of subchannel analysis in the field of nuclear safety calculation methods. Subchannel analysis offers a more detailed description for local conditions of the active zone. Further sections involve its history and possible use of subchannel analysis for benchmarking, code-to-code comparisons and coupling.

2.1 Brief History of Subchannel Analysis

Experiments of rod bundles has a long history reaching back to 1960s. Measurement of heat transfer characteristics, pressure drop across the rod bundle, flow velocity and its distribution, secondary flow vortices inside the subchannel, turbulence quantities, behaviour of fluids influenced by grid spacers and others gave basics of nowadays advanced computational methods and mathematical models [1].

The experience gained from the experimental and analytical methods that are being developed for more than a half of a century represent a key step in the description of the nuclear fuel.

The gradual increase of computing power offered more opportunities for detailed numerical solution methods describing nuclear fuel performance, such as CFD models etc. One of these methods is subchannel analysis.

Subchannel analysis is a method used for the description of nuclear power plant behaviour during steady-state and transient conditions. Nowadays it is one of the essential method used for design optimization, experiment planning and interpretation of safety analysis. It is implemented in various codes and used in a majority of nuclear research institutes all over the world e.g. Karlsruher Institut für Technologie (KIT) [2], Idaho National Laboratories (INL), National Nuclear Laboratory Limited (NNL) [3] and others.

One of the codes used for final safety analysis reports (FSAR) used in the Reasearch Centre Řež (CVR) and the National Radiation Protection Institute in the Czech republic (SURO) is called SUBCHANFLOW. This code is based on COBRA family codes, which was first introduced in 1960s in Pacific Northwest National Laboratories in the USA. This

code allowed two-dimensional, multiphase hydrothermal modelling of a reactor and other complex systems [4].

The following paragraphs will describe various use of subchannel analysis. Different approaches in the subchannel analysis are more specifically described in the literature [5]. However, the objective of the thesis is not to make code-to-code benchmark.

2.2 Nowadays Status of Subchannel Analysis

As it was mentioned above, subchannel analysis codes are used for safety analyses in the nuclear energy field. It represents a powerful tool that can describe the active zone behaviour of a reactor, spent fuel pool or spent fuel container.

The nuclear accidents demonstrated the importance of performing safety analyses in past hence it is necessary to deepen the knowledge of system codes and nuclear devices [6].

2.3 Code-to-Code Benchmark

Code-to-code benchmarking and validation of computer codes is an important activity that can facilitate international cooperation or exchange of information, which is important for comparison of software codes. It is necessary for regulatory commissions such as NRC (The U.S. Nuclear Regulatory Commission) to support decision making procedures based on the results obtained from codes used in nuclear energy engineering. In order to get certification, the code has to be realistic and reliable. This may be achieved by benchmarking with other codes where the reliability was previously validated by comparison e.g. with experimental data.

In the next subsections will be described nowadays approaches and topics of studies related to code-to-code benchmarking of subchannel software.

2.3.1 Shin Kori 3&4

Comparison of VIPRE-01 (Versatile Internals and Component Program for Reactors: EPRI) and THALES (Thermal Hydraulic AnaLyzer for Enhanced Simulation of core) subchannel codes using power distribution for sample departure from nucleate boiling analysis in South Korean nuclear power plant Shin Kori 3&4 final safety analysis report was done in 2014.

VIPRE-01 is a subchannel code considering more used approach of coolant-centered and rod centered division. The code is possible to use for description of Light Water Reactors (LWR) and Boiling Water Reactors (BWR) thermal hydraulic behaviour.

THALES was developed by KEPCO Nuclear Fuel (KNF) to analyse core thermal hydraulics for OPR1000 and APR1400. The main differences between the codes are in the implemented correlations for two-phase friction multipliers, subcooled boiling, bulk void/quality, heat transfer and critical heat flux.

The result of the study showed negligible difference in the prediction of MDNBR. On the other hand, after enabling the conduction model there were significant differences in MDNBR-time functions between the codes. During LOCA the VIPRE-01 is giving much more conservative results after 3 seconds from the beginning of the calculation [7].

2.3.2 BWR

Subchannel codes can assess the thermal hydraulic behaviour of fluid in BWRs (Boiling Water Reactors). One of the newly developed two-phase flow porous media code is TWOPORFLOW. This code is being developed in KIT and recent articles were comparing the results obtained from TWOPORFLOW with codes NEPTUNE-CFD, COBRA-TF, SCF, TRACE and ATHLET. The results gathered from these codes were reasonably comparable with negligible differences during steady-states and few transient tests [8].

2.3.3 Turbine and Reactor Coolant Pump Trip

During 2012 was performed a study comparing few codes (TRACE, COBRA-TF, SCF, NEPTUNE CFD) simulating turbine and a reactor coolant pump trip using database provided within the Nuclear Power Engineering Center (NUPEC) BWR Full size Fine mesh Bundle Test (BFBT) benchmark [9].

There has been done a comparison for three densitometers experimental data axially positioned in the AZ. At the top level, TRACE code gives the best results for the transient while COBRA-TF and SCF catch the steady-state conditions better than system codes. The computational fluid dynamic code NEPTUNE CFD gives only good agreement in accordance to the experimental data at the middle level of the AZ. The study showed noticeable differences between few codes e.g. in the results of transient void fraction during turbine trip accident [9].

2.4 Coupling

There are plenty possible variations of coupling between subchannel codes and neutronic codes such as PARCS (Purdue Advanced Reactor Core Simulator), thermal-hydraulics codes (e.g. TRACE - TRAC/RELAP Advanced Computational Engine) or radiation transport codes like MCNP (Monte Carlo N-Particle Transport Code). Coupling may be also established between different other reactor dynamic solvers such as CRONOS,

DYN3D and COBAYA3 or three-dimensional continuous-energy Monte Carlo reactor physics burnup calculation code SERPENT.

Between subchannel and other thermal hydraulic codes that are being coupled belong, besides SCF, also already mentioned VIPRE, THALES, COBRA codes, CTF (COBRA-TF) or FLICA. Few examples of coupling are mentioned in the further subsections.

2.4.1 TRIGA

For TRIGA (Training Research Isotope General Atomics) MARK II reactor has been done a study in Jožef Stefan Institute (JSI) in 2018 describing coupled system MCNP/SCF to predict pin-power distribution in a PWR assembly. The study compared the coupled model with power and fuel temperature measurement during a control rod extraction. There was also a brief description of coupling SERPENT/SCF to simulate a full PWR under hot full power conditions.

The main conclusion for the coupling are the results from comparison of using subchannel analysis and CFD (Computational Fluid Dynamics) approaches. The authors selected implementation of CFD instead of SCF due to observed strong recirculation inside the core. The simple geometry of TRIGA reactor core and coolant filled pool made the CFD models easier to solve the issue but this approach is not appropriate for commercial reactors [10].

2.4.2 REA

REA stands for Rod Ejection Accident. It is a design basis accident that should be examined in order not to exceed the acceptance criteria. This type of accident has been studied in 2019 on a newly developed boron-free light-water small modular reactor (LW-SMR). To follow a conservative approach, the beginning of life (BOL) was chosen for simulation using coupled codes PARCS/SCF [11].

Recently, there is a high interest in the SMRs and it is still necessary to make detailed safety analysis. The results would help for getting the projects of SMRs closer to commercialization.

During this study has been also done a sensitivity analysis on importance of flow mixing. It was simply turned off in SCF and it showed that the effect of flow mixing was negligible. The results showed that if the research is based on FA (channel-based) and not subchannels level simulation, it is possible to neglect the flow mixing between channels [11].

2.4.3 NURESIM

NURESIM (European Nuclear Reactor Simulation) is a platform established by consortia of more than twenty European countries. The goal of NURESIM is to develop a multi-scale and multi-physical simulation platform with a flexible and automatic coupling approach based on validated neutronics, thermal hydraulics and pin mechanics solvers also including powerful pre and post-processing tools.

In order to implement SCF as a powerful simulation tool, there has been done a lot of work in the field of coupling with other codes. In 2013 there was done an extension between the 3D neutron diffusion codes COBAYA3 and DYN3D, and SCF for the simulation of boron dilution transients. Boron transport models are important for the simulation of boron dilution transients following a small break LOCA (SBLOCA). In this case, the mixing is a key mechanism determining the positive reactivity insertion in the core [12].

Within the NURESIM platform has been done also validation of coupled COBAYA3/SCF through the benchmark validation based on the american nuclear power plant Three Mile Island 1 (TMI-1) main steam line break (MSLB) and the russian nuclear power plant Kalinin-3 Cooling Transient. TMI-1 MSLB benchmark is code-to-code comparison meanwhile Kalinin 3 benchmark is code to data comparison. The study proved that the implemented coupling scheme was successfully implemented inside the NURESIM platform [13].

2.4.4 VVER

Particular attention has been paid to the VVER coupling studies, due to their possible contribution on this thesis development.

A study from KIT mentions two possible approaches of SCF, namely coolant subchannel model and fuel-centered. SCF input file works only with the hydraulic parameters of the subchannels and not with the exact subchannel geometry shape. One of the noticeable result was that during coupling of SERPENT2/SCF, the SCF used only 0.01 % of the running time for finding a converged solution [14].

Using the ECI-Module (Exterior Communication Interface Module) was coupled TRACE/SCF and validated due to data provided by the VVER-1000 coolant mixing benchmark. A study describes the optimization of two temporal coupling schemes for the steady-state and transient simulations to improve the calculation efficiency of the coupled system. The simulation done in this work shows that TRACE/SCF predicts better result at least for two hot legs which lay much closer to the measured data compared to TRACE-standalone [15].

2.4.5 DYN SUB

DYN SUB is a two-way pin-based coupling of the simplified transport (SP3) version of DYN3D with the SCF.

The key element was replacing the code FLOCAL from previous coupling schemes with SCF which required several changes and modifications of involved codes as well as the writing of new subroutines. After the compilation, a SCF library was created and linked to the DYN3D-SP3 source, for a later compilation as a coupled code.

The main changes of the code are described below.

- * Source code extensions to have an additional option for direct allocation of the power distribution in every node of a 3D problem representation allowing a different axial profile for every single rod.
- * Implementation of a time dependent pin power map taking into account local changes. Such development replaces the former global definition of the power in which the change in power was taken into account as a global change (the original power multiplied by the fractional change in power).
- * Development of a generic and flexible Pre-processor for SCF that is needed for the automatic input deck generation of very large calculations (large number of channels and rods in the model). This capability was also necessary for DYN SUB to represent accurately a core configuration or even a FA for which different tables with hundreds of rows (one for each sub-channel considered) have to be created. This Pre-processor is able to generate all the tables needed by SCF with all the possible details e.g. the definition of an irregular cluster of assemblies each one with different inner configurations that are characterized by different type of rods with different thermal properties and control rod positions, with or without wetted boundary, etc. The Pre-processor works for the standalone version of and it is also directly implemented in DYN SUB as a subroutine.

This study also covered practical issues like involving one eighth of a PWR core [16].

DYN SUB was used for calculation of steady-state from hot zero power (HZP) and for calculation of REA transient by two time schemes (explicit and fixed point iteration FPI) and the effect of FPI was shown to be very important [17].

2.4.6 RIA

RIA stands for the Reactivity Insertion Accident. This accident has been modelled with data from SPERT III (Special Power Excursion Reactor Test III). There has been done a study describing coupling of SERPENT2/SCF and also briefly SCF, mentioning that there are available three kinds of solvers: a direct Gauss elimination solver for small

problems, a SOR and a BiCGStab iterative solver. Due to its solution method, SCF is restricted only to upward flow [18].

The objective was to validate the SERPENT2-DYNSUB code utilizing the SPERT III E-core experiment series and the DYNSUB stationary simulations were compared well to the Monte Carlo neutron transport reference solutions obtained with SERPENT 2 (cold startup conditions) and SERPENT2/SCF (operating power conditions) [18].

2.5 Summary

Computational analysis and benchmarking the results with experimental data are necessary approaches for the safety analysis conclusions. Topics of nowadays interest of computational methods are flexibility, stability and time efficient calculations providing best estimates.

The subchannel analysis is a strong tool which is worldwide applied on a large number of nuclear reactors and facilities connected to the nuclear fuel. Although the research of this topic has a long history, progress in computer performance power, same as evolution of the nuclear power plants generations, requires actual engineering methods and codes results.

Chapter 3

VVER-440

Chapter 3 describes the evolution of soviet pressurized water reactors VVER-440 and its basic design. Briefly are also depicted the operating conditions, the most important materials used in this design and type of used nuclear fuel.

3.1 Description

VVER stands for водо-водяной энергетический реактор (Water Water Power Reactor). This reactor is pressurized homogeneous water reactor working on thermal neutrons.

The first commercial pressurized water reactor VVER-210 was built and commissioned in 1963 at Novovoronezh. This reactor was followed by the 365 MWe prototype and these two projects are representing the predecessor of VVER-440 design. The first nuclear power plant VVER-440 is considered to be Novovoronezh Unit 3 type V-230 [20].

VVER-440 have a six loops configuration each with horizontal steam generator (SG) and main steam isolation valve. Every unit uses two 220 MWe turbines.

VVER-440 type V-213 is modified version of VVER-440 type V-230. It was introduced in 1980/1981 in Rovno as Unit 1 and 2 [20]. A 3D scheme of the main primary circuit devices of VVER-440 V213 is presented in picture 3.1.1. In picture are visible six SGs, six loops (each with hot leg, cold leg and main isolation valves), six RCPs and reactor. In picture 3.1.2 is presented schematic layout of VVER-440 V-213 primary circuit with main devices.

In comparison to V-230 design, the V-213 has been improved by many safety upgrades like enhancement of signal logic to be more sophisticated, no main isolation valve water sealing, high inertia sealed shaft pump GCN-317 on MCPs, higher pump efficiency or MCP anti-reverse protection. V-213 principally reaches higher safety also due to a fact, that as a maximum design basis accident (DBA) was assumed a guillotine rupture of 500 mm reactor coolant system pipe. During the accident leaking steam would reach bubbler tank where it would condense [20].

As a coolant is used light demineralized water with boric acid H_3BO_3 . It is used as a

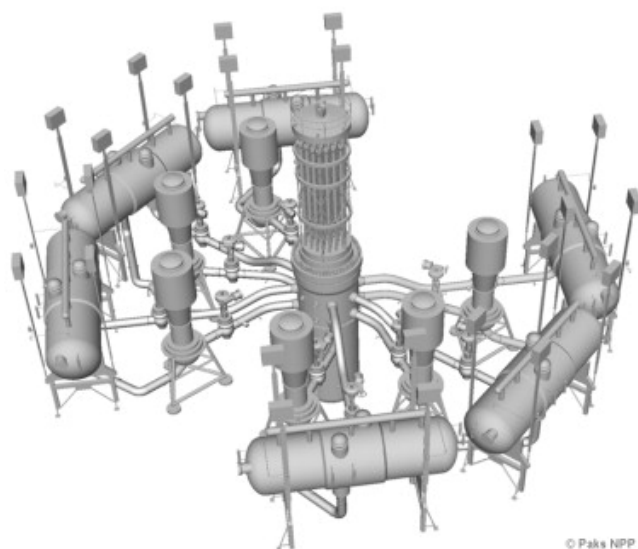


Figure 3.1.1: 3D figure of VVER-440 reactor primary circuit [19].

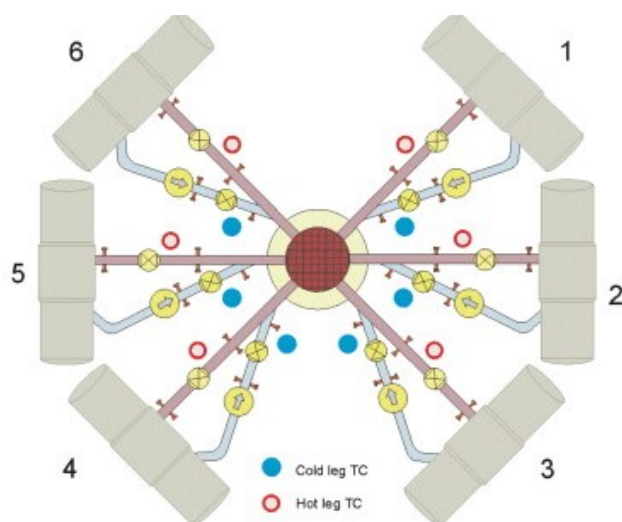


Figure 3.1.2: 2D figure of VVER-440 reactor primary circuit [19].

compensator of reactivity and the H_3BO_3 concentration in the cooling medium is reduced according to the burnout of fuel. Boron additions have acidic tendencies which affects coolant pH, therefore, coolant has to be diluted by chemical solutions that help to solve the issue of chemical purity.

3.2 Operating Conditions

The operating conditions of the power plant VVER-440 (type V-213) listed below, will be implemented as operating conditions in the SCF code.

Nominal heat power production during steady-state:	1444 MW
Minimal flow:	40 000 m ³ /h
Nominal flow:	41 500 m ³ /h
Nominal pressure in the outlet of the AZ:	12.26 MPa
Average temperature in the inlet of the AZ:	265-270 °C
Average temperature in the outlet of the AZ:	293-302 °C

There are 312 fuel cassettes and 37 control assemblies. Due to this assumption, flow rate through one fuel cassette is $\dot{V} = 41500/(312+37) = 118 \text{ m}^3/\text{h}$, because in VVER-440 design is assumed uniform distribution of mass flow through the fuel cassettes [21].

According to FSAR the bypass flow represents 6.55 % of total flow [21], and for this analysis SCF requires value of mass flow per FA \dot{m}_i .

3.3 Material Properties

Due to ongoing experience in the field of material engineering, the connection with computational methods is necessary. It is essential to derive many information covering materials used in nuclear engineering and new findings, which influence nuclear safety analyses. The need of connection of thermal hydraulics and material research is significant and cooperation with progress in both sciences determines successful evolution of the nuclear research in general. Besides, this subsection focuses on fuel and cladding materials.

Materials selected for nuclear fuel and fuel structural components has to fulfil following conditions: reliability, economical operation, safety, high corrosion resistance, radiation stability, high technological parameters and other conditions. These limitations depend on the material functionality and its location in the primary circuit.

VVER fuel cassettes materials are marked according to russian standards. Steel materials used in nuclear power plants are characterized by their high corrosion resistance, radiation stability and high technological parameters (due to GOST 5632-72 standard) [21] e.g. for fuel type Gd-2M⁺ austenite stainless steels 12Ch18N10T, 08Ch18N10T or 06Ch18N10T. These austenite steels are main components of the cassettes and they are welded by electronic arc in argon.

In table 3.3.1 are physical values of specific materials at the testing temperature T_t . Fuel is represented by UO₂ and also by UO₂+3,35 % Gd₂O₃. As a cladding material is E110. Values were obtained from FSAR.

Table 3.3.1: Thermomechanical properties of cladding and fuel materials [21].

Material	T_t [°C]	$\alpha_T \cdot 10^{-6}$ [K ⁻¹]	λ [W/m/K]	c_p [J/kg/K]	ρ [kg/m ³]
E110	380	5.5	20.3	361	6550
UO ₂	627	~ 9.2	8.2	288	~ 10600
UO ₂ +Gd ₂ O ₃	627	~ 9.2	5.7	287	~ 10600

3.3.1 Cladding

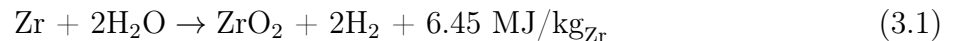
There are high requirements on the fuel and cladding materials in the AZ e.g. low effective cross sections for thermal neutrons, high resistance to pressure gradients and mechanical deformation or high corrosivity resistance, which these alloys fulfil [21].

As a fuel cladding of Gd-2M⁺ fuel is used E110 zirconium alloy (Zr+1 % Nb) and for control assemblies envelopes and control assemblies fuel parts is used E125 (Zr+2.5 % Nb).

The research of E110 thermomechanical properties is considerable because it has a usage also in VVER-1000 and other PWRs. It shows e.g. the stability of the E110 alloy structure even after 50 years of irradiation time [22], also according to [21] irradiation of the material leads to material strengthening while the plasticity maintains.

During the construction of the cladding, it is inevitable to focus on the main impurities in the natural zircon. Besides, it contains from 1-5 % of hafnium. Reduction of Hf is necessary, because effective cross section of absorption is approximately 600 times higher in comparison with nuclear Zr alloys, which contain less than 0.03 or 0.01 % depending on the fuel [21].

Crucial issue of Zr is chemical behaviour dependent on the temperature. Oxidation of Zr begins approximately around 350 °C where the fragility of the surface is increased. Up to 800 °C Zr cladding begins exothermal reaction with steam and from 1200 °C the problem of autocatalytic reaction appears. This reaction is described by equation 3.1, where is visible 6.45 MJ of energy released by one kg of Zr.



The autocatalytic reaction temperature also depends on hydrogen percentage volume in the system. If the concentration of hydrogen is higher than 400 ppm, the temperature of autocatalytic reaction decreases on 1121 °C [21].

3.3.2 Fuel

The AZ is 2.48 m high and each cassette has 126 fuel rods and one guiding rod. The control assembly is designed as a combination of a fuel cassette and an absorber part,

which is made of boron steel that effectively absorbs neutrons. The control assembly drive mechanism is rack and pinion type. During normal operation the electro-engine is energized until the emergency mode, when the control mechanism starts to pull the control assembly fuel part out of the AZ due to power cut-off.

Unlike PWRs western projects the AZ of VVER has hexagonal fuel cassettes with triangular symmetry. The AZ containing hexagonal fuel cassettes is more effective in comparison with rectangular fuel assemblies, these types of reactors, however, are more difficult to manufacture.

The fuel itself is enriched sintered uranium dioxide UO_2 ceramic pellet, 7.6 or 7.8 mm in diameter depending on the fuel specifications [21].

For extension of the fuel life is used Gd_2O_3 as a burnable absorber, then the resultant material is $\text{UO}_2\text{-Gd}_2\text{O}_3$. This material has high neutron absorption cross section and it decreases fuel reactivity in the BOC.

The subchannel analysis requires knowledge of specific material parameters in order to calculate e.g. heat transfer phenomena for fuel, cladding or coolant. Required parameters for fuel and for cladding are conductivity, specific heat, density, emissivity, thermal expansion, dimensions and specifically cladding roughness for certain correlation. For the gap between fuel and cladding it is necessary to obtain conductance, pressure and volume.

Gd-2M⁺

Gd-2M⁺ represents fuels of 2nd generation in VVER-440 design. This fuel is improvement of previous generations and the differences are between fuel cassettes and also control assemblies [21]. The main differences in comparison with previous versions are following:

- Strengthen fuel cassette stability: The first spacer grid is in a lower axial position. This was done due to the higher hydrodynamical forces in the lower part of the fuel cassette.
- Increase UO_2 weight in the AZ (fuel cassettes and control assemblies): Inner diameter of cladding was increased; Outer diameter of a fuel pellet was increased; Fuel pellet without burnable absorber is without central hole; Fuel column length increase.
- Heat transfer between cladding and fuel increase (fuel cassettes and control assemblies): Gap between fuel and cladding was decreased.
- Reduction of local unevenness in fuel burnout of control assemblies: Summary of gaps between pellets was lowered.
- Decrease absorption of control assemblies thermal neutrons: Hafnium maximum weight volume decrease in the fuel cassette envelope.

3.4 Summary

This chapter involved a brief introduction to VVER-440 design project, main specifications of operating conditions and basic materials in the primary circuit.

Due to an ongoing process of the nuclear fuel evolution it is necessary to use safety analysis methods with actual physical parameters of modern materials.

Chapter 4

Phenomenology During Transients

This chapter describes the term of transients and phenomenology of specific LOFA transients which may occur during the nuclear power plant operation. Unlike projects from Siemens, Framatom and Westinghouse, it is allowed for VVER to work with lower number of RCPs than maximum [23]. Due to this possibility, variations of RCPs trip have to be examined.

4.1 Introduction

Objective of the safety analysis is to ensure nuclear safety which means to eliminate the possibility of an accident causing significant radioactive release.

Task of the safety analysis is to evaluate the physical barriers integrity in order to provide tightness of the system against radioactive materials leakage. The first three physical barriers are the fuel matrix, the fuel cladding, the boundary of the primary coolant system and the fourth barrier is the containment [20].

One of the crucial safety analyses approach are computational methods which includes subchannel analysis.

Subchannel analysis is useful for evaluation of transient states, which may occur with certain possibility during the nuclear power plant operation. In this thesis were selected and simulated LOFA transients by subchannel analysis accordingly to the FSAR specifications [21].

Transient is an event or series of events which may occur in the nuclear facility due to the system malfunction or series of particular devices defects. Transients lead to the change of temperatures, pressures or power of a unit which may lead to the reactor trip.

Between design basis accidents that are proposed for consideration in the project are included reactivity accidents, loss of flow accidents (LOFAs), loss of coolant accidents (LOCAs), loss of integrity of secondary circuit, loss of power supply, primary circuit malfunctions, secondary circuit malfunctions, forces on reactor internals, components (e.g. valves) and piping during accidents, cold water impact on the reactor vessel material

during overcooling transients, interfacing system LOCA, anticipated transients without SCRAM (ATWS), fuel handling accidents, accidents in auxiliary system and accidents due to external events [20].

4.2 LOFA

For VVER-440 (type V-213) are specified different types of transients in the project. This thesis focuses on LOFAs. These transients may be reached by six groups of initiated events which were postulated in the project that may directly affect the safety of the power plant [20]:

1. Trip of different number of reactor coolant pumps (RCPs)
2. Loss of power supply to all RCPs
3. Seizure of one RCP
4. Break of the one RCP shaft
5. Inadvertent closure of one main isolation (shut-off) valve
6. Partial blockage of the coolant flow through the FC

In order to meet the safety criteria there are three parameters that must not be exceeded: critical heat flux on the external surface of every single fuel rod, fuel melting temperature and allowed value of pressure in the primary and secondary circuit. The results of various analyses showed that by compliance of these three criteria a conservative approach is fulfilled in its essence [21].

The subchannel analysis is suitable in order to investigate possible undesirable boiling in the primary circuit. During the heat transfer it is necessary to stay away from the higher heat flux when boiling regimes are initialized. This phenomenon is described in figure 4.2.1.

In the lowest horizontal position are described boiling regimes, upper is a heated rod with pictorial description of boiling regimes and pool boiling curve for water at atmospheric pressure above all [24]. In this picture are visible few points from which the most important is point A when the nucleate boiling begins. An appropriate value for research of safety operation is departure from nucleate boiling ratio (DNBR). This value is defined by equation 4.1

$$\text{DNBR} = \frac{q_{cr}(z)}{q(z)}, \quad (4.1)$$

where $q_{cr}(z)$ is the critical heat flux at the position z and $q(z)$ is the actual heat flux at the position z . Highly important for PWRs is maintenance of safe margin to DNB.

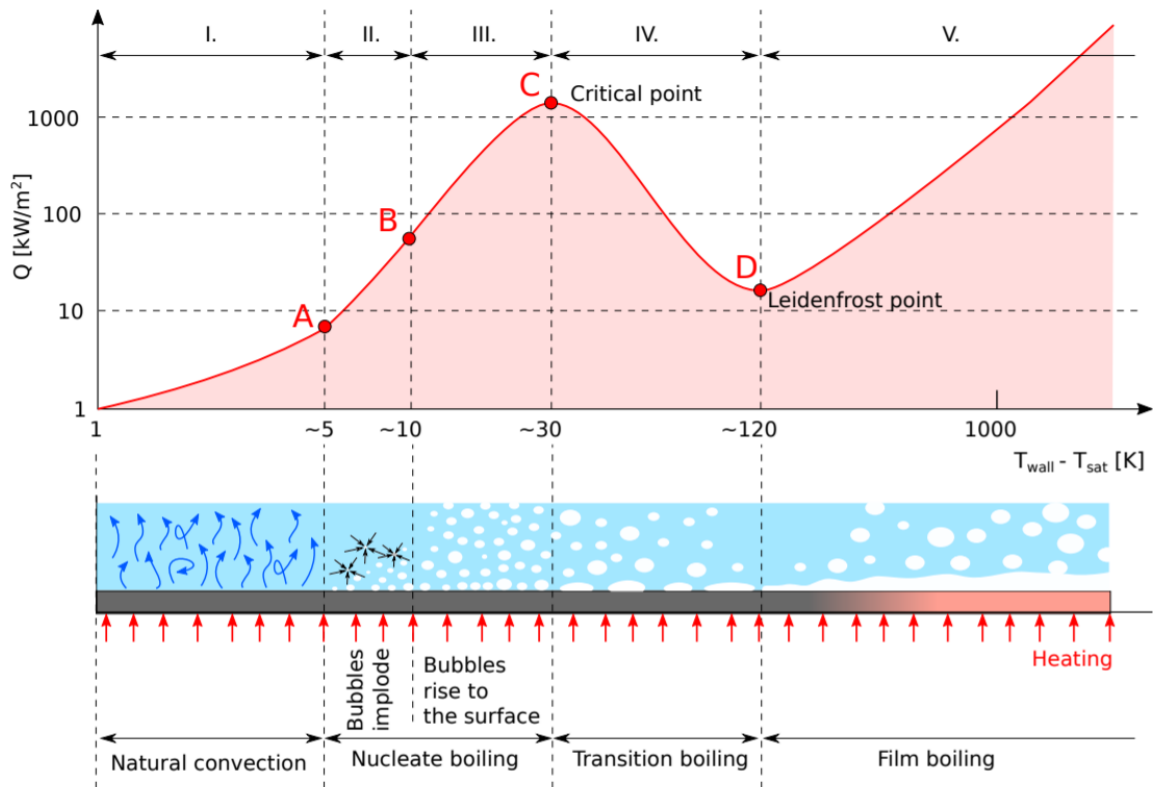


Figure 4.2.1: Pool boiling curve for water at atmospheric pressure with boiling regimes [24].

4.2.1 Trip of Different Number of RCPs

The initialization of this accident is caused by a reactor coolant pump trip, power supply failure, operator's error or trip caused by the RCP protection system.

Trip of the RCPs will cause reduction of the coolant flow through the AZ. This would lead to the AZ medium temperature increase which would increase the primary circuit pressure and this may lead to the loss of integrity.

In the case there are three or more working RCPs, the reactor limitation system (RLS) decreases reactor power generation. In the case there are less than three RCPs working, the system orders to shut down the reactor.

Detailed criteria that has to be met are: departure from nucleate boiling ratio higher than 1.125 for correlation PG-I (1.0 for OKB), pressure in primary circuit lower than 15.2 MPa and fuel temperature lower than $T_{melt} = 2480$ °C [21]. Another three criteria that are required during accidents: Limit value radially centered enthalpy in a fuel pellet 690 J/kg, cladding temperature limit value 1200 °C and limit value for fuel cladding total local oxidation 18 % based on the correlation VNIINM.

4.2.2 Loss of Power Supply to all RCPs

The cause of this accident is total power outage for all RCPs. As a result there is intensive decrease of flow through the AZ. The reduction in flow leads to the fuel cladding temperature increase, deterioration of cooling conditions and the primary circuit pressure increase.

The worst scenario assumes failure of the RLS. This system would insert the control assemblies to the AZ and it also would forbid increasing of the power to the RCS system [21].

4.2.3 Seizure of One RCP

The possibility of occurrence of this accident is very low hence the possibility of rotor seizure by more than one RCP is not considered. After rotor seizure there is a rapid decrease of flow through the AZ. This incident may lead to, same as in the previous scenario, increase of temperature in the AZ, deterioration of the cooling conditions and the primary circuit pressure increase [21].

4.2.4 Break of the One RCP Shaft

Advantage against rotor seizure in this case is possible free movement of the RCP in the flow hence the flow decrease is not as significant as in previous accident.

Rupture of only one RCP shaft is assumed due to the same reasons as in the previous accident. The possibility of the shaft breakage occurrence is very low.

RCP rotor seizure and RCP shaft rupture are similar accidents which may be replaced by one single accident. This hypothetical accident begins with rotor seizure and immediate discontinuation of the flow through a loop. This accident continues with reversal flow where the rotor freely rotates.

Criterion on pressure limits is covered by main isolation (shut-off) valve closure, which stops the flow. Even though the flow decreases slowly than during RCP rotor seizure, important is the fact that one steam generator (SG) has completely lost its possibility to transfer heat with the secondary circuit.

The shaft rupture also influences moment of the RCP inertia, therefore, rotation in the opposite way of original flow may begin faster the moment of inertia is lower [21].

4.2.5 Inadvertent Closure of One Main Isolation (Shut-off) Valve

Main isolation valve closure is an incident which happens after defect in circuits or after wrong intervention of operator (human error).

As was mentioned, the difference against remaining scenarios is elimination of one whole loop (heat exchange in the SG) which causes deterioration of cooling conditions

consequently the temperature in the AZ increase and the primary circuit pressure increase. Moreover a possibility of zero flow through the SG is increased. This loop does not contribute to the heat exchange with the second circuit.

During the simulation of this accident is assumed inaction from the side of the operator for 30 minutes [21].

4.2.6 Partial Blockage of the Coolant Flow through a Fuel Cassette

This incident is commonly known for its results e.g. in NPP Jaslovské Bohunice, unit A1. Reduction of flow through a FC began thanks to the forgotten silica gel, which was initializing element for the meltdown.

The cause of this accident may be impurities which lower heat transfer between coolant and fuel. These impurities may occur after fuel exchange or after maintenance activity. The main influenced parameters are fuel and fuel cladding temperature which may considerably increase. It is also possible an occurrence of two phase flow in the FC [21].

4.3 Reactor Coolant Pumps Trip Scenarios

In this section are described step-by-step scenarios of different number of the RCPs trip. For this thesis are calculated four scenarios, which progress is described in FSAR [21]. These scenarios were simulated in the code TRACE and resulting mass flow through the RPV and power of the reactor were used as input values for the calculation of transient in the SUBCHANFLOW software.

During the calculation is not involved any action from the operator in the modelling process. This approach leads to high contribution on conservatism.

The study of following four scenarios are sufficient from the conservative point of view due to many similarities in the LOFA accidents.

These scenarios have following limitations, where the first three are required during transients and last three are required also during accidents.

- Sufficient DNBR. MDNBR has to be higher than correlation limit (for OKB 1.0, for PG-I 1.125).
- Limitation of maximum pressure. Pressure in P.C. has to be lower than 15.2 MPa and in the S.C. lower than 6.15 MPa.
- Maximum fuel temperature (melting temperature). Limit value is 2480 °C.
- Not exceeding radially centered enthalpy in a fuel pellet. Limit value is 690 J/kg.

- Not exceeding cladding temperature. Limit value is 1200 °C.
- Not exceeding fuel cladding total local oxidation. Limit value is 18 % based on the correlation VNIINM.

In order to satisfy the MDNBR criterion, the operation of the RTS is necessary. This system consists of three independent channels. Failure of any of these channels leads to the system function fulfilment. The maximum pressure criterion has to involve possible failure of the safety valve opening in the pressurizer. This sequel of events supports the conservative approach of the accident modelling.

4.3.1 One of Six RCP Trip

Final safety analysis report does not contain simulation of 1/6 RCP trip [21]. This scenario is conservatively covered by scenarios 2/6 RCPs trip and 3/6 RCPs trip. Time sequence of this scenario, created for the purpose of this thesis, is in table 4.3.1.

Table 4.3.1: 1/6 RCPs trip sequence simulated in TRACE.

t [s]	Event	Description
-5.0	Beginning of the calculation	Stabilization of the parameters
5.0	1/6 RCP trip	
34.0	SCRAM	

4.3.2 Two of Six RCPs Trip

Time sequence of this scenario is in table 4.3.2. This scenario is studied from the point of maximum pressure in the P.C.

4.3.3 Three of Six RCPs Trip

Step-by-step scenario of this accident is in table 4.3.3. This calculation is stopped after 700 seconds due to not including LOOBP.

4.3.4 Total LOFA (Six of Six RCPs Trip)

Scenario for the total LOFA was simulated with step-by-step from the point of MDNBR. It is highly conservative analysis due to low possibility of occurrence of this accident. The time sequence of this accident is in table 4.3.4.

Table 4.3.2: 2/6 RCPs trip sequence [21].

t [s]	Event	Description
-510.0	Beginning of the calculation	Stabilization of the parameters
0.0	2/6 RCPs trip	Modelling of trip of RCPs 1 and 2, failure of the system TE and showering of the pressurizer, in closed position is also blocked valve on the way from the pressurizer to the BT
1.0	Signal from the RLS on power lowering	Conservatively not included
1.8	Initialization of pulling out of the control assembly	Involvement of RCS from lowering of the power
23.0	LOOBP	Quick-closing valves closing of both turbines, power cut of electric feed water pump, trip of the rest RCPs
22.8	Pulling out of control assembly stopped because of high pressure in the P.C.	Pressure in the reactor outlet $p=13.12$ MPa
25.1	MDNBR reached	Limit for PG-I is 1.125
25.5	1st signal RTS from 4 or more RCPs trip	Signal not reflected (conservatively)
26.8	2nd signal RTS from high pressure in the P.C.	$p=13.72$ MPa
29.0	Beginning of programme ELS	
29.1	SCRAM from 2nd signal RTS	Delay 2.3 seconds
31.0	Opening of all SGs safety valves	Opening pressure 5.78 MPa + uncertainty 0.06 MPa
31.9	Opening of 2nd safety valve of pressurizer	Pressure in pressurizer 14.7 MPa + uncertainty 0.15 MPa
32.7	Maximum pressure in the P.C.	$p=15.14$ MPa (bottom of the RPV)
47.0	Maximum pressure in the S.C.	$p=5.96$ MPa (bottom of the SG5)
51.0	Running up of the DGs	
200.0	The end of the calculation	

Table 4.3.3: 3/6 RCPs trip sequence [21].

t [s]	Event	Description
-500.0	Beginning of the calculation	Stabilization of the parameters
0.0	3/6 RCPs trip	Consequently modelling failure of TK and failure of PH system
1.0	Signal from RLS on lowering of power	Not used in conservative approach
1.8	Initialization of pulling out of the control assembly	During lowering of power of the reactor
19.8	Opening valve on the way from pressuriser to BT	$p=13.03$ MPa
22.0	Pulling out of the control assembly stopped because of high pressure in the P.C.	Outlet pressure in the reactor $p=13.12$ MPa
27.1	Forming of 1st signal RTS "high temperature in the reactor outlet 312 °C"	By temperature on outlet 314 °C; Delay by temperature inertia of sensor and delay of logic
29.4	SCRAM from 1st signal RTS	Delay 2.3 seconds
29.5	MDNBR 1.131	Correlation PG
31.0	Maximum pressure in the P.C. 13.73 MPa	Bottom of the pressurized vessel of reactor
34.4	Closing of quick closing valve of both TGs	5 s after SCRAM
34.5	Opening of the BVC	
37.5	Working of the BVA	
42.0	Maximum pressure in the S.C. 5.49 MPa	In the SG5
200.0	The end of the calculation	

Table 4.3.4: 6/6 RCPs trip sequence (Total LOFA) [21].

t [s]	Event	Description
0.0	6/6 RCPs trip	At the same time is modelled failure of TK and PH systems.
1.0	Signal from RLS on lowering of power	Not used in conservative approach
1.1	Initialization of pulling out of the control assembly	RCS in N regime
4.1	1st signal RTS from power failure of 4 or more RCPs lasting more than 3 s	
6.4	SCRAM	Delay 2.3 s
6.6	MDNBR reached	Limit for PG-I is 1.125
10.0	Maximum pressure in the P.C.	$p=12.85$ MPa (bottom of the RPV)
11.4	Closing of quick-closing valve of turbines	5 seconds after LOOBP
11.6	Opening of the BVC	
17.0	Maximum pressure in the S.C.	$p=5.16$ MPa (bottom of the SG2)
200.0	The end of the calculation	

4.4 Summary

The topic of this chapter were transients and description of initiating events that are postulated in the project. Due to the neutronic and thermal hydraulics software it is possible to assess appearances of physical phenomenons in the reactor and avoiding the limits during transients. Time sequences of particular transients reached from FSAR were attached on the end of this chapter.

Chapter 5

Subchannel Analysis

This chapter describes theoretical approach of the subchannel analysis and includes basic approximations and simplification methods.

5.1 Introduction

Subchannel analysis is a special case of the porous media approach. This analysis is specified by fundamental relations between solid structures and fluid. Equations solving single and two phase flow physical phenomenons will be described further.

Subchannel analysis is not describing a fully three-dimensional flow because the simplification is in the lateral exchanges between the neighbouring subchannels. When the flow is leaving the region of a subchannel, it is assumed that this flow loses its sense of direction. This approach simplifies the lateral convection terms of the linear momentum balance equations [5].

Subchannel analysis's topic of interest is clearly described in picture 5.1.1. This picture shows typical PWR rectangular assembly AZ, with detail of one FC. The control volume defined in a subchannel code is in the right lower corner.

5.2 Terminology

Subchannel analysis operates with few terms which is necessary to define. These terms are described below.

5.2.1 Geometry

The first important parameter in the equation of subchannel analysis is geometry. There are two approaches of the subchannel analysis which refer to the coolant or the rod. The first is the coolant centered subchannel and the second is the rod centered subchannel. In this thesis (for VVER-440 hexagonal scheme) will be described the coolant centered

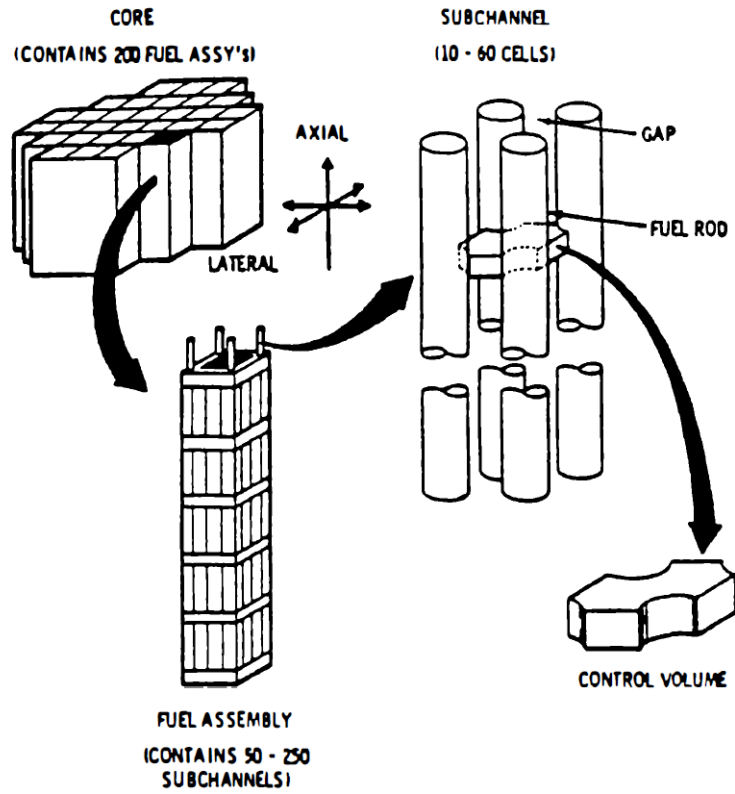


Figure 5.1.1: Relation of subchannel control volume to the AZ [5].

approach which is also more traditional. On the other hand, the results for two phase flow, particularly annular flow, are better for the rod centered subchannel [5]. These two possible subchannel area definition approaches around the rod are visible in picture 5.2.1.

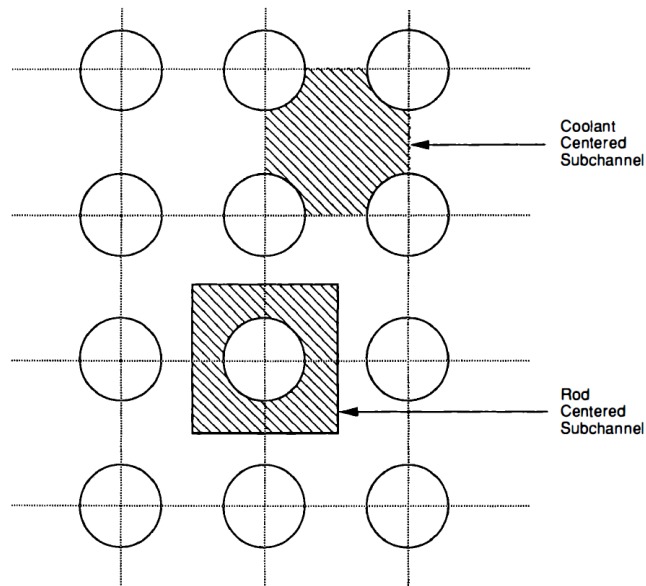


Figure 5.2.1: Difference between two possible approaches in subchannels definition [5].

For definition of geometry have to be specified spacing gap s_{ij}^x and s_{ij}^y , where ij represents flow from subchannel i to j and superscripts x and y represent direction. It is

necessary to realize that these gaps are not constant in the real device [5].

5.2.2 Mass Flow Rate

In the case of mass flow rate it is important to take into consideration the transverse component which is associated with the control volume same as axial part [5].

5.2.3 Axial Mass Flow Rate

Axial mass flow rate in the channel i \dot{m}_i is given by equation

$$\dot{m}_i = \int_{A_{fi}} \rho u_z dA, \quad (5.1)$$

where A_{fi} [m²] stands for the total axial cross-sectional area of the subchannel [5].

5.2.4 Momentum and Energy Transfer Rates

There are three types of transfer: transport by diversion cross flow, transport by turbulent interchange and viscous transfer due to the transverse gradients of axial velocity and temperature.

Transport by diversion cross flow is based on product of density and velocity in the direction x : ρu_x , and also as a product with velocity in axis x or enthalpy $\rho u_x u_z$, respectively $\rho u_x h$.

Transport by turbulent interchange uses time averaged balance equations and viscous transfer due to the transverse gradients of axial velocity and temperature redefine parameters to include viscous effects [5].

5.2.5 Transverse Mass Flow Rate per Unit Length

Transverse mass flow rate per unit length W_{ij} is given by equation

$$W_{ij}^x = \frac{1}{\Delta z} \int_{\Delta z} \int_{s_{ij}^y} \rho u_x ds dz. \quad (5.2)$$

Superscripts x and y stand for flow along x direction and for y direction respectively. There are two transverse mass flow creation mechanisms.

The first are pressure gradients and the second are turbulent fluctuations. The pressure gradient is given by differences in the geometry or by variations in the fluid density. The subchannel analysis also calculates the bowing and swelling of the rods and this phenomenon creates the differences in the pressure field.

Turbulent fluctuation differs in superscript $'D$. In single phase flow it is assumed that $W_{ij}'^D = W_{ji}'^D$. This approximation is based on the idea that during single phase flow there is similar density in both channels hence there is no net mass exchange [5].

5.3 Conservation Equations

For the following relations are assumed only single phase flow models which are proceeded by volume averaged porous body equations [5].

5.3.1 Geometric Relations

In the geometric equations appears volume porosity $\gamma_V = V_f/V_t$, where V_f stands for fluid volume and V_t stands for total volume. The geometric equations are

$$V_t \gamma_V = V_f \quad (5.3)$$

$$V_t \gamma_{Az} = A_f \Delta z \quad (5.4)$$

$$V_t \gamma_{Ax} = s_{ij}^y \Delta x \Delta z \quad (5.5)$$

$$V_t \gamma_{Ay} = s_{ij}^y \Delta y \Delta z \quad [5]. \quad (5.6)$$

5.3.2 Continuity Equation

Continuity equation for subchannel i is

$$A_{fi} \frac{\partial}{\partial t} \langle \rho_i \rangle + \frac{\Delta \dot{m}_i}{\Delta z} = - \sum_{j=1}^J [W_{ij} + W_{i \leftrightarrow j}'^D], \quad (5.7)$$

where J is a number of neighbouring subchannels and $i \leftrightarrow j$ means flow between subchannels i and j . This equation is also possible to simplify in order to get equation only for single phase flow [5].

5.3.3 Energy Equation

For single phase flow it is possible to obtain equation

$$A_{fi} \frac{\partial}{\partial t} [\langle \rho h \rangle_i] + \frac{\Delta}{\Delta z} [\dot{m}_i h_i] = \langle q_i' \rangle_{rb} - \sum_{j=1}^J W_{ij}^{*H} [h_i - h_j] - \sum_{j=1}^J W_{ij} \{h^*\} + A_{fi} \left\langle \frac{Dp_i}{Dt} \right\rangle. \quad (5.8)$$

The brackets $\langle \rangle$ and $\{ \}$ are related to the volume average and the surface average respectively.

5.3.4 Axial Linear Momentum Equation

For transverse momentum equation in the case of subchannel to subchannel in COBRA IIC is used equation

$$\frac{\partial W_{ij}}{\partial t} + \frac{\partial(uW_{ij})}{\partial x} = \frac{s}{z}(p_i - p_j) - F_{ij}, \quad (5.9)$$

which is also used for assembly to assembly equation. In this equation z is axial dimension, F_{ij} is force on the solid for vertical flow over the solid surfaces in the control volume, p_i is pressure in the subchannel i [25].

5.4 Summary

Subchannel analysis includes various of advanced thermal hydraulics equations which were described in this chapter. Also were defined main terms used in the mathematical and physical description of the AZ. This analysis is difficult from the point of geometry definition, possible two phase flow or turbulent mixing of the flow. Equations mentioned above are fundamental for subchannel calculation and flow behaviour modelling in the AZ.

Chapter 6

SUBCHANFLOW

This chapter briefly describes subchannel analysis software and then focuses on the SUBCHANFLOW 3.5 fundamentals, main parameters required for the calculation and on the input system characteristics.

6.1 Subchannel Analysis Software

This section gives basic overview of the evolution in numerical codes dealing with subchannel analysis. There is a variety of subchannel software which differ in specific usage, calculation approaches or number of correlations used for two-phase friction multipliers, subcooled boiling models, bulk void/quality correlations, heat transfer correlations etc.

SCF was developed in order to provide flexible, stable and fast running tool for nuclear safety analysis. It is based on $3 + 1$ equation model for the conservation of mass, energy and momentum (axial and lateral) for the water vapour mixture. There is also included fully implicit iteration solver for steady-state and transients research and for heat conduction is applied finite volume approach.

SCF can be used to model systems cooled/operated with water, air, helium, lead, lead–bismuth and sodium in quadratic and hexagonal lattices using subchannel or sub-assembly discretization of the AZ [9].

Depending on the void fraction the heat transfer regime is selected. In SUBCHANFLOW the boiling curve is divided into four sections following the COBRA IVi approach [9].

6.1.1 COBRA-IIIC

COBRA-IIIC is software based on COBRA family software. This code enhanced COBRA-III code in 1973 and it is possible to calculate steady-states and transient conditions. The essential benefit of this programme was implementation of heat transfer in the fuel, forced mixing of transverse flow and complete momentum equation in the transverse direction.

This programme also calculates the flow and enthalpy in 1-D geometry in all subchannels before and during the boiling [25].

6.1.2 COBRA-IV-I

COBRA-IV-I is another evolution of COBRA-III. This update contains correlation methods for subcooled boiling, boiling and overheated boiling. Moreover, this version involves calculations of heat transfer in fuel rods in both axial and radial directions and calculation of reverse flow [26].

6.1.3 VIPRE-01

VIPRE-01 stands for Versatile Internals and Component Program for Reactors: EPRI [7]. It was developed by Battelle Pacific Northwest Laboratories under the sponsorship of the Electric Power Research Institute (EPRI). This code was submitted to the NRC for generic review in 1984 [27].

Besides, VIPRE-01 is used nowadays for subchannel analysis of steady-states and abnormal events or accidents by ÚJV Řež for safety analyses of VVER.

6.2 SUBCHANFLOW Code Description

SCF is software developed in Karlsruher Institut für Technologie (KIT). This software is based on COBRA code family (COBRA-IIIC [25], COBRA-IV-I [26], COBRA-EN [28]) [2].

It is able to compute the results for steady-state and for transient conditions. The advantages of this software are fast and stable executions and it is based on semi-implicit SOLA method [29].

Version 3.5 is using Fortran 2003 which is advantageous in using of simple structures and it is also possible to use the coupling to the external GUI program SALOME by an interface module to the C++ language [2].

6.3 Input Parameters

SCF requires input of parameters, correlations, dimensions etc. into input text file. This file is divided into 16 groups. Mainly important for the calculation are following 10.

6.3.1 Properties

Properties of the coolant are gained from the IAPWS-97 libraries moreover liquid metals (sodium and lead) and gases (helium and air) properties with two phase flow for water

and sodium are available. For lead-bismuth are used Lead-Bismuth HLMC properties and for lead are used Lead HLMC properties [2].

6.3.2 Correlations

Correlations are highly important computational tool for thermal hydraulics phenomena determination. There is vast number of correlations that are used for calculation of mixing coefficients, friction factors, critical heat flux etc. It is important to use appropriate correlations for specific operational conditions or particular nuclear reactors designs.

The first group of correlations are calculating sub-cooled boiling. These correlations are Levy, Saha-Zuber, Unal, Bowring and none.

The second group in correlations are models for vapor slip behavior. There are three models: Modified Armand, Smith slip ratio and Chexal-Lellouche.

Friction factors for two phase friction and turbulent friction are more described in Appendix, specifically Armand and Lockhart-Martinelli friction factors correlations.

Single phase heat transfer is group number 5 in correlations. There are three options: Dittus-Boelter heat transfer, Gnielinski heat transfer and Subbotin for liquid metals.

The sixth group are correlations for critical heat flux in the water boiling curve. There is possible to choose between Biasi, OKB, W-3, Levitan , EPRI with shape function and Doroshchuk.

The last group calculates cladding gap: Simplified model, TRANSURANUS-Model and Benchmark VVER-1000 cold gap [2].

Specific equations for majority of the mentioned correlations are described in the Appendix.

6.3.3 Special Parameters

Special parameters section requires input of rod pitch and rod diameter. It is also possible to input axial wire wrap pitch, wire diameter and wetted perimeter. If Rehme average pressure loss model is used, it is possible to use these three last parameters instead of detailed calculation model in the group Grid spacer wire wrap which description will follow in the text [2].

6.3.4 Axial Heat Flux

Axial heat flux is important for axial heat distribution in the fuel cassette or fuel assembly. Axial heat flux is written to the input as relative axial location and power in this location. It is possible to write total power in the input text file, therefore, write only relative axial heat flux.

If positions 0.0 and 1.0 are missing, the code calculates them by the linear extrapolation [2]. Axial heat flux for the calculation was obtained from the code TRACE.

6.3.5 Rods and Channels Layout

Rod layout part requires detailed material properties as was described in section 3.3. It is possible to use already implemented libraries of material types for fuel (UO_2 , UO_2PuO_2 , Boron Nitride/Nichrome, PWR and VVER benchmarks) or for cladding materials (Zircaloy, Stainless steel SS316, Inconel 600 and VVER-1000 benchmark). The fuel rod heat transfer is calculated by the standard finite volume method. Material properties of fuel UO_2 and UO_2PUO_2 are coded from the code TRACE.

It is possible to specify more materials and define different types of fuel rods in the FC.

Solution of pin radial heat conduction may be done by finite volume method using SOR iteration procedure or by method taken from COBRA-EN [2].

There is also implemented possibility of simulation transient burn-up simulation and burn-up dependent fuel pin behaviour e.g. fuel swelling or fission gas release.

6.3.6 Calculation Control

This part defines one of the fluid flow solver, upward flow (UPWA) which is fully implicit COBRA type solver or SOLA, which is more robust for cases including downward flow, buoyance driven flow, strong lateral flow, small axial flow rates or pressure boundary conditions at the top and the bottom [2].

Calculation control allows to use boron transport during transients, sets total axial length, flow convergence, calculation time steps, maximum reachable parameters during the calculation, Courant number for SOLA, minimum and maximum number of iterations etc.

This part is crucial for the realization of calculation due to the boundary conditions, which are represented by three maximum temperatures change types, maximum void change or maximum iteration number. Due to the difficulty of numerical calculation there has been done convergence analysis of the steady-state calculation

6.3.7 Grid Spacer Wire Wrap

Important input for VVER is the relative axial position of grid spacers and their loss coefficients. Besides, SCF is able to implement information about wire wraps [2]. Detail description of each grid spacers and its loss coefficient may be searched in the Final safety analysis report of particular project.

6.3.8 Lateral Transport

Lateral transport is group for choosing one of four single phase mixing correlation: constant mixing coefficient, Rogers-Tahir rectangular, Rogers-Tahir triangular and Rogers-Rosehart. Further equal mass or equal volume exchange is chosen [2]. According to [2] the difference between equal mass or equal volume exchange is that equal mass exchange is more numerically stable than equal volume exchange.

6.3.9 Operating Conditions

This group defines flow conditions and global parameters of the calculation such as exit pressure, inlet temperature, inlet boron concentration, inlet flow rate or inlet mass flux, total power, average heat flux, pressure drop and heat fraction moderator [2].

This group requires detailed information from TRACE study that defines steady-state or transient scenario.

6.3.10 Point Kinetics

The last part solves point kinetics of the system by explicit Euler-forward method. It is possible to input fractions of six delayed neutron groups, six decay constant groups and coefficient for calculation: Doppler, coolant temperature, void and boron [2].

6.4 Output

As it was said in section 1.1, the main results from the subchannel analysis are temperature profile in the rods (outer and inner cladding temperature and outer and center fuel temperature) and channels (coolant temperature), DNBR, equilibrium quality or pressure.

Other physical values reached for the rods are coolant density, heat transfer coefficient, fuel cladding gap and heat gap coefficient. In the subchannels are calculated pressure, temperature, density, void fraction, velocity, mass flow, flow rate, boron concentration and cross flow.

6.5 Geometry

For the triangular symmetry FA geometry was developed a software named HEGGS (Hexagonal Geometry Generator Software). This software was written in Python 3.6.0 language [30] and the main goal of this software was hexagonal fuel assemblies geometry generating simplification especially for the SUBCHANFLOW 3.5, which requires particular input text files.

The main issue of the geometry is in the rods and subchannels numbering. In order to get general solution it is easier to number the rods and the subchannels from the center of the FA. This was done in anticlockwise system. The approaches given e.g. by [31] are obviously not general and it would be much more complicated to reach the generalization by the software.

It is possible to input four parameters to the software HEGGS which are connected to the geometry. The first is number of hexagonal groups in the fuel assembly, the second is pin pitch (PP), the third is FA pitch and the last is rod diameter (RD).

Geometry generated for VVER-440 is in picture 6.5.1. The geometry was defined in Cartesian coordinates where rod number 1 is in the center in point (0,0). The rods numbering is above of each rod. The numbering system may be set as clockwise or anticlockwise which improves the possibility of code-to-code benchmarking and also the geometry correctness verification.

There are 258 subchannels and the numbering system is in picture 6.5.2. The numbering system was designed with the same philosophy as in the case of rods i.e. anticlockwise numbering with the beginning in the FA center.

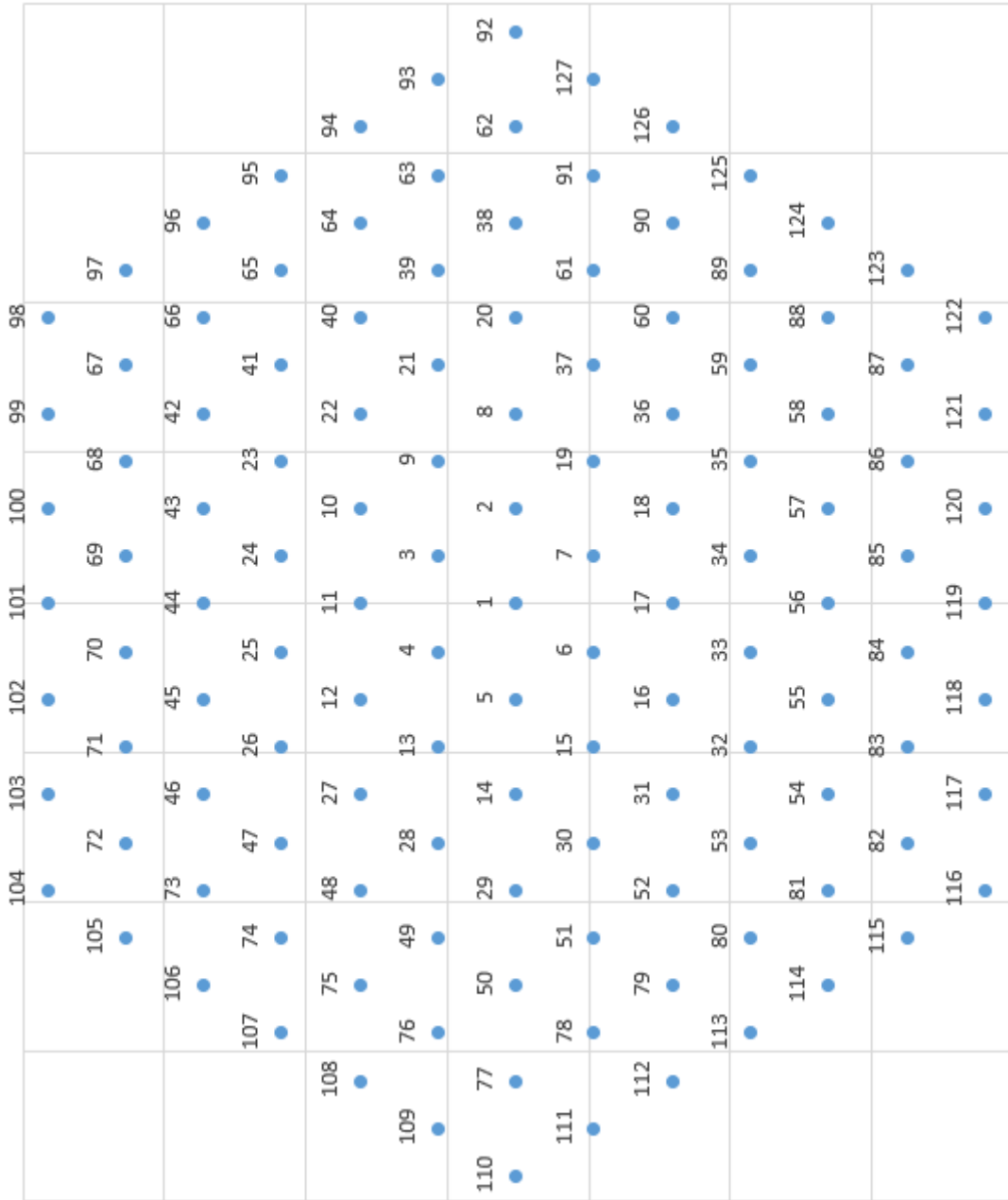


Figure 6.5.1: Rods positions in VVER-440.

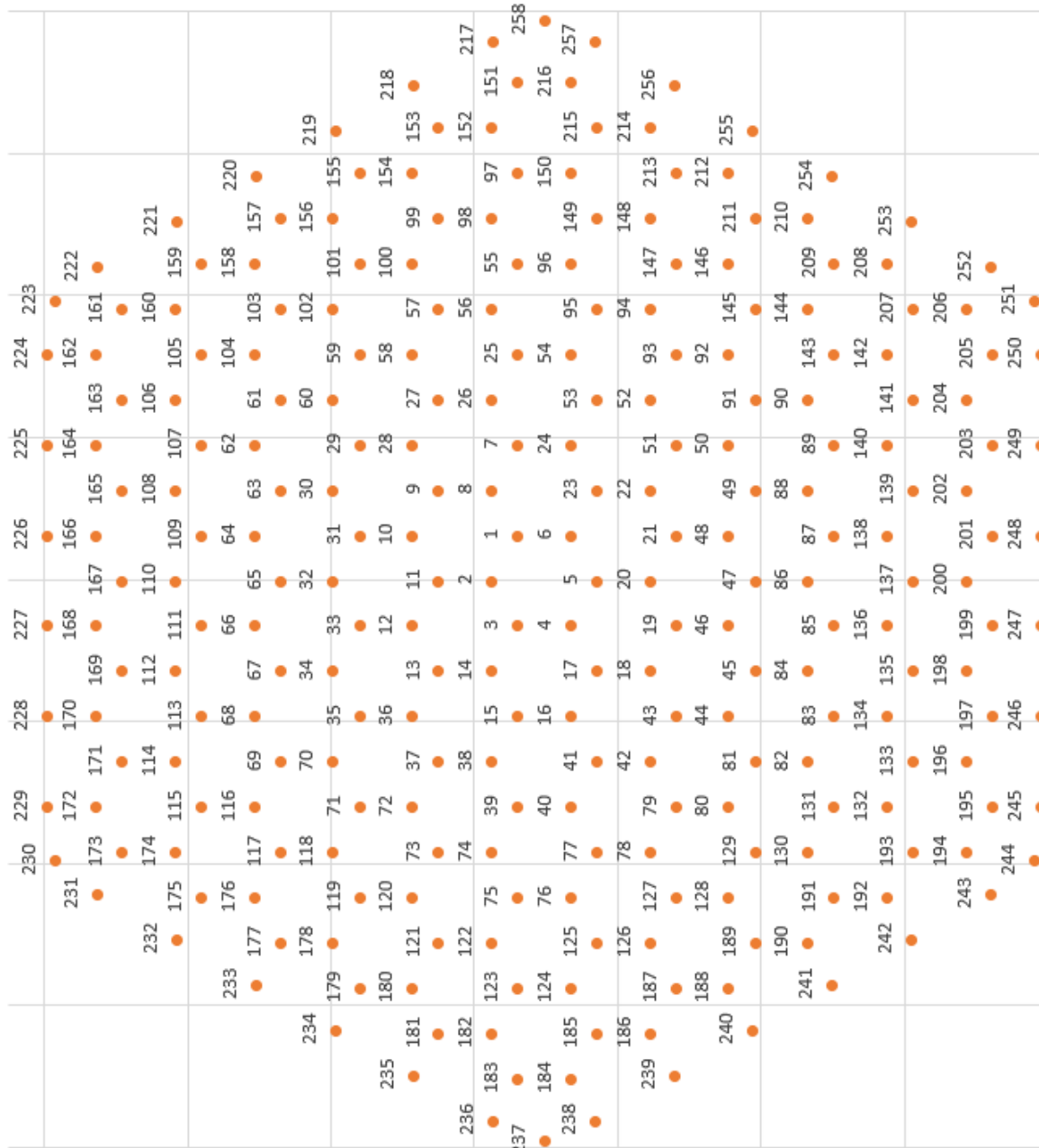


Figure 6.5.2: Subchannels positions in VVER-440.

6.6 Benchmark with TestCase

The so called TestCase is a hexagonal FA implemented by the SCF developers. This geometry contains 37 rods and 72 subchannels which are numbered from the FA edge. This layout is visible in figure 6.6.1.

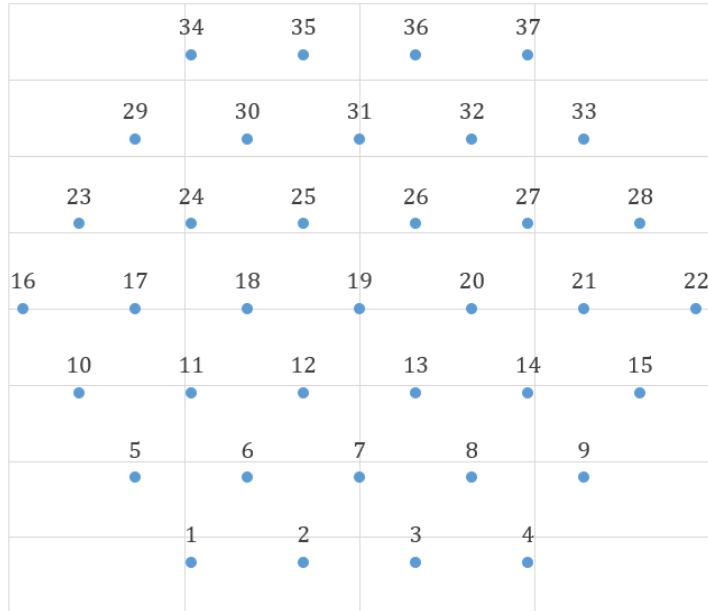


Figure 6.6.1: Edge numbering of the rods in TestCase.

The input values for this benchmark are in table 6.6.1. For this benchmark were used same correlations, numerical methods and operating conditions.

Table 6.6.1: Physical values of benchmarking with TestCase.

p_{ex} [MPa]	T_{in} [°C]	\dot{m}_{in} [kg/s]	P_{tot} [GW]
15.52	286.85	14.12	2.017

The geometry generated by HEGGS is numbered from the center and includes 37 rods and 78 subchannels.

The subchannels number differs due to the different FA segmenting approach. The difference is visible in figure 6.6.2.

In figure 6.6.3 are visible three hexagonal groups. The first is from the rod number 2 to the rod number 7. The second is from 8 to 19 and the last is from 20 to 37. The geometrical dimensions of the FA are: $d=9.1455$ mm, FA pitch=82.1136 mm and PP=12.8138 mm. These parameters were taken from TestCase input tables.

The MDNBR was in the case of TestCase geometry 7.6111 on the rod 34 and in the case of HEGGS geometry 5.4076 on the rod 23.

Due to the different numbering the rods are in both cases on the same corner position. The difference in the MDNBR are given by a different value of the corner channel area.



Figure 6.6.2: Corner subchannels geometry generated by HEGGS (left) and geometry in TestCase.

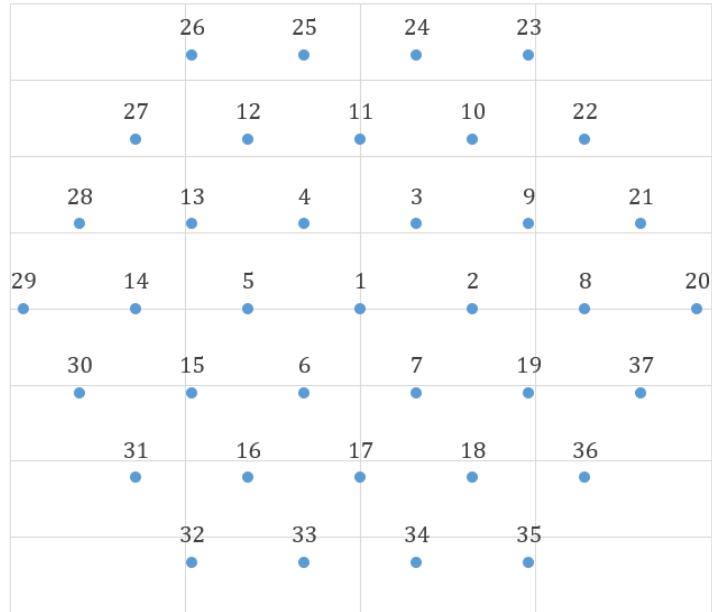


Figure 6.6.3: Centered numbering of the rods done by HEGGS code.

From the input table was calculated the edge channel area as $3.8102\text{E-}05 \text{ m}^2$, but in the TestCase table_channel.txt input table is written number $6.66576\text{E-}05$. From this point of view it is visible that the HEGGS geometry results are more conservative. The benchmarking was done also with this different channel area and the axial temperature on the hot rod is in figure 6.6.4. This benchmarking with different channel area in HEGGS method was marked as HEGGS v2 and the results are compared in table 6.6.2.

Table 6.6.2: Benchmarking results of HEGGS method with TestCase.

	TestCase	HEGGS	HEGGS v2
MDNBR [-]	7.61	5.41	7.61
Rod number [-]	34	23	20

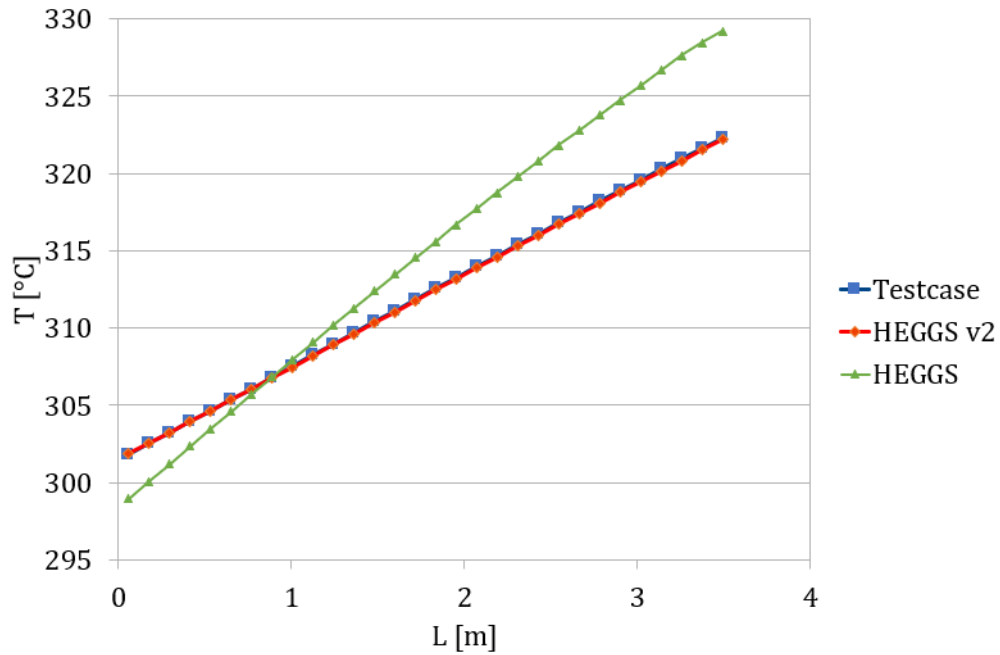


Figure 6.6.4: Axial temperature on the HR outer cladding diameter.

6.7 Summary

Chapter 6 briefly summarized main subchannel analysis software that preceded SCF. Due to the possible future work was also mentioned subchannel analysis software VIPRE-01. There were depicted groups of input parameters that are included in the SCF. The correlation methods will be described in more details in the Appendix. In the end of this chapter was briefly described initial benchmark of constructed geometry created in the software HEGGS. The benchmark pointed to the different number of corner subchannels area in the TestCase files. After implementation of the same channel area as in the TestCase files to the geometry generated by HEGGS, the results were similar.

Chapter 7

Methodology Description

Steady-state is a term used in the nuclear engineering describing operational mode of a reactor when the physical parameters are stabilized. Nuclear reactors are operating in steady-state majority of its operational time. The steady-state analysis is necessary for validation of a computational method, for simulating transients and for optimal choice of numerical parameters for the null transient i.e. for time period before the accident begins.

7.1 Operational Conditions for VVER-440

For the steady-state analysis was chosen the beginning of cycle (BOC) in order to be more conservative in the safety approach. The operational conditions for steady-state were extracted from FSAR and they are listed below.

Nominal heat power production:	1 444 MW
Nominal flow rate:	41 500 m ³ /h
Mass flow per FC:	24.13 kg/s
Exit pressure:	12.26 MPa
Nominal temperature at the AZ inlet:	268 °C

FSAR offers flow information in m³/h, while SCF needs the inlet flow to be in kg/s. Therefore, it was necessary to convert the nominal flow rate to mass flow rate per FC. The water density was obtained from CoolProp thermodynamic libraries [32], hence mass flow per FC in VVER-440 is $\dot{m}_i = 24.13$ kg/s.

For axial and radial power profile are theoretically used cosine respectively Bessel function of order 0 J_0 . This function may be defined as infinite power series

$$J_0(z) = 1 - \frac{z^2}{2^2} + \frac{z^4}{2^2 \cdot 4^2} - \frac{z^6}{2^2 \cdot 4^2 \cdot 6^2} + \dots [33], \quad (7.1)$$

which may be also defined using gamma function Γ

$$J_0(z) = \sum_{k=0}^{+\infty} \frac{(-1)^k}{k! \Gamma(k+1)} \left(\frac{z}{2}\right)^{2k} \quad [34]. \quad (7.2)$$

For the input of the subchannel analysis was used the relative axial power profile P depending on the relative axial location z from the code TRACE. The axial power profile is in figure 7.1.1.

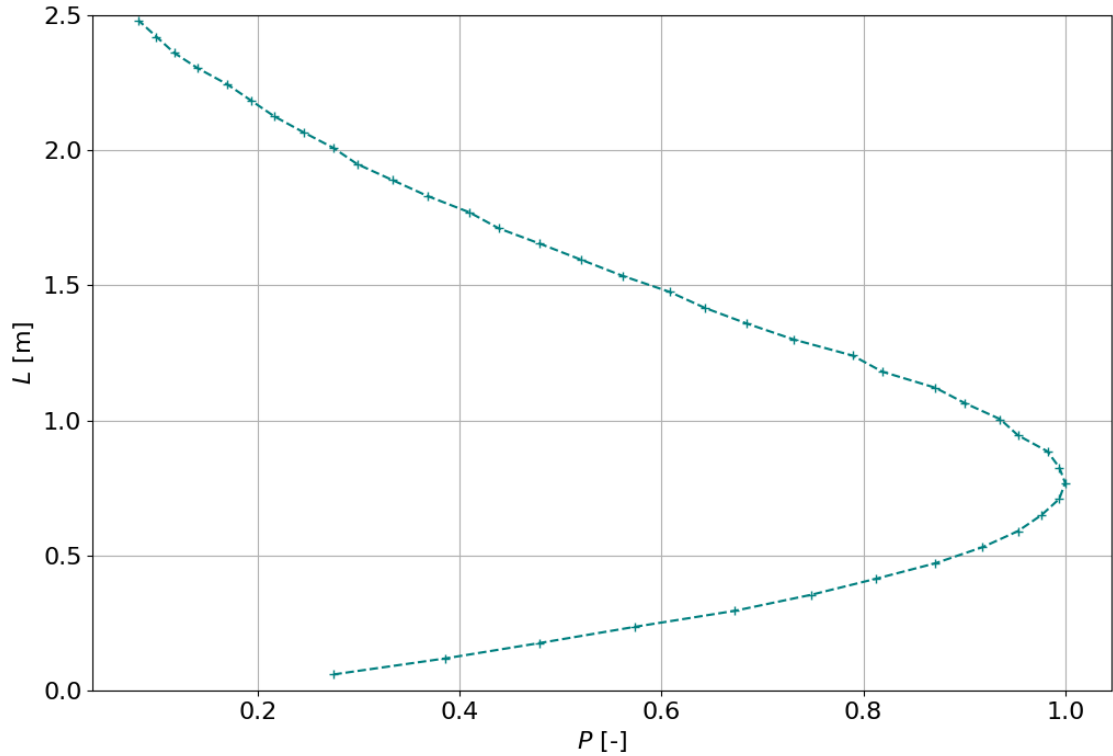


Figure 7.1.1: The relative axial power profile vs. the relative axial location.

The temperature (267 °C) was extracted from the steady-state calculation performed using the existing Dukovany model in the TRACE code.

7.2 Calculation Procedure

In picture 7.2.1 is presented the calculation procedure scheme.

In the beginning of the process were extracted all necessary information from NPP Dukovany Final safety analysis report. Then a LOFA scenario was simulated in TRACE code. Results from TRACE code which are used in SCF are mass flux, the AZ power change and the AZ axial power profile. Meanwhile, geometry relations of the VVER-440 fuel cassette were obtained using automatic processes of Python programming language. The geometry and information extracted from TRACE were used as input files for the

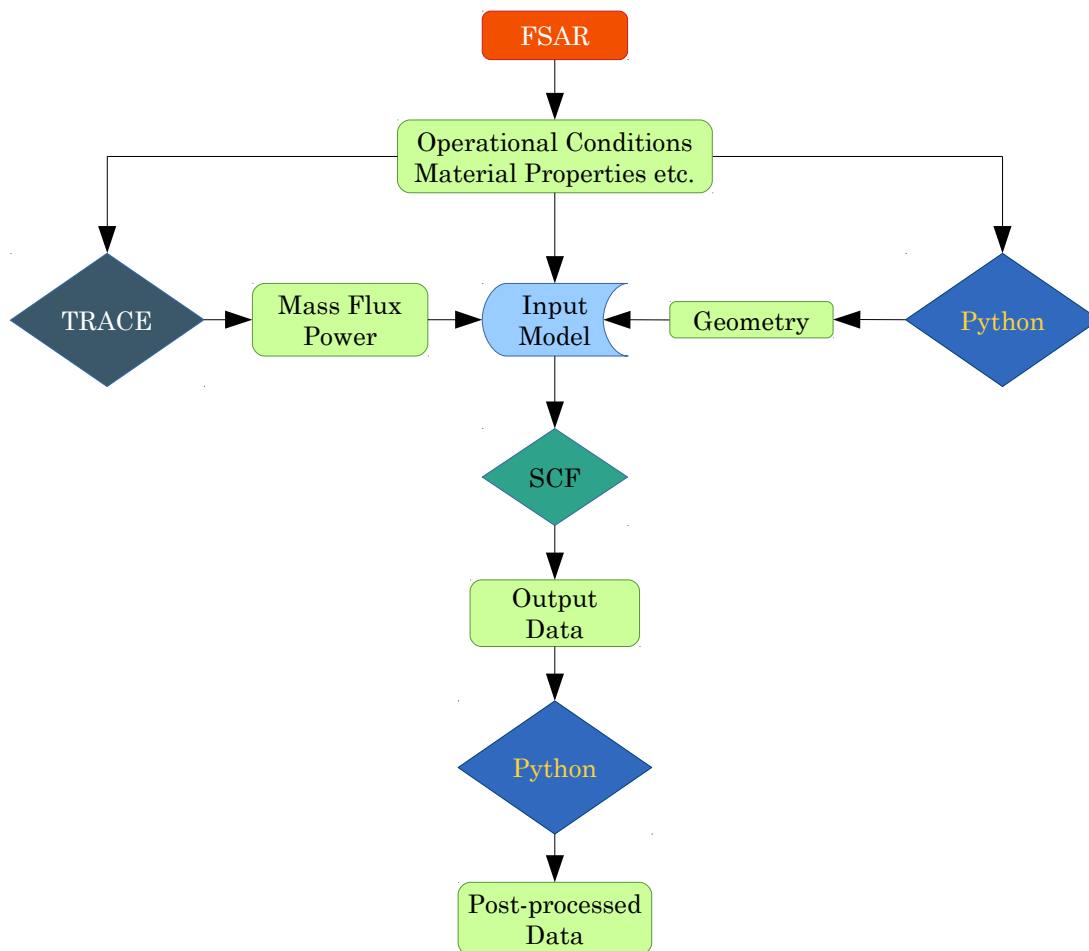


Figure 7.2.1: Calculation procedure scheme.

SCF subchannel analysis calculation. After receiving the final data from SCF software, these results were adapted for specific needs of the post-processing using the scripts in Python.

For proper calculation approach was done firstly steady-state analysis in order to reach optimal parameters for numerical solution. This analysis searches for minimum possible value of cladding maximum temperature changes, central fuel and coolant temperature and minimum value of maximum void change.

Calculation time for steady-state was five seconds with time step 0.1 s. Every calculation was completed with minimum flow iterations 20.

True vapour quality due to sub-cooled boiling was modelled by Saha-Zuber correlation. Vapour slip ratio was calculated by modified Armand model, two phase wall friction multiplier by Armand correlation and for single phase friction was used Blasius correlation. Single phase heat transfer was defined by Dittus-Boelter correlation in the simple form and for CHF calculation was used OKB correlation. Last group of correlations is applicable for the fuel cladding gap heat conductance and for this calculation was set benchmark

VVER-1000 cold gap.

It is possible to observe three main parameters of the numerical calculation itself. The first is maximum axial velocity change during last iteration related to the maximum axial velocity u_{ax}^{err} , the second is maximum lateral velocity change during the last iteration related to the maximum lateral velocity u_{lat}^{err} and the last is maximum coolant temperature change in °C during the last iteration T^{err} [2].

7.3 Python Software

Part of this thesis was the Python scripts development that speed up the calculation process and analysis of the results. For SCF 3.5 were written four programmes in Python 3.6.0 programming language [30].

The first programme HEGGS was mentioned in section 6.5. This programme generates a geometry of arbitrary hexagonal fuel assemblies for random hexagonal dimension with the triangular symmetry.

The second programme is called SSASA (Software for SUBCHANFLOW Automatic Sensitivity Analysis). This software enables automatic calculation of SCF for various input parameters in order to save time with rewriting them manually in the input text file.

The following two programmes are post-processing software which enable quick and clear orientation in the output results of the SUBCHANFLOW calculations. Due to the large number of time steps in the calculation the output files achieve more than 10 GB and it is necessary to speed up the post-processing.

The third programme is called SPA (SUBCHANFLOW Post-processing Analysis). This code enables to choose any physical parameter from the calculation in any position of the AZ and plot given value depending on the time. It is possible to plot average, maximum or any value in specific axial location for chosen rods or channels. This programme enables plotting of 3D scatter plots or simple 2D plots.

The last programme was named SUBVID (SUBCHANFLOW Video Analysis). This programme creates videos of average or maximum values in particular axial location depending on time, or physical value depending on axial location in the AZ.

These programmes are useful for a detailed post-processing analysis and for better understanding of physical phenomena which happen and may occur in the reactor and for orientation between the physical values that are changing in time in the AZ.

7.4 Summary

This chapter described the main approaches in the steady-state analysis calculation, operational conditions, used correlations, calculation procedure scheme etc.

From the steady-state calculation results was evident the sufficiency of lasting time five seconds. This conclusion reduces the calculation of transient scenarios.

The last part of this chapter described the software developed in Python programming language.

Chapter 8

Results

This chapter focuses on the operational conditions description, steady-state, four LOFA scenarios and results from the calculation in SCF are given. The sequence of events and the detailed description of the AZ behaviour during particular transients were presented in sections 4.2 and 4.3.

8.1 Steady-state

Steady-state is a term describing a reactor operational mode when the physical parameters are stabilized. The steady-state represents the first five seconds of LOFA scenarios and the parameters can be seen in table 8.1.1.

Table 8.1.1: Steady-state parameters

P [MW]	\dot{m} [kg/s]	T_{in} [°C]	p_{ex} [MPa]	MDNBR [-]	HR [-]	HC [-]
6.58	24.13	268	12.26	1.93	105	176

The steady-state calculation results are depicted by figures of MDNBR and the hot rod position 8.1.1. From the figure is visible MDNBR steady value and the HR 105 steady position during the calculation.

8.2 LOFA Calculation

As was mentioned in section 7.2, four LOFA scenarios have been simulated in the TRACE code.

The LOFA calculation accident begins with the steady-state calculation in order to lower the oscillations for the numerical solutions of the model. The steady-state analysis prior to the accidents offers a better initialization.

A convergence analysis of minimum values of maximum temperature changes and maximum void change has been done for all transient scenarios and the combination of

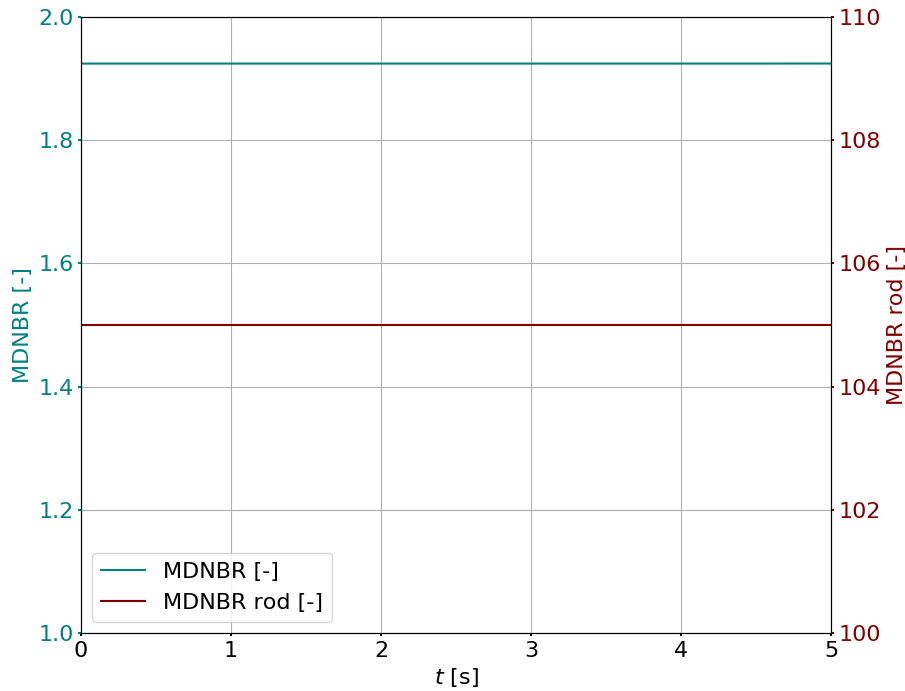


Figure 8.1.1: MDNBR and the HR position during steady-state.

minimum temperature changes have been selected and implemented in the model.

The input values necessary to be implemented in the LOFA models were mass flow time dependency and power of the active zone during the whole transient. These values were extracted from the TRACE code. These two parameters were recalculated as a relative value in comparison with mass flow and power to be same as for the steady-state ($G = 41500 \text{ m}^3/\text{h}$ and $P = 1444 \text{ MW}$). The density was obtained from CoolProp open-source thermophysical properties library [32].

8.3 One RCP trip

The first scenario simulates one of six RCP trip scenario. The relative mass flow \dot{m}/\dot{m}_0 related to the time and the relative power are presented in figure 8.3.1. The pump trip begins at second 5. In TRACE, before the sixth second is simulated null-transient for 10 seconds. For a better initialization and for reducing the calculation time in SCF the null transient was set to 5 seconds, id est the first five seconds of null-transient from TRACE calculation were neglected.

In figure 8.3.2 is plotted the HR positions (rod with the MDNBR) vs time of the scenario.

As observed in figure 8.3.2, rod 105 is identified as the hottest for a longer period of time, while between 43rd and 55th second is the HR at the position 73.

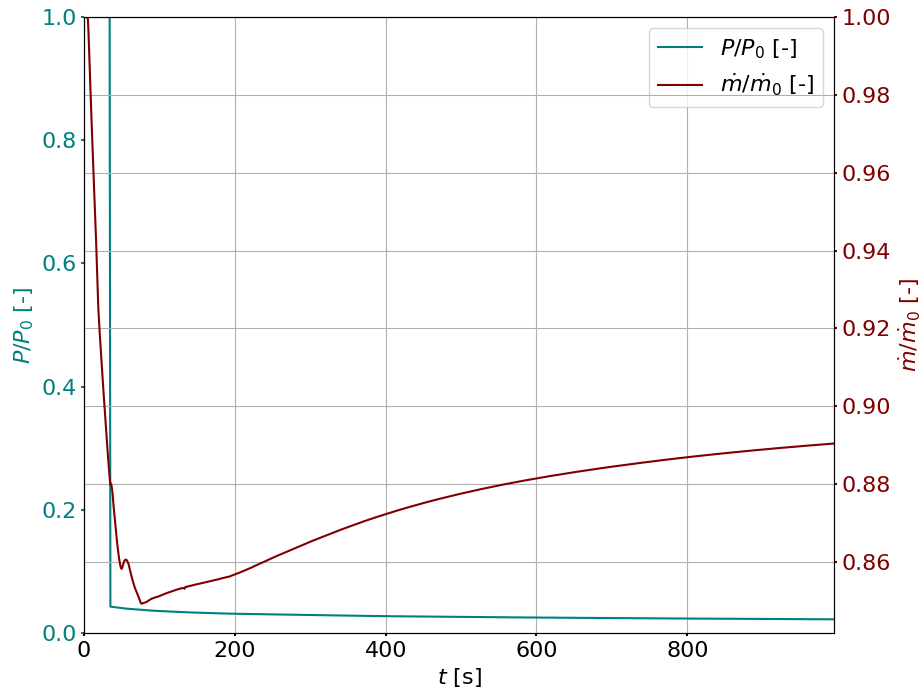


Figure 8.3.1: Relative mass flow \dot{m}/\dot{m}_0 and relative power \dot{P}/\dot{P}_0 .

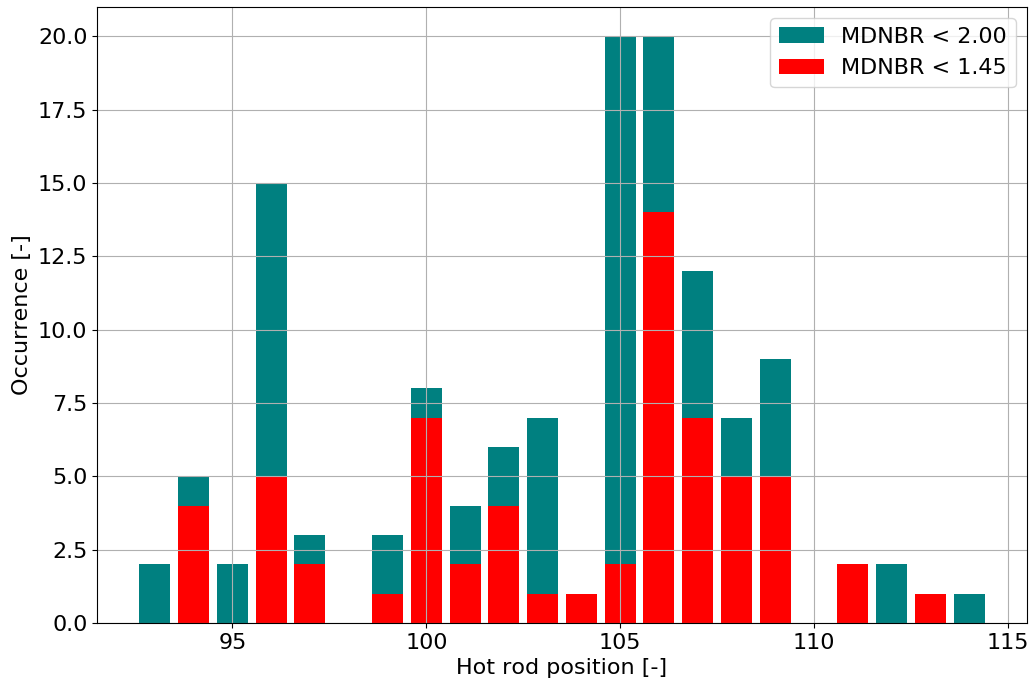


Figure 8.3.2: Bar chart of MDNBR rods occurrences between 31.5 s and 34.7 s.

The bar chart 8.3.2 signalizes that the most burdened area is the edge line of rods in FC (rods 93-127). According to [21], in case of LOFA scenario with one RCP trip, SCRAM

signal occurs at 34th second, which is clearly visible in the further plots, position of the HR begins to stabilize, and also the MDNBR starts to grow as a reaction on bringing negative reactivity to the AZ. The bar chart shows HRs for each time step between 31.5 and 34.7 s. In the same plot is described the position of the HR when the MDNBR is lower than 1.45 and this bar chart differs by colour.

In figure 8.3.3 is shown the MDNBR change in the whole FC related to the time of the accident. According to used OKB correlation the limit value for MDNBR is 1.0. It is noticeable that the time period when the HR is at the position 73 (after SCRAM) is not important for the calculation, because the MDNBR is far from the limit to neglect this period from safety analysis requirements and the power is too low to expect boiling crisis in the FC.

The most interesting section of the plot when the oscillations begin is zoomed between seconds 20 and 37 in figure 8.3.3, which is time period before SCRAM and three seconds after SCRAM. The influence of SCRAM at the beginning of 36th second is visible. Due to oscillations in the data was used Savitzky-Golay filter [35]. This digital polynomial filter was used in order to smooth the data and for better orientation in the results.

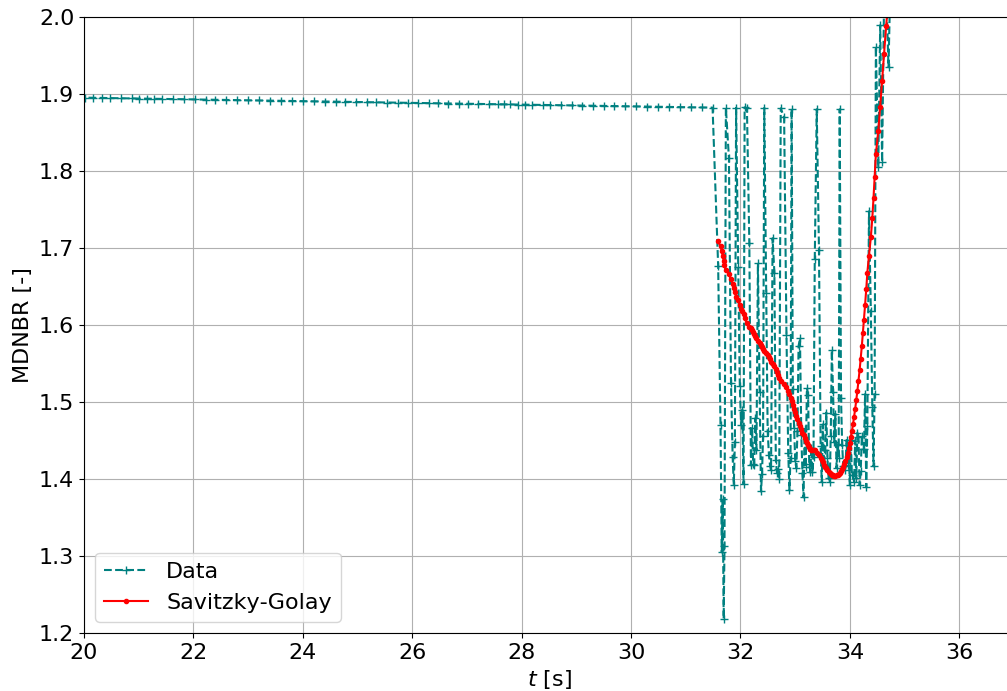


Figure 8.3.3: MDNBR in FC during 1/6 RCP trip.

Figure 8.3.2 refers to the hottest area during the accident and the area with the lowest MDNBR is between rods 105 and 108. MDNBR for these rods was plotted in figure 8.3.4.

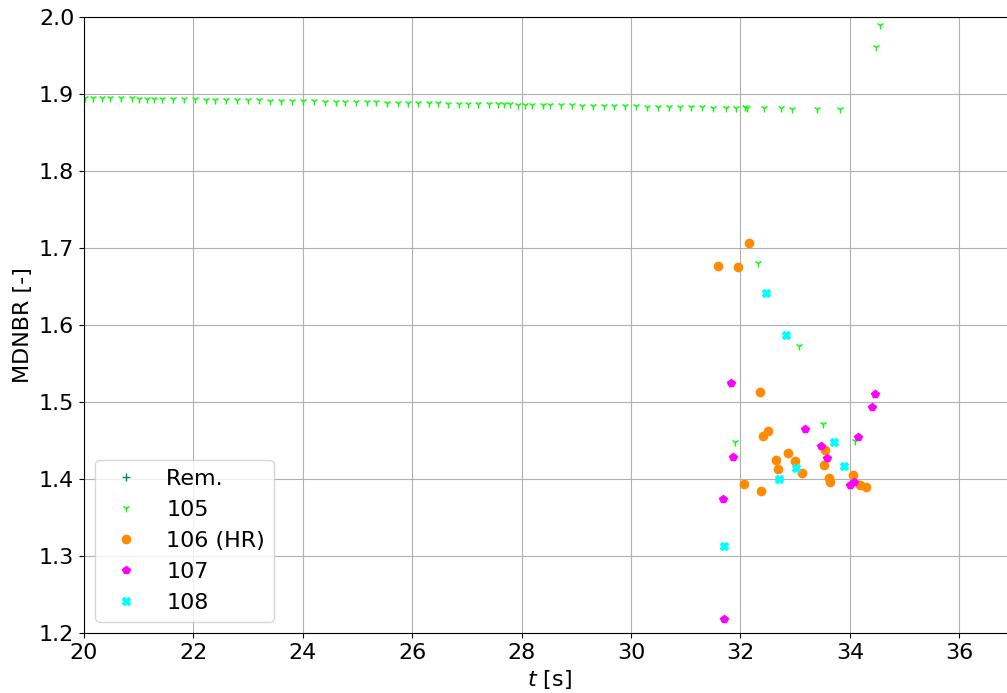


Figure 8.3.4: MDNBR of rods 105-108 and the remaining HRs between particular time period.

The hottest rod was identified as a rod at the position 106. This identification is done due to the results visible in figure 8.3.2. The acceptance criteria and limitations that must not be exceeded during the transient will be verified for the HR. These criteria were described in section 4.3.

The first MDNBR criterion was not exceeded, which is visible in figure 8.3.3. In figure 8.3.5 is MDNBR time dependency. The lowest reached MDNBR value was 1.22 at $t=31.7$ s for rod at the position 107 and MDNBR=1.39 at $t=33.2$ s for the HR 106.

In figure 8.3.6 is represented the maximum fuel pellet center temperature. The melting temperature $T_m = 2480$ °C was not exceeded in any time during the whole transient.

In figure 8.3.7 is presented the temperature in the nuclear pellet center depending on axial location for the HR. This temperature is plotted for four times at $t_1=5$ s, $t_2=20$ s, $t_3=33$ s and $t_4=40$ s. The first time t_1 is the end of steady-state before the RCP trip, t_2 is 15 seconds after the RCP trip, t_3 is the last time calculation step before SCRAM (34 s) and t_4 is six seconds after SCRAM.

The last criterion is related to the maximum cladding temperature. This value has to be lower than 1200 °C. Figure 8.3.8 shows that this criterion was not exceeded.

After the HR determination, the HC was identified for further flow investigations. It is one of the five neighbouring channels around the HR and during the whole simulation was the HC at the position 176. Further analysis is done for this particular subchannel.

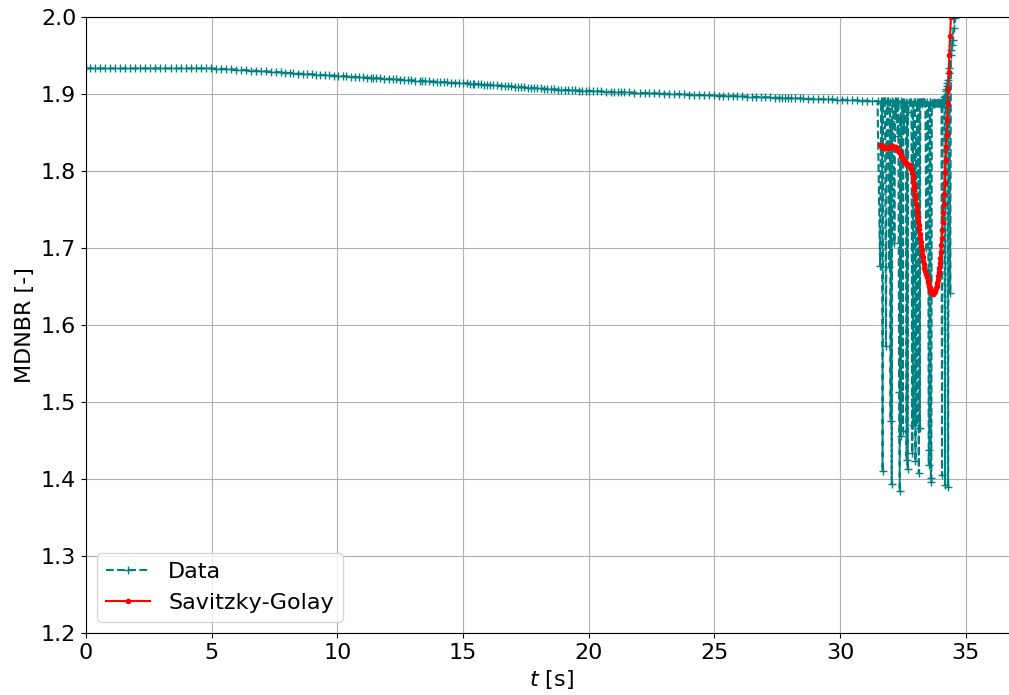


Figure 8.3.5: The HR 106 MDNBR.

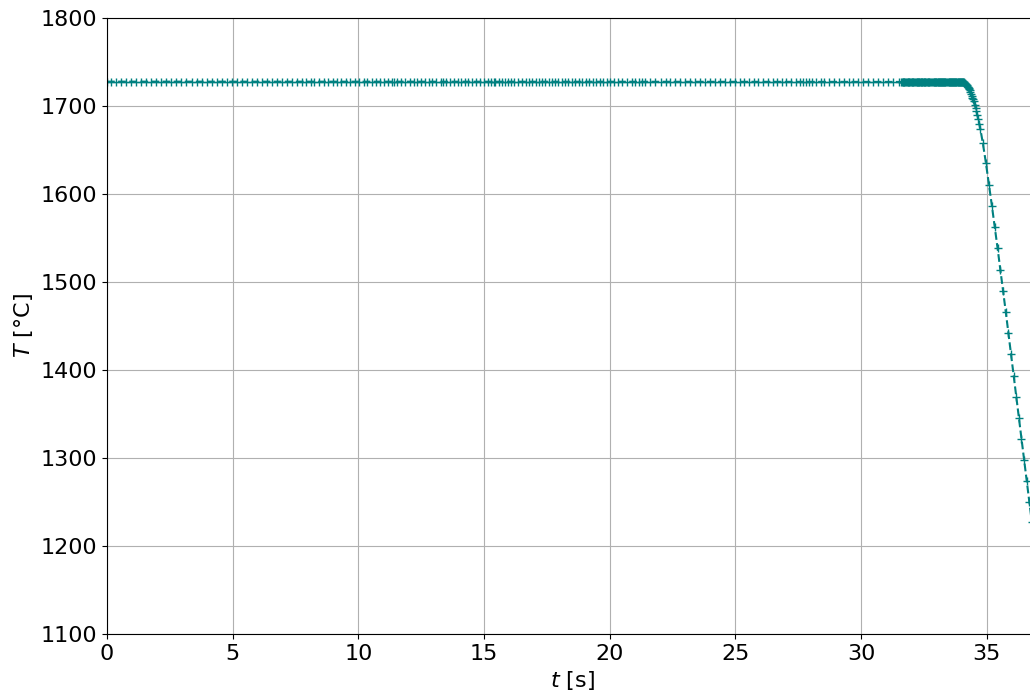


Figure 8.3.6: The HR 106 maximum fuel center temperature.

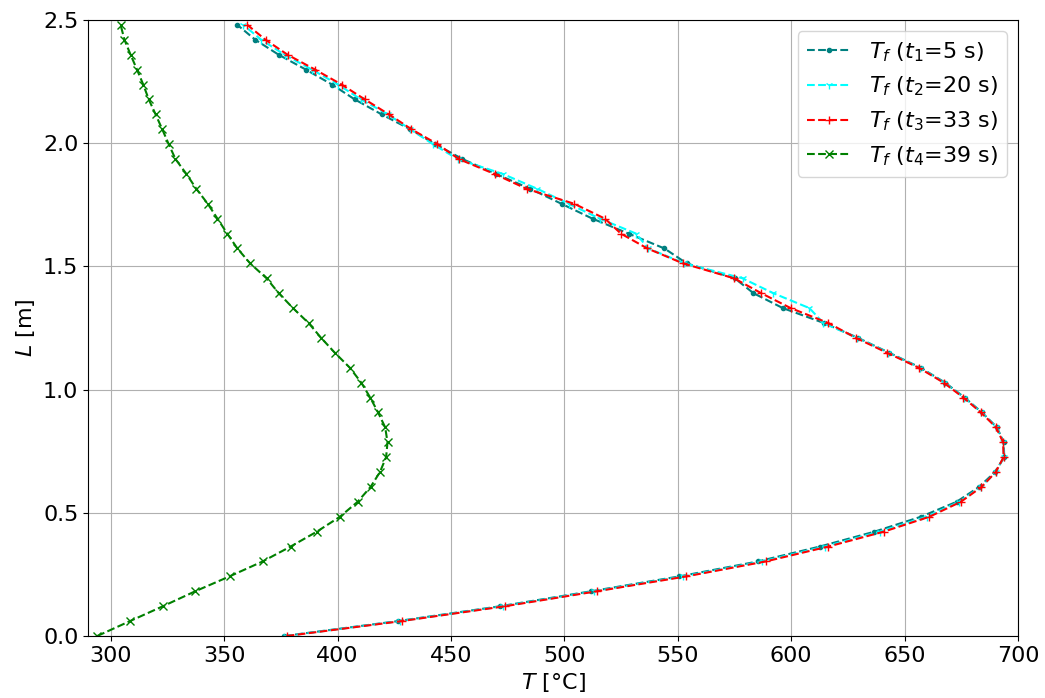


Figure 8.3.7: The HR 106 fuel center temperature at t_1 , t_2 , t_3 and t_4 .

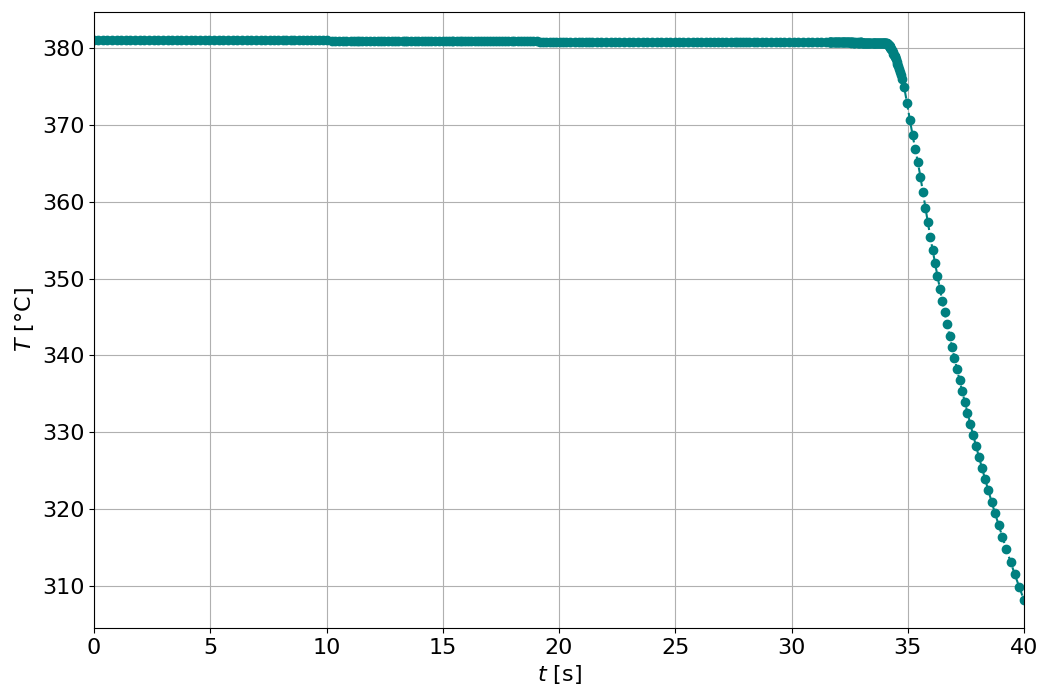


Figure 8.3.8: The HR 106 maximum cladding temperature.

The HC was studied from the point of maximum equilibrium quality x around the HR. In figure 8.3.9 is visible the highest equilibrium quality. This value occurs on the top of the AZ above 2.25 m.

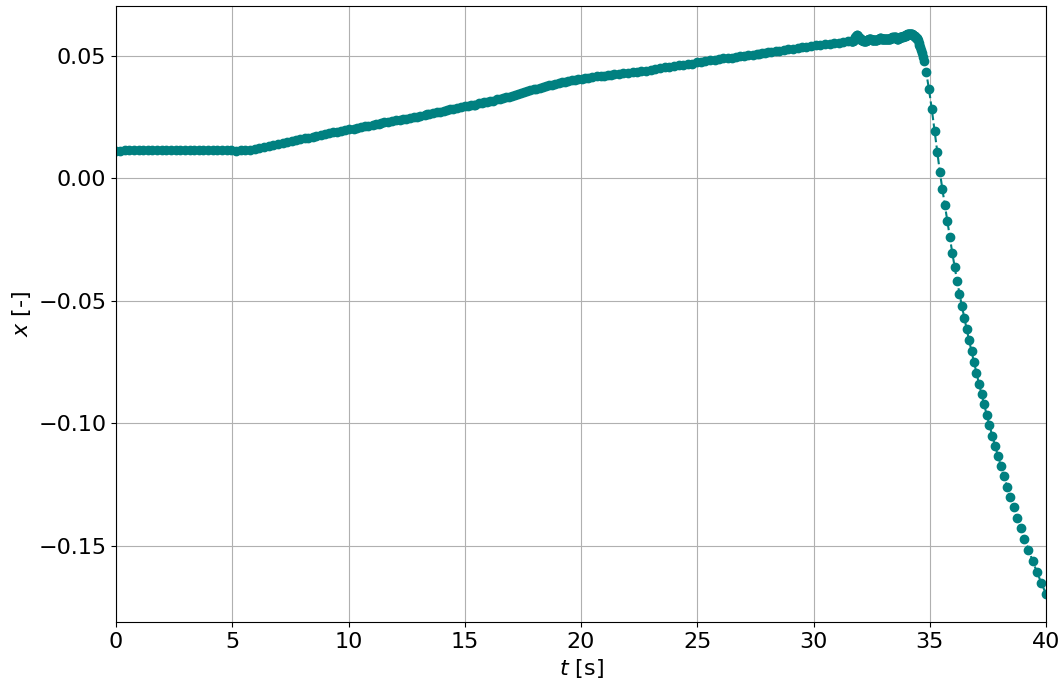


Figure 8.3.9: The highest equilibrium quality x in the HC 176.

8.4 Two RCPs Trip

The following LOFA scenario simulates two RCPs trip. The relative mass flow \dot{m}/\dot{m}_0 and relative power \dot{P}/\dot{P}_0 related to time are presented in figure 8.4.1. The pump trip starts at the sixth second. Also for this scenario, the null-transient was decreased to 5 seconds for reducing the calculation time.

In figure 8.4.2 is visible the change of the hot rod positions (rod with the MDNBR) versus time of the accident. As mentioned above, a null transient is simulated for 5 seconds.

The HR is identified as 105 same as in the first scenario for majority of the simulation. However, after the SCRAM signal, between 42-55 seconds the HR was at the position 73 (as in the case of the first scenario). The HR position starts to oscillate much faster than in the first scenario. The plot signalizes that the most burdened area is again the edge line of rods in the FC (rods 93-127).

The HR position instability starts at 16.7 s and lasts until 35.1 s. Figure 8.4.2 shows the HR position bar chart versus HR occurrences. The bar chart shows the HRs for each

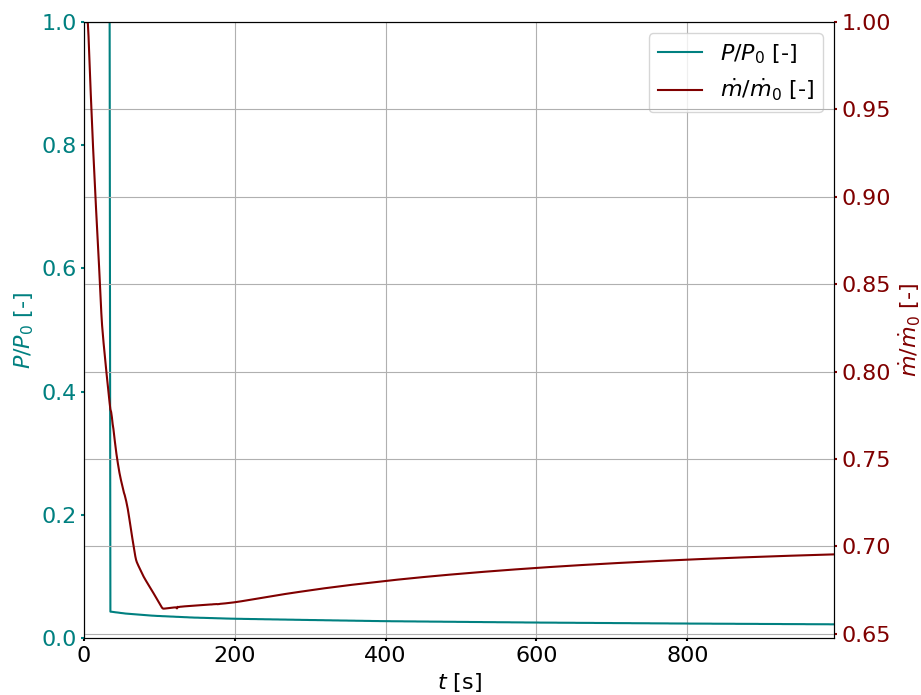


Figure 8.4.1: Relative mass flow \dot{m}/\dot{m}_0 and relative power \dot{P}/\dot{P}_0 .

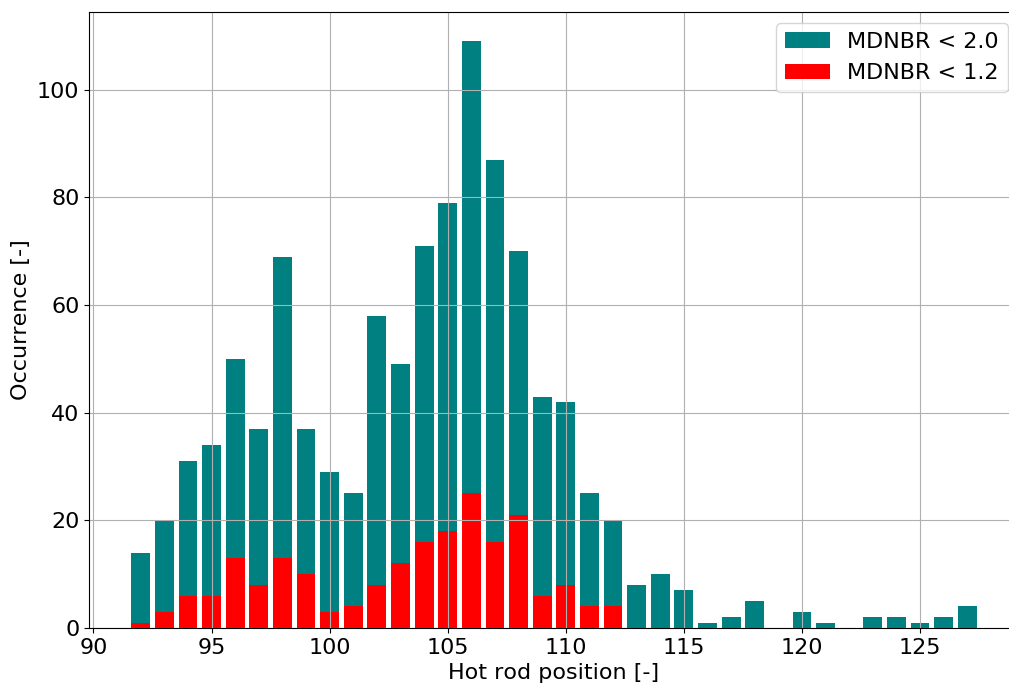


Figure 8.4.2: Bar chart of MDNBR rods occurrences between 16.7 s and 35.1 s.

time step during the oscillations. More interesting is the HR position when the MDNBR is lower than 1.2. Figure 8.4.2 refers to the hottest area during the accident.

In figure 8.4.3 is the MDNBR change in the whole FC related to the time of the accident. It is noticeable that the time period when the HR is at the position 73 (after SCRAM) is not important for the calculation, because the MDNBR is high enough to neglect this period from safety analysis requirements.

The most interesting section of the plot when the oscillations begin is zoomed between seconds 15 and 37 which is the time period before SCRAM and three seconds after SCRAM. The area with the lowest MDNBR is between rods 104 and 107. MDNBR for these rods was plotted in figure 8.4.4.

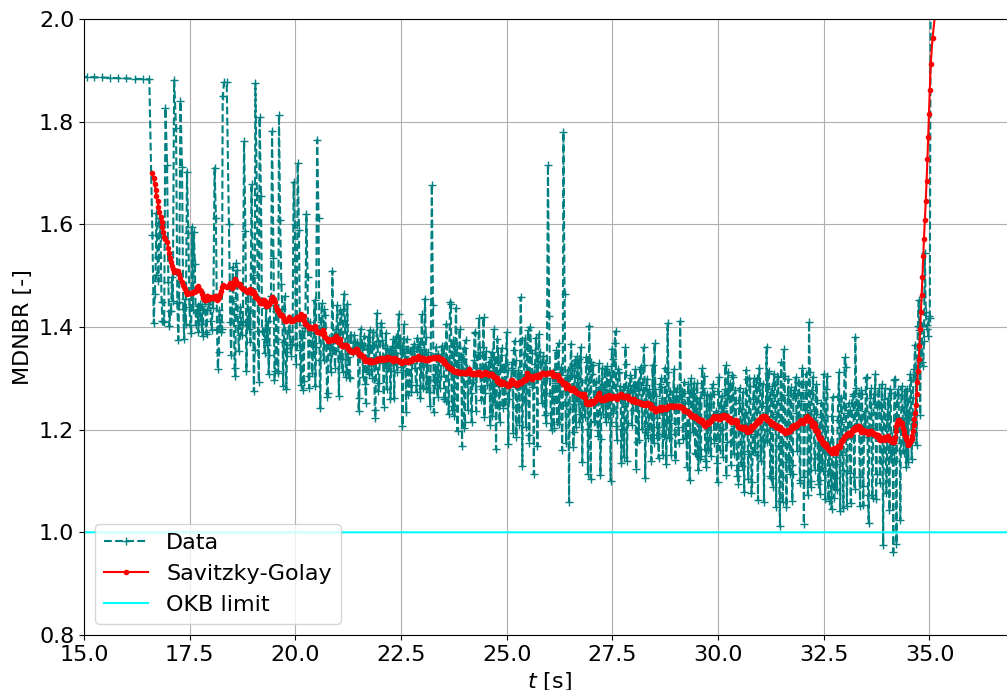


Figure 8.4.3: MDNBR in the whole FC.

As in previous scenario, the HR was identified as a rod at the position 106. The identification was done based on the results presented in figure 8.4.2.

The first MDNBR criterion was exceeded only for one time step for the rod 106, which is visible in figures 8.4.4 and 8.4.5. The lowest reached MDNBR was 0.96 at $t=34.1$ s. This result may be neglected due to the MDNBR oscillations in the calculation and the overall MDNBR is higher than the limit value 1.0. In figure 8.4.4 is also visible that the MDNBR criterion was exceeded only by three chosen rods from the most problematic area and only in one time step for each, namely rods 104, 106 and 107.

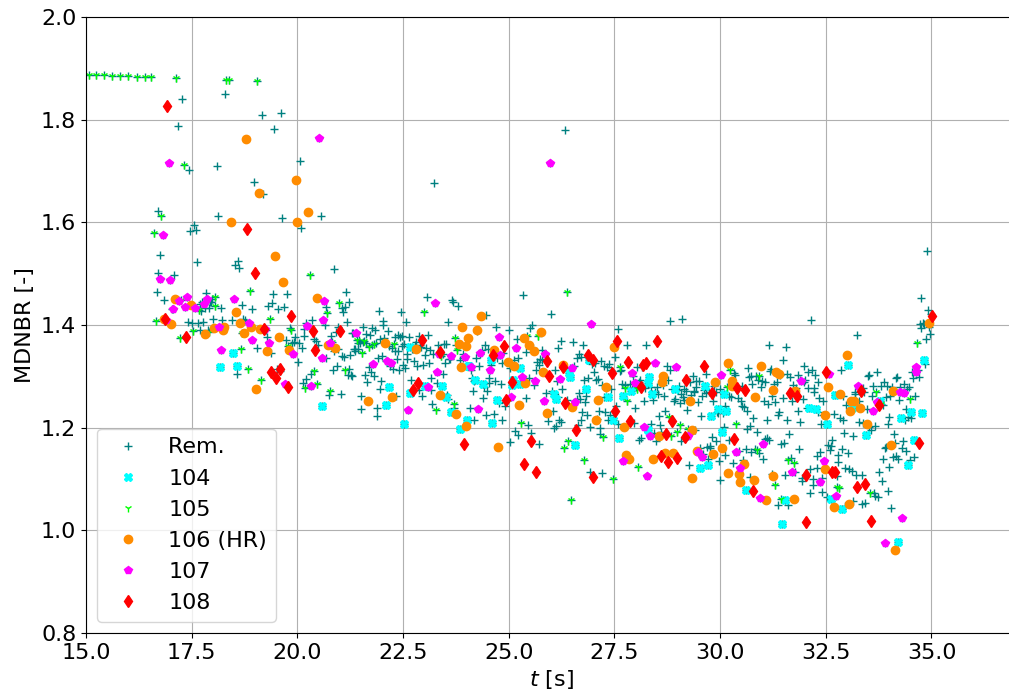


Figure 8.4.4: Rods 104-107 and the remaining HRs MDNBR between particular time period.

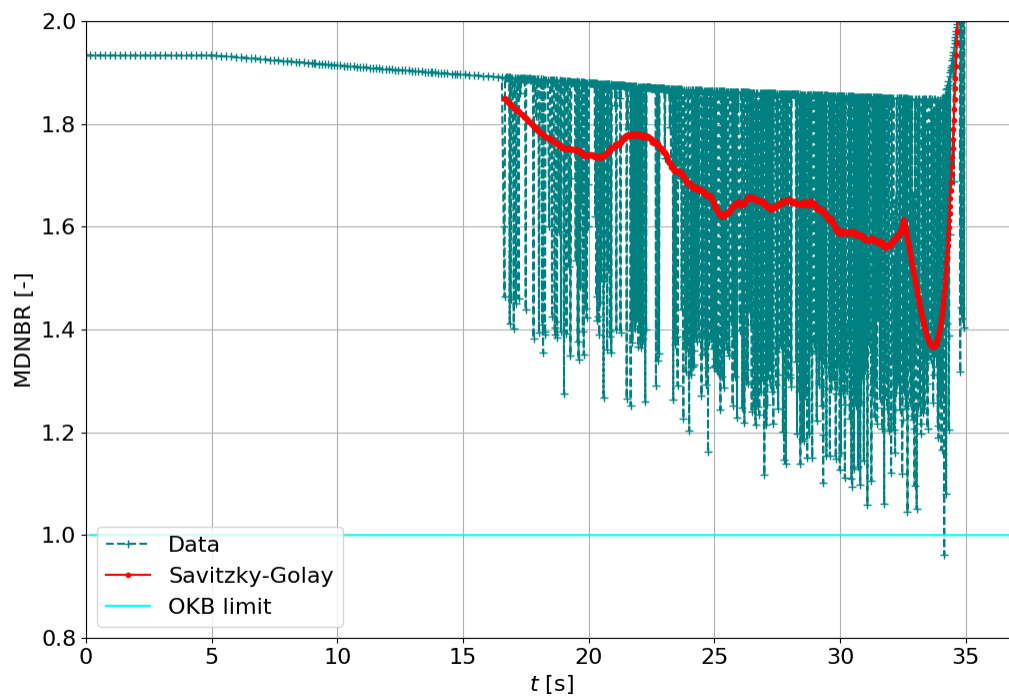


Figure 8.4.5: The HR 106 MDNBR.

On the other hand, using Savitzky-Golay filter for data smoothing, it is visible, that the MDNBR criterion for the HR was not exceeded.

In figure 8.4.6 is the maximum fuel center temperature. The melting temperature $T_m = 2480$ °C was not exceeded in any time of the calculation.

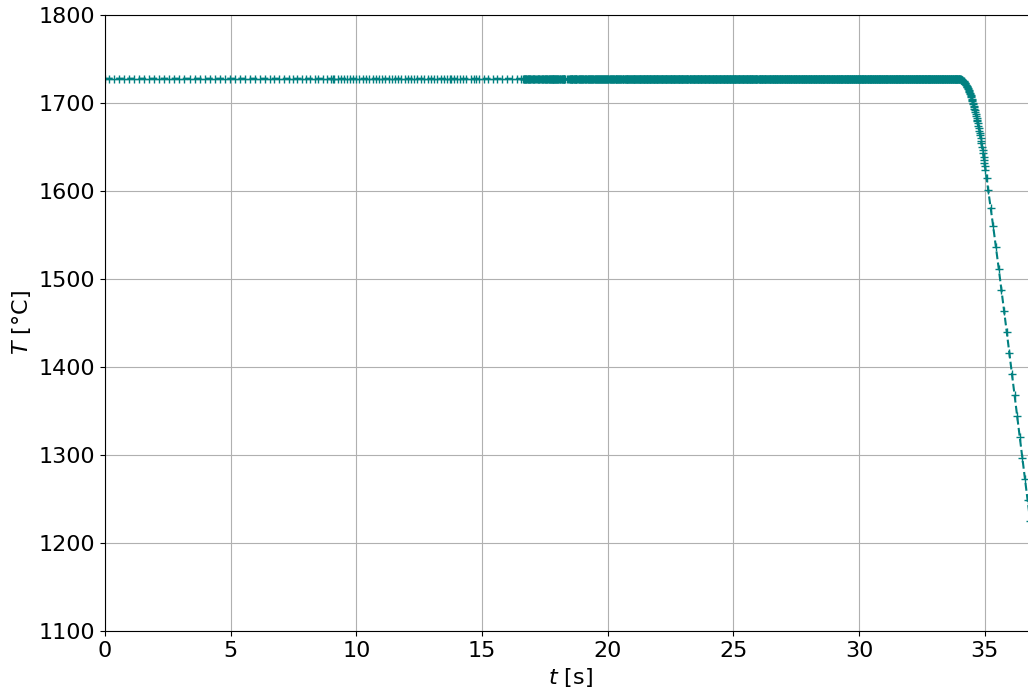


Figure 8.4.6: The HR 106 maximum fuel center temperature.

Fuel temperature in the center is showed in figure 8.4.7. This figure shows four times at $t_1=5$ s, $t_2=20$ s, $t_3=33$ s and $t_4=40$ s same as in the first scenario. The first time t_1 is the end of steady-state before the RCP trip, t_2 is 15 seconds after the RCP trip, t_3 is the last calculation time step before SCRAM (34 s) and t_4 is six seconds after SCRAM.

Figure 8.4.8 shows that the maximum cladding temperature criterion was not exceeded, but there is a visible slight temperature decrease after circa 10 seconds after the RCPs trip.

As a hot channel was identified the channel at the position 176, same as in previous scenario. The maximum equilibrium quality in the whole AZ for the HC is in figure 8.4.9. This value occurs again on the top of the AZ above 2.25 m.

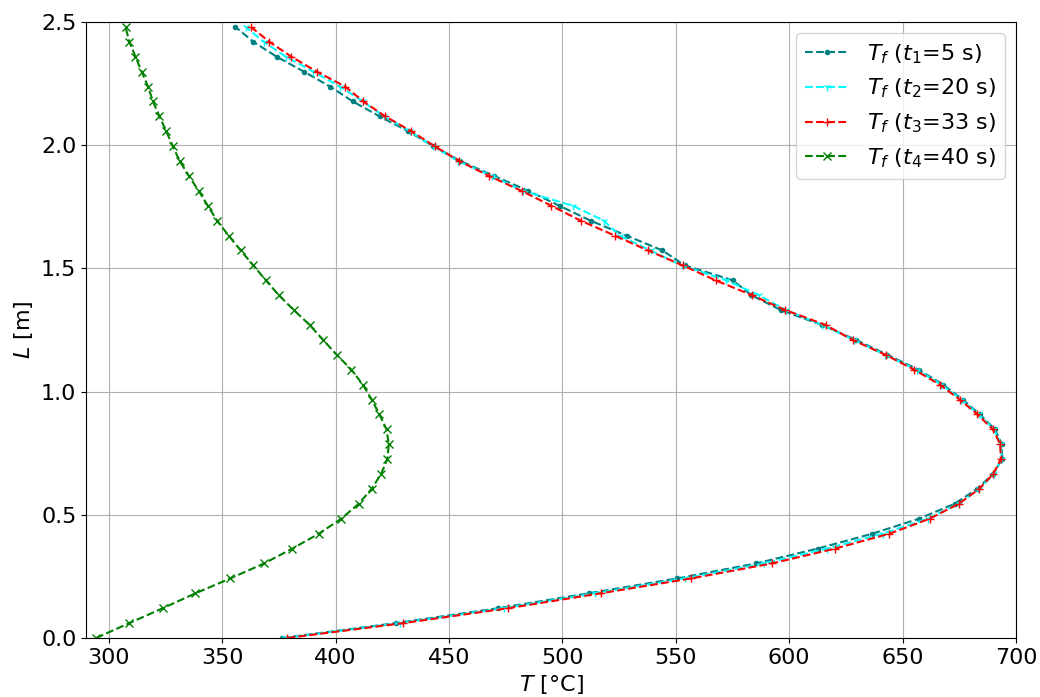


Figure 8.4.7: The HR 106 fuel center temperature at t_1 , t_2 , t_3 and t_4 .

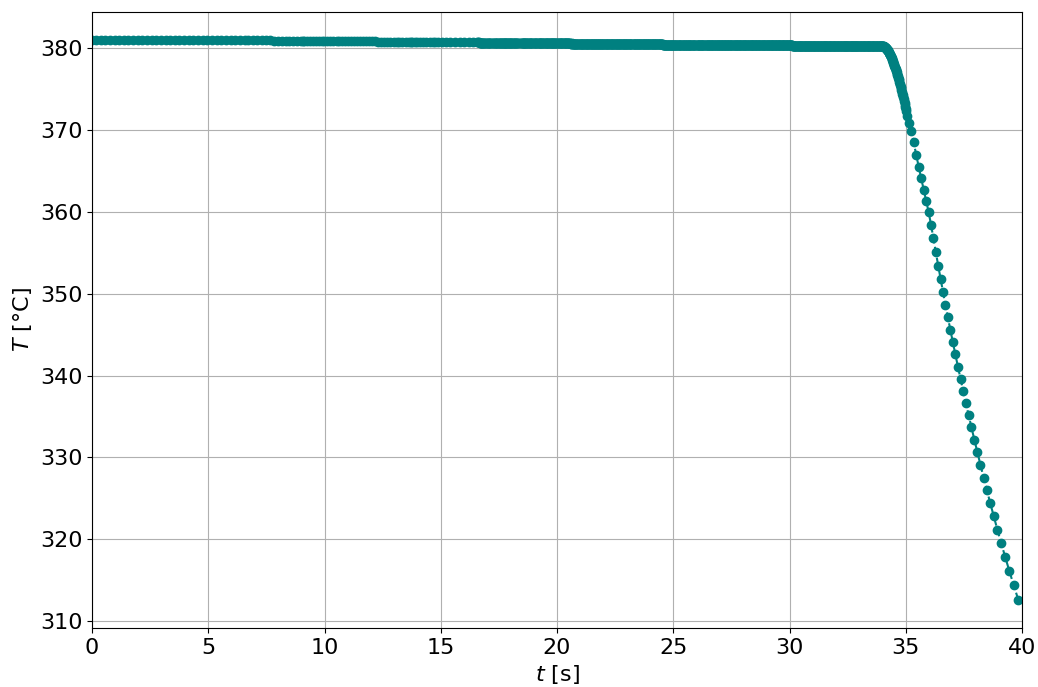


Figure 8.4.8: The HR 106 maximum cladding temperature.

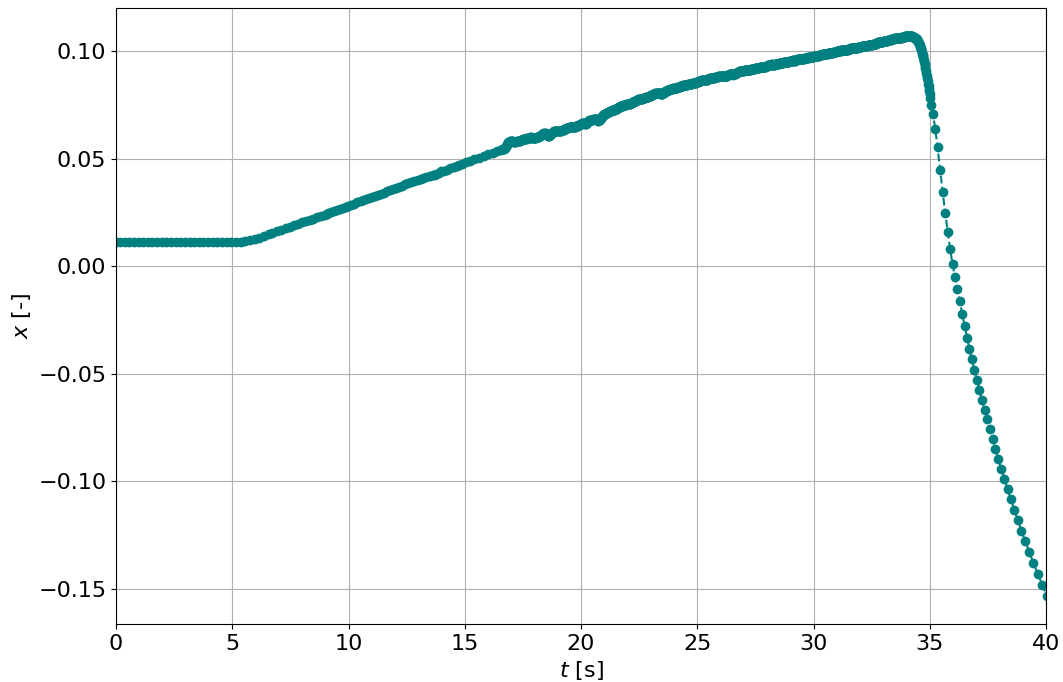


Figure 8.4.9: The highest equilibrium quality x in the HC 176.

8.5 Three RCPs Trip

The input values for the calculation of the third transient is mass flow through the nuclear reactor and power obtained from the code TRACE, same as in previous scenarios. The relative mass flow and power changes are in figure 8.5.1. In this scenario SCRAM is initiated at second 34 same as in previous scenarios.

In figure 8.5.1 is visible mass flow decrease in the first seconds after RCPs trip which reaches the lowest value 47.85 % after 160 seconds. The mass flow stabilizes after circa 600 seconds after the RCPs trip.

In figure 8.5.2 is presented change of the particular rod, where is the MDNBR. For the majority of time the HR is number 106. Between 41.7 s and 55.5 s the HR is 73. As in previous scenarios the results for time from 37th second is neglected.

A detailed study of the hot rod position indicates that the possible system overload may be located between the FC edge positions as in previous scenarios. The bar chart in figure 8.5.2 shows the MDNBR of the HRs for values lower than 2.0 and 1.2.

From figure 8.5.2 is clearly visible the different ratio for the rod 104 between occurrence for the whole time period and explored time period when the MDNBR < 1.2. Due to this, the attention will be paid to rods 105-108 same as for scenario 1 and 2.

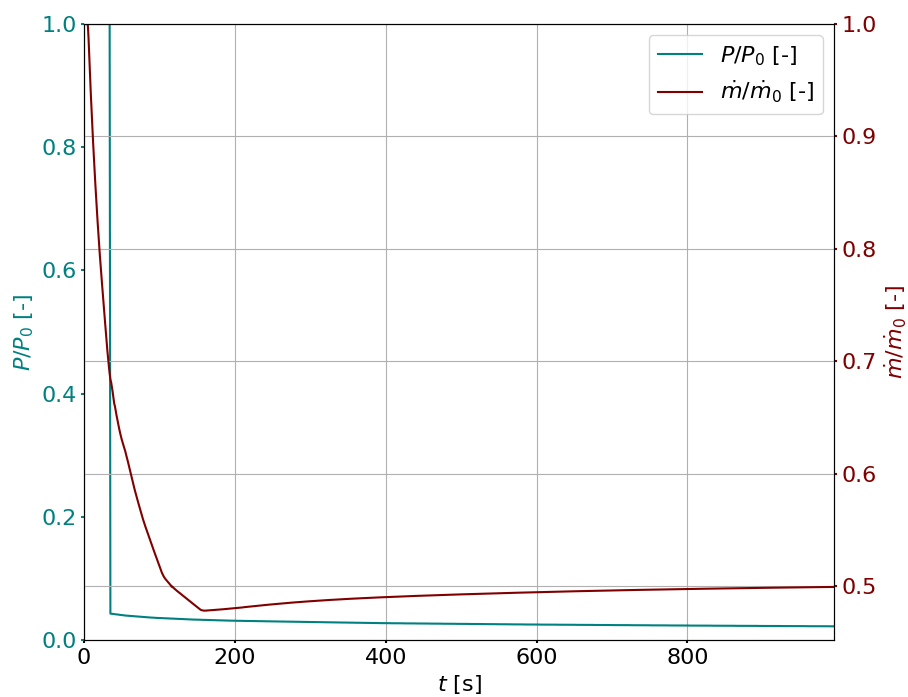


Figure 8.5.1: Relative mass flow \dot{m}/\dot{m}_0 and relative power \dot{P}/\dot{P}_0 .

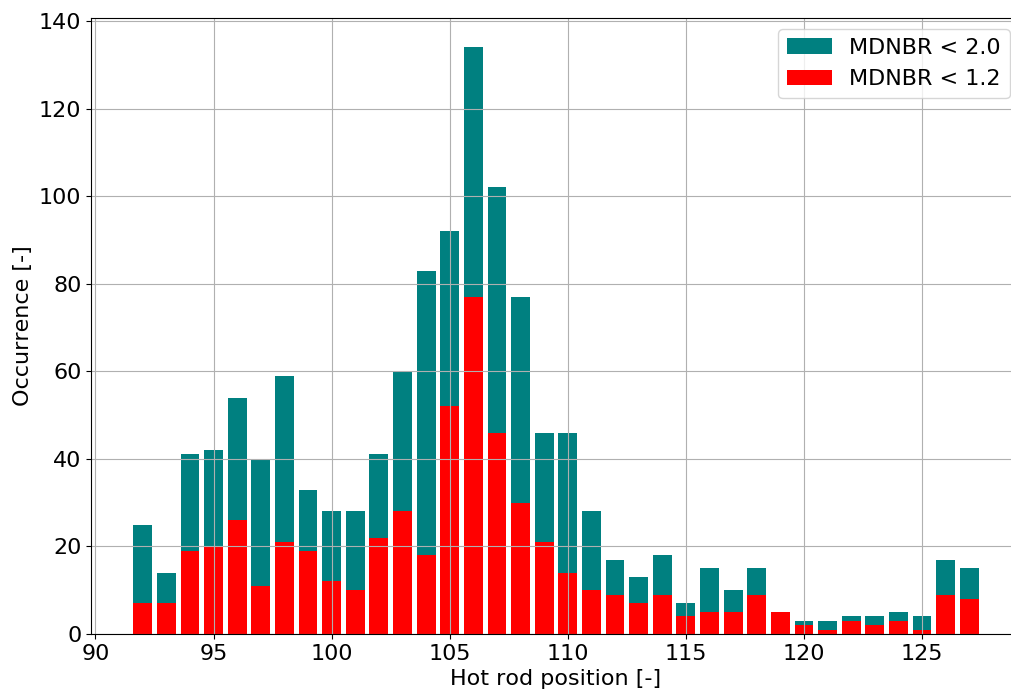


Figure 8.5.2: Bar chart of MDNBR rods occurrences between 12.4 s and 35.5 s.

The HR for the third scenario is at the position 106 (viz figure 8.5.2), same as in the previous scenarios. This rod was identified due to the high occurrence between problematic HRs positions if the MDNBR is lower than 1.2.

The first MDNBR criterion was exceeded for a number of HRs between 25th and 36th second, which is visible in figure 8.5.3. For a better orientation in the plotted MDNBR serves plot 8.5.4. In figure 8.5.5 is time dependency of the MDNBR for rod at the position 106. The lowest reached MDNBR was 0.82 at $t=31.4$ s. This result shows possible exceeding of the first criterion, because the calculation shows the MDNBR lower than 1.0 for almost 10 seconds. On the other hand, the lowering MDNBR trend may not exceed the OKB limitation, because the majority of the results for the MDNBR is higher than the correlation limit.

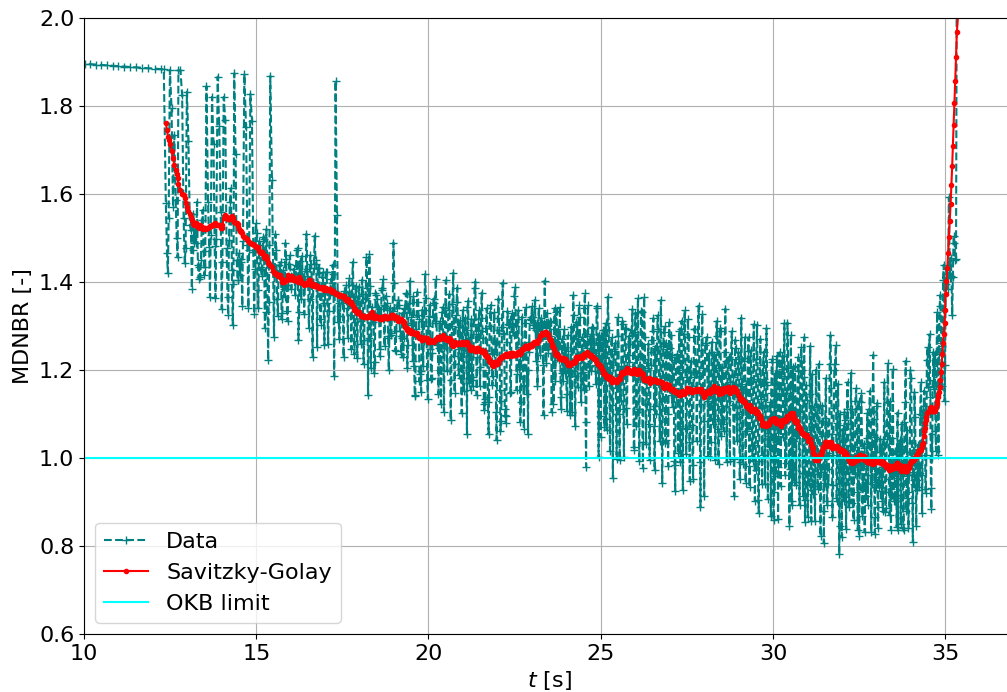


Figure 8.5.3: MDNBR versus time t between seconds 10 and 37.

The melting temperature $T_m = 2480$ °C was not exceeded in any time of the calculation, which is visible in figure 8.5.6.

The fuel center temperature is presented in figure 8.5.7. This figure shows four calculation times same as for previous scenarios. The first time t_1 is the end of steady-state before the RCP trip, t_2 is 15 seconds after the RCP trip, t_3 is the last calculation time step before SCRAM (34 s) and t_4 is six seconds after SCRAM.

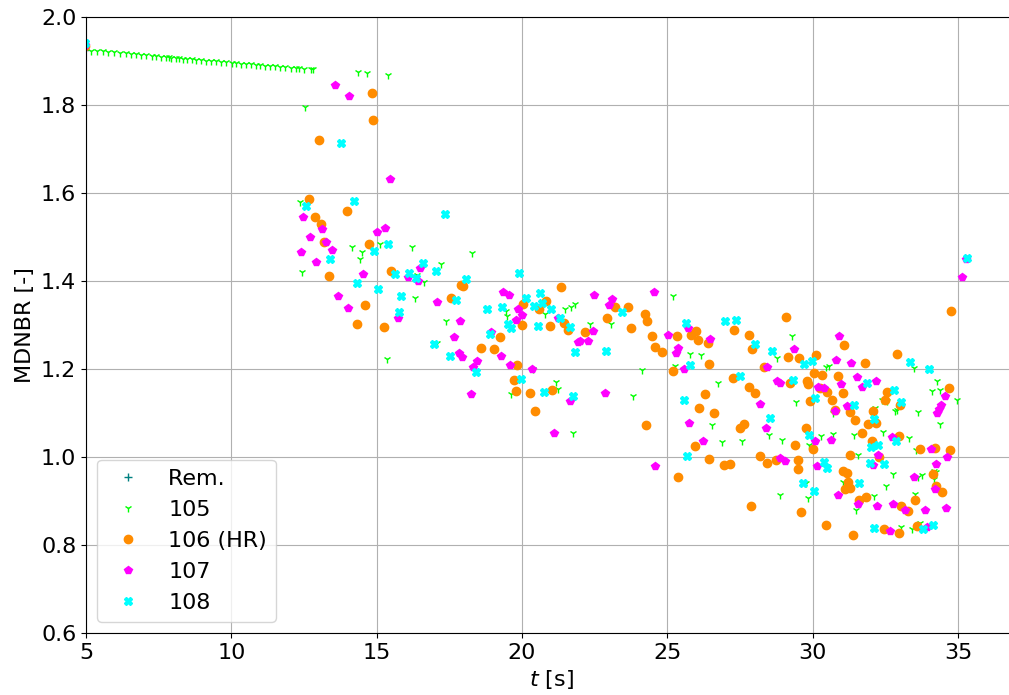


Figure 8.5.4: Rods 105-108 and the remaining HRs MDNBR between particular time period.

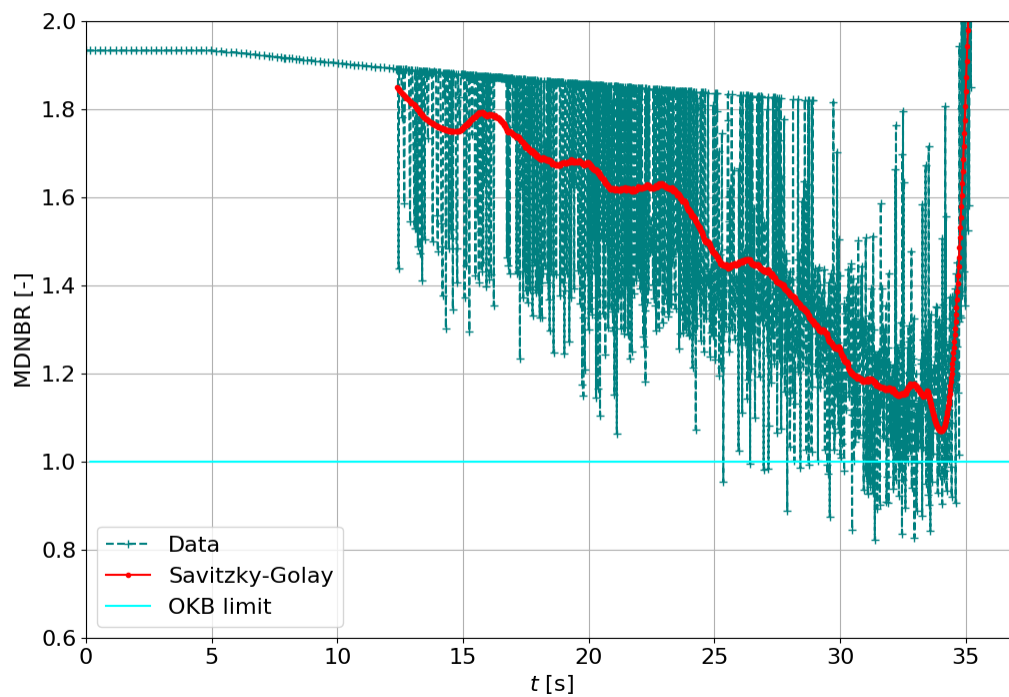


Figure 8.5.5: The HR 106 MDNBR.

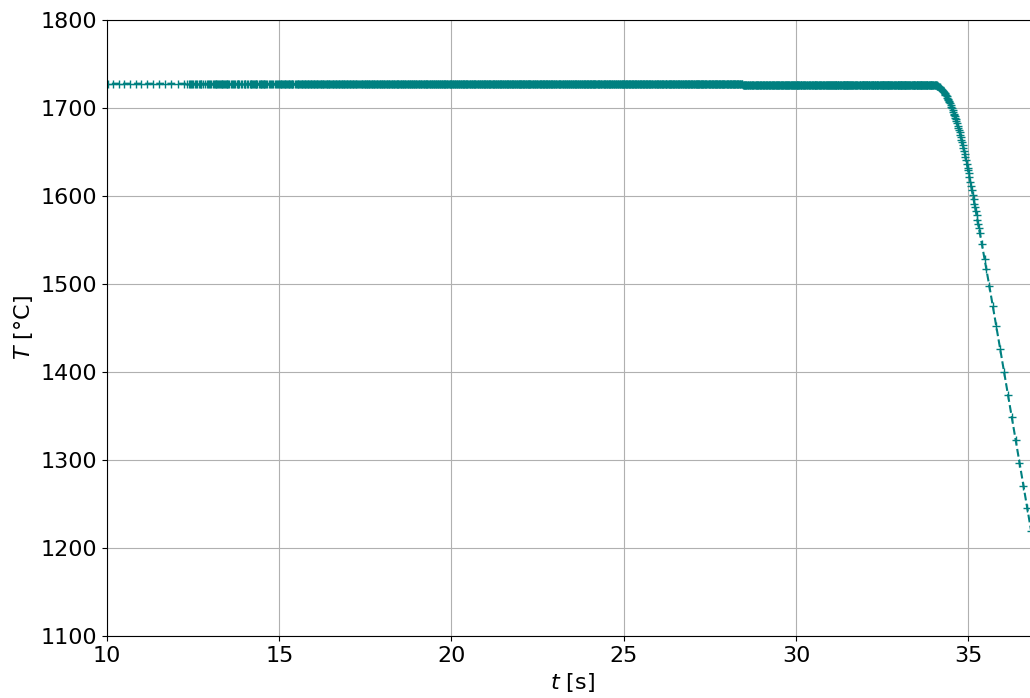


Figure 8.5.6: The HR 106 maximum fuel center temperature.

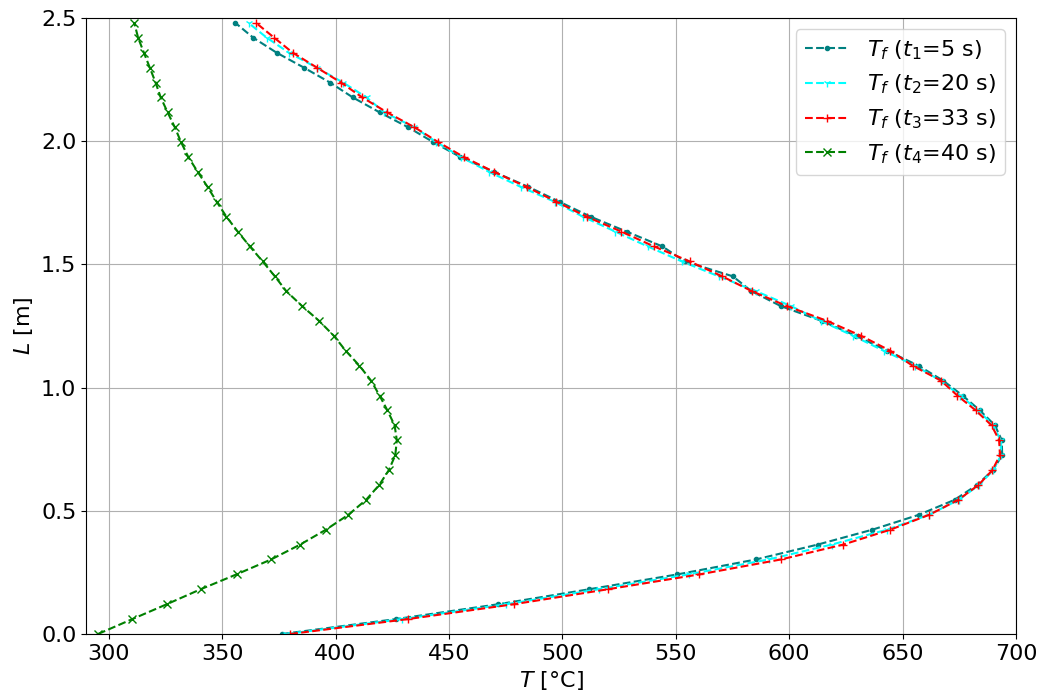


Figure 8.5.7: The HR 106 fuel center temperature at t_1 , t_2 , t_3 and t_4 .

Figure 8.5.8 shows that maximum cladding temperature criterion was not exceeded.

Same as for both previous scenarios, a hot channel was identified at the position 176. The HC position was stable during the whole studied time period from the beginning of RCP trip until 41st second. The maximum equilibrium quality in the whole AZ for the HC is in figure 8.5.9. This value occurs again on the top of the AZ above 2.25 m.

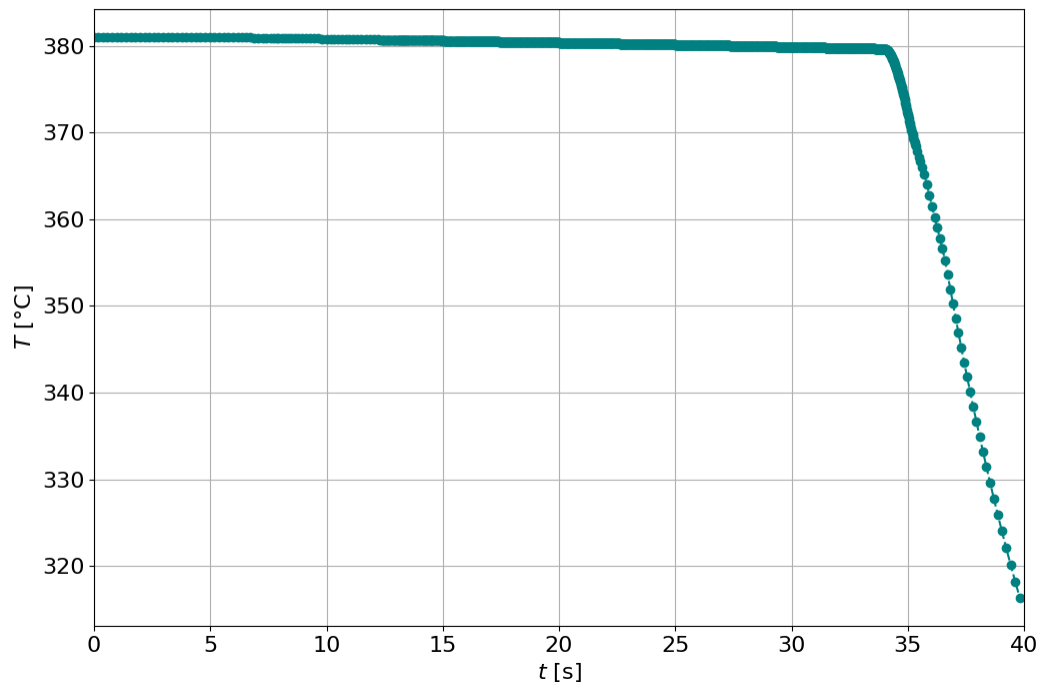


Figure 8.5.8: The HR 106 maximum cladding temperature.

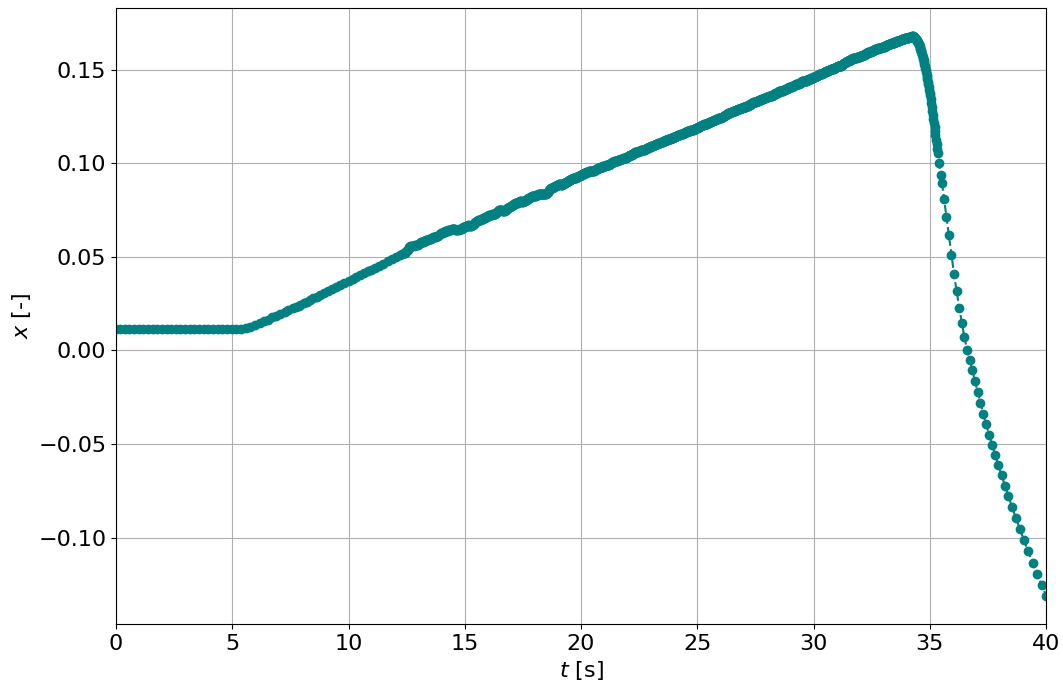


Figure 8.5.9: The highest equilibrium quality x in the HC 176.

8.6 Total LOFA (Six RCPs Trip)

Total LOFA (meaning all six RCPS trip) can be simulated considering either an average power $P = 4.303$ MW or a more conservative approach considering a maximum power per cassette. In this scenario the maximum power per FC $P = 6.58$ MW was implemented. The average power is chosen during the partial blockage of the coolant flow through a FC [21]. Selecting the maximum power is a part of conservative approach.

The relative mass flow through the AZ and the relative power obtained from the code TRACE are presented in figure 8.6.1. The six RCPs trip begins at second 5 and SCRAM is initiated 6 seconds after the RCPs trip. Remaining flow through the AZ is given by the natural circulation.

This transient sequence was reached from the FSAR [21] and was described previously in section 4.3.

A fundamental figure for the analysis is the hot rod position. During steady-state and 19 seconds after SCRAM the HR was at the position 105, likewise in previous scenarios. The results for this scenario differs mainly due to an earlier SCRAM implementation.

The HR position bar chart is presented in figure 8.6.2. This figure shows the earlier SCRAM influence in comparison with other scenarios.

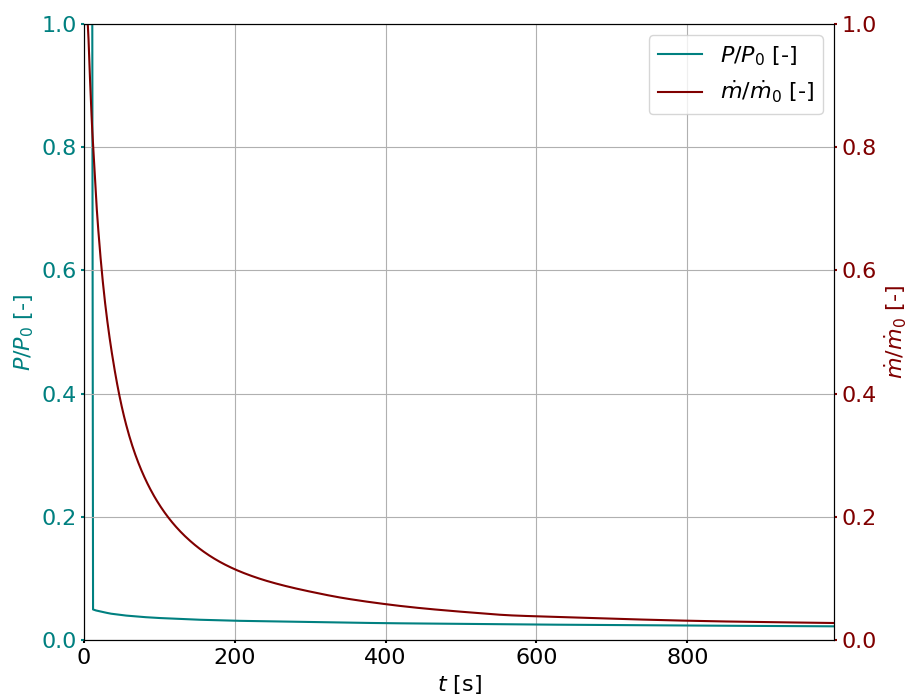


Figure 8.6.1: Relative mass flow \dot{m}/\dot{m}_0 and relative power \dot{P}/\dot{P}_0 .

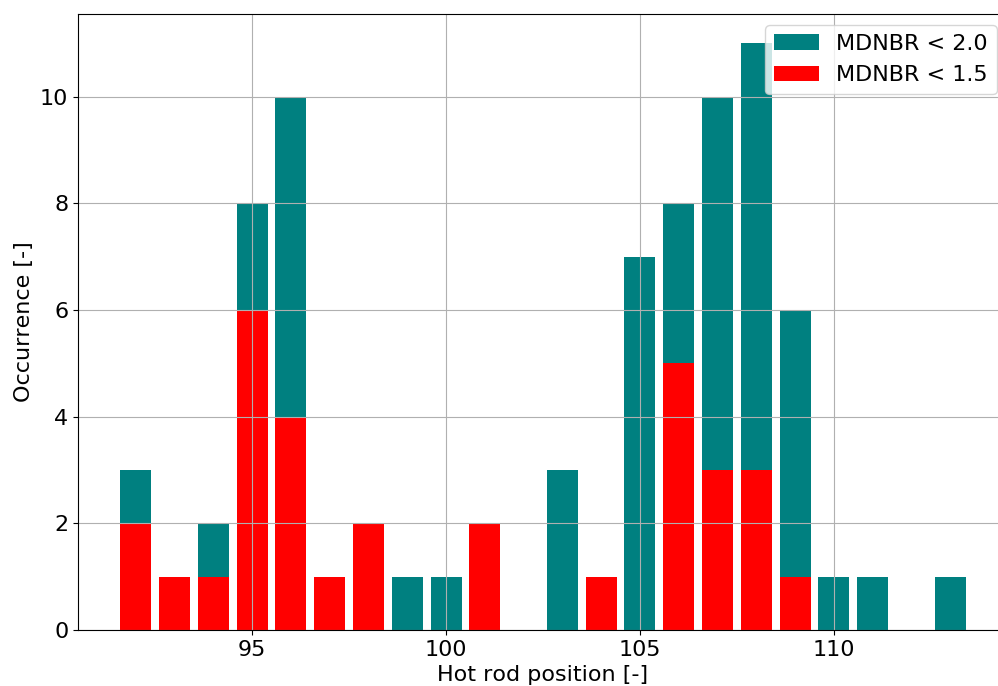


Figure 8.6.2: Bar chart of MDNBR rods occurrences between 9.2 s and 11.9 s.

Unlike other scenarios, for the total LOFA scenario was identified the HR at the position 95 (viz figure 8.6.2). The first MDNBR criterion was not exceeded for any of the rods, which is visible in figure 8.6.3 and also in figure 8.6.4 which describes the MDNBR for the HR 95.

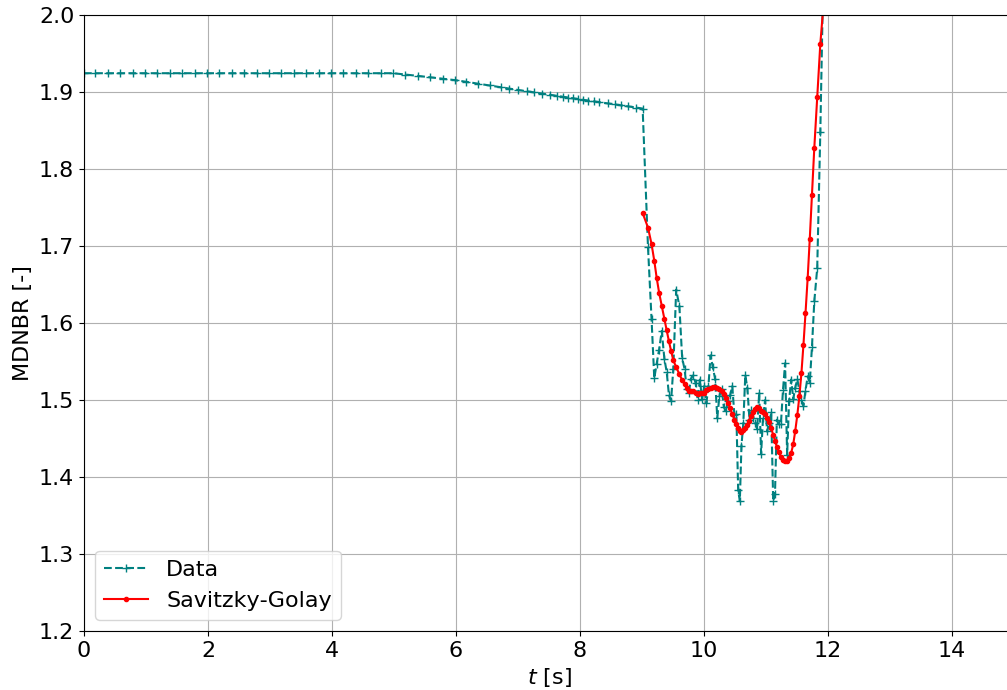


Figure 8.6.3: Minimum departure from nucleate boiling ratio against time t .

The melting temperature $T_m = 2480$ °C was not exceeded in any calculation time, which is visible in figure 8.6.5.

In figure 8.6.6 are fuel center temperatures at four calculation times. The first time t_1 is the end of steady-state before the RCPs trip, t_2 is 2 seconds after the RCPs trip, t_3 is the last calculation time step before SCRAM (11 s) and t_4 is nine seconds after SCRAM.

Figure 8.6.7 shows that the maximum cladding temperature criterion was not exceeded and the temperature stabilizes around 276.5 °C after 35 seconds.

Due to the HR position different number, the hot channel differs from previous scenarios. Between the neighbouring subchannels was identified the HC 156 representing the HC until 41st second. The maximum equilibrium quality in the whole AZ for the HC is in figure 8.6.8. This value occurs again on the top of the AZ above 2.25 m.

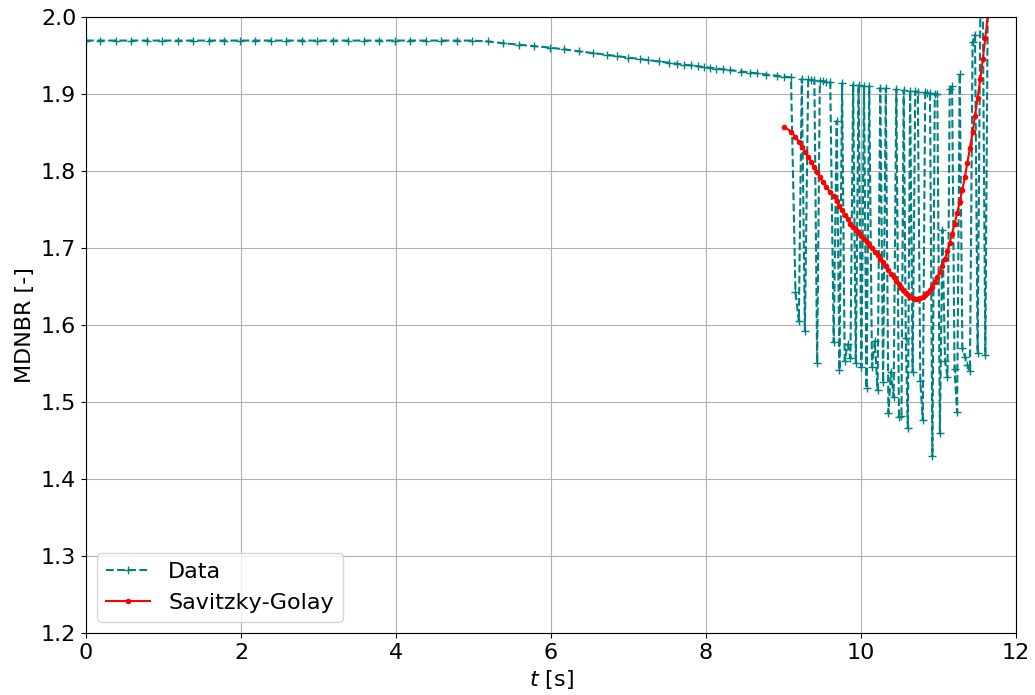


Figure 8.6.4: The HR 95 MDNBR.

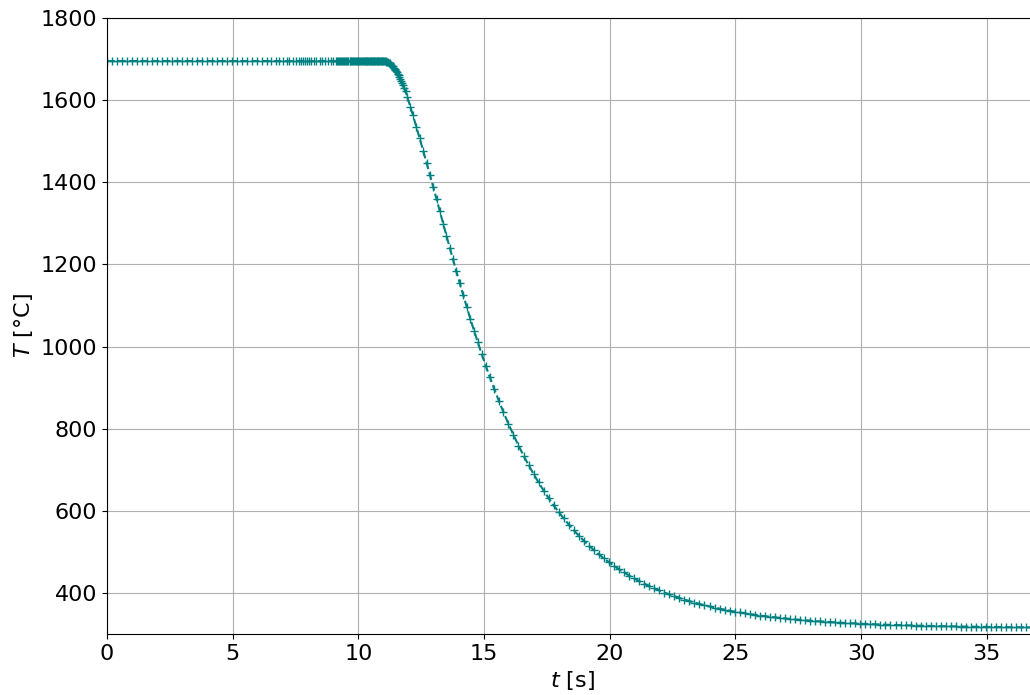


Figure 8.6.5: The HR 95 maximum fuel center temperature.

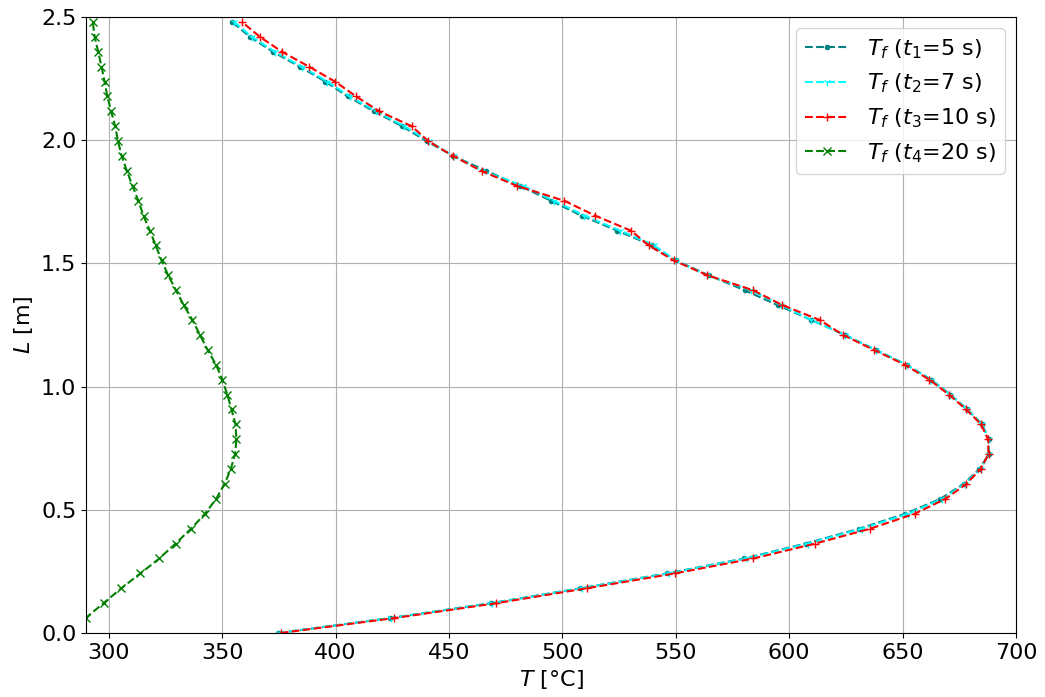


Figure 8.6.6: The HR 95 fuel center temperature at t_1 , t_2 , t_3 and t_4 .

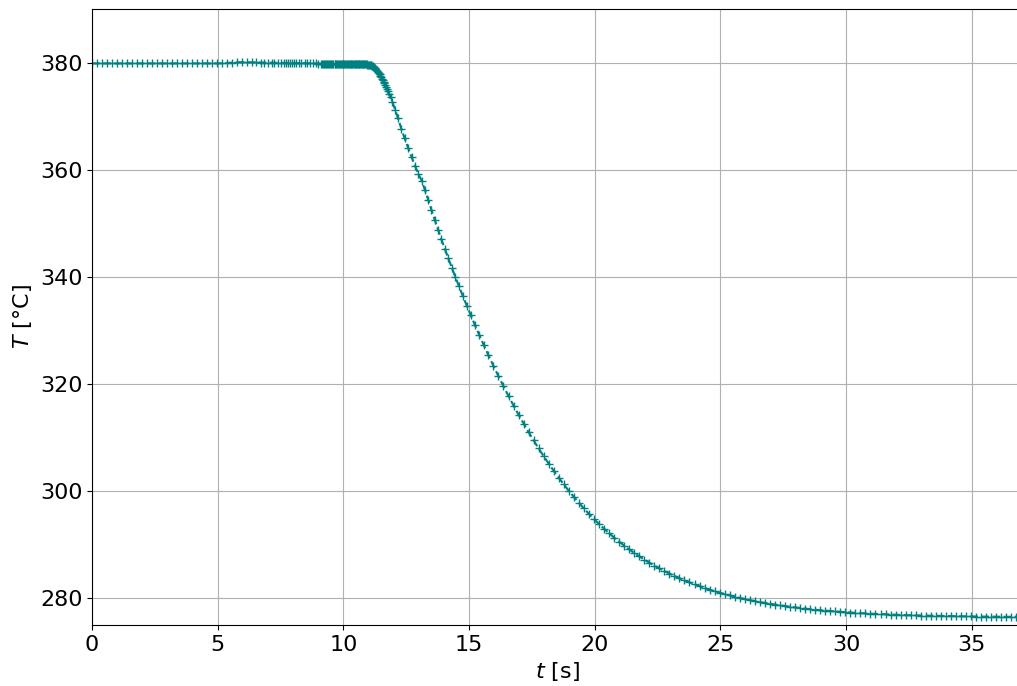


Figure 8.6.7: The HR 95 maximum cladding temperature.

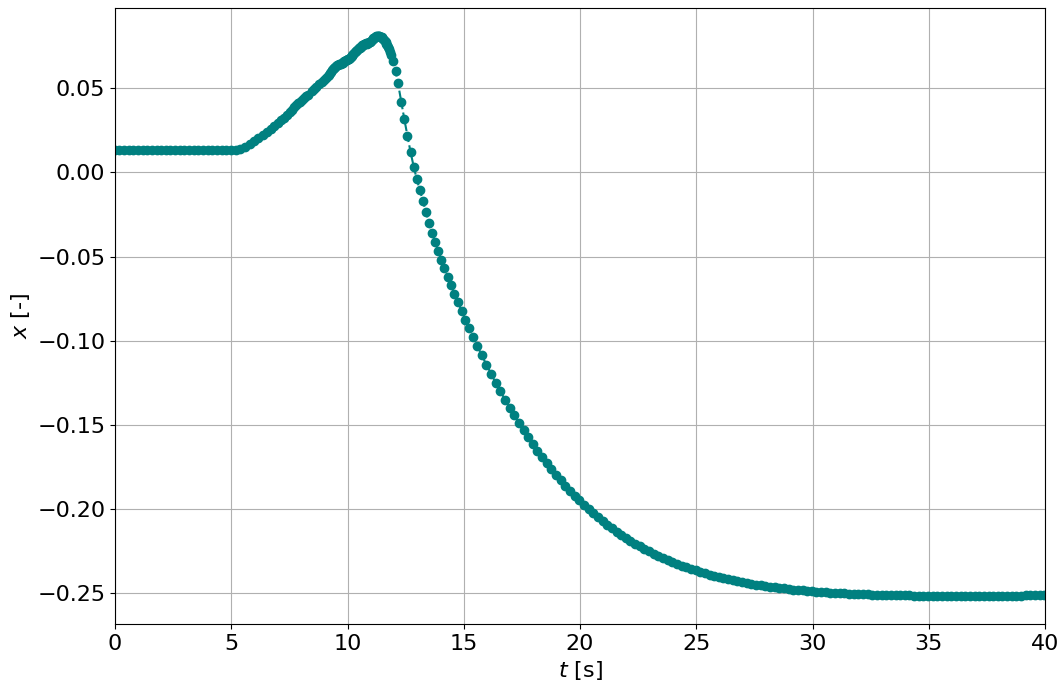


Figure 8.6.8: The highest equilibrium quality x in the HC 156.

8.7 Final Outcome

Table 8.7.1 summarizes the results from the subchannel safety analysis which was calculated in the SCF code. The first criterion is given by limitation of the critical heat flux correlation. In the case of OKB correlation the MDNBR has to be higher than 1.0. The third row is related to the MDNBR calculated by Savitzky-Golay smoothing data filter, which describes obtained data appropriately.

The second criterion is maximum pressure in the P.C. This criterion was not exceeded for any of scenarios due to the definition of outlet pressure in SCF calculation and this criterion is studied by different codes.

In the FSAR safety analyses the pressure increases during transient, on the other hand, lower pressure has negative effect on the MDNBR and due to this the first criterion is more easily exceeded [21]. In the first three scenarios the emergency operational procedures were implemented accordingly to the FSAR.

The third studied criterion was the maximum temperature in the fuel pellet $T_{f_{max}}$ center. The criterion defines the maximum temperature 2480 °C, which is the fuel melting temperature. The calculation proved that this criterion was not exceeded in any case.

The last criterion is the maximum cladding temperature $T_{c_{max}}$, which is defined as 1200 °C. It is visible, that all four scenarios did not exceed the criterion.

Table 8.7.1: Final results.

Scenario	1/6	2/6	3/6	6/6
MDNBR [-]	1.39	0.96	0.82	1.37
MDNBR S.-G. [-]	1.64	1.37	1.07	1.63
HR [-]	106	106	106	95
HC [-]	176	176	176	156
$T_{f_{max}}$ [°C]	1727.7	1727.7	1727.7	1727.7
$T_{c_{max}}$ [°C]	383.4	382.4	382.1	380.1

8.8 Summary

This chapter described the final results from specific LOFA scenarios safety analysis using subchannel software SUBCHANFLOW. The table of events was implemented accordingly to Emergency operating procedures found in the Final safety analysis report for NPP Dukovany, which gave inputs to the TRACE code. The results have been compared against the safety criteria.

Chapter 9

Conclusion

This thesis presented the application of subchannel analysis for VVER technology using a specific methodology. In particular, there was described the nuclear power plant VVER-440 (type V-213), the new fuel Gd-2M⁺ and subchannel analysis terminology. The thesis also performed simulations of steady-state and loss of flow accident scenarios for VVER-440 type using SUBCHANFLOW. The main results have been verified against safety criteria listed in the Final safety analysis report.

VIPRE-01 as a subchannel software for safety analyses does not calculate the AZ reflooding, because it can not solve quench front. It also can not simulate transients with blowdown in details, because the program assumes incompressible fluid [27].

On the other hand, SCF limitations have also been encountered during the simulations. For instance, the code does not offer information about the hot channel, therefore, the user needs to identify it. For a better post-processing and code handling, series of Python scripts have been created.

From the results described previously in this thesis it is also visible, that the chosen methodology of the analysis is conservative. In FSAR the subchannel analyses were performed by consecutive steady-states series. However, the adopted methodology simulated steady-state with continuation of the whole transients.

The applied safety criteria extracted from FSAR are: minimum departure from nucleate boiling ratio, the maximum fuel temperature $T_{f_{max}}$ and the maximum cladding temperature $T_{c_{max}}$.

The first scenario 1/6 reactor coolant pump trip did not exceed any of the given criteria. The MNDBR for the hot rod 106 was 1.64.

Even though the second scenario exceeded the lowest MDNBR criterion, the results may be neglected due to oscillations in the calculation. The MDNBR was lower than limit value for OKB correlation 1.0 only in one calculation time step. After using Savitzky-Golay data filter, it is visible, that the limit was not exceeded for the HR nor for the whole fuel cassette (MDNBR=1.37).

The third scenario is the most problematic analysed sequence. This is due to exceeding

the first criterion, where the MDNBR was lower than 1.0 for circa 10 seconds. From the numerical calculation it is visible, that the value oscillated during transient, and overall results may be influenced by this computational oscillations. After using Savitzky-Golay data smoothing algorithm, it is visible, that for the whole fuel cassette the criterion was exceeded for circa 3 seconds. On the other hand, the key information is connected to the HR. The HR is at the position 106 and after applying Savitzky-Golay it is visible that the MDNBR trend did not exceed the first criterion.

The last scenario is characterized by the trip of all six RCPs. Due to the complete loss of flow, the SCRAM signal is implemented earlier than in the previous scenarios [21].

For all scenarios, MNDBR has not exceeded the criterion for the HR. The second and the third criterion have not been exceeded in any of the simulated scenarios. In particular, the fuel center temperature change in four different times (the end of steady-state t_1 , before SCRAM t_2 , last time step before SCRAM t_3 and after SCRAM t_4) was also plotted and enclosed in the results.

For each scenario were identified also the HCs. In these channels was studied the maximum equilibrium quality. The highest equilibrium quality $x = 0.16$ was reached during 3/6 RCPs trip scenario. This result points out the presence of boiling in the HC. Nevertheless, the limitations for equilibrium quality in the HC during LOFA are not included in the safety criteria [21].

The experience gained from the safety analysis calculations in this thesis will be helpful in future for comparison of SUBCHANFLOW with other software for subchannel analyses, and it is also possible to perform code-to-code benchmarks with other subchannel codes used in the Czech republic.

Important by-products of this thesis are programmes which were made for steady-state analysis speed up and post-processing. These programmes may be extended in order to be more automatic and user friendly even for users not familiar with Python programming language.

Future work will also focus on the coupling of TRACE and SCF, which may speed up the calculation processes and extend sensitivity analyses possibilities.

Bibliography

- [1] A. Moorthi, Anil Kumar Sharma, K. Velusamy, *A review of sub-channel thermal hydraulic codes for nuclear reactor core and future directions*, Nuclear Engineering and Design, Volume 332, 2018, Pages 329-344, ISSN 0029-5493, <https://doi.org/10.1016/j.nucengdes.2018.03.012>.
- [2] U. Imke *User manual for SUBCHANFLOW 3.5*, KIT, 2017.
- [3] P. Van Uffelen, J. Hales, W. Li, G. Rossiter, R. Williamson, *A review of fuel performance modelling*, Journal of Nuclear Materials, Volume 516, 2019, Pages 373-412, ISSN 0022-3115, <https://doi.org/10.1016/j.jnucmat.2018.12.037>.
- [4] *Discovery in Action Through Years* [online]. Pacific Northwest National Laboratory, 2015 [cit. 2020-02-06]. Available from: https://www.pnnl.gov/about/pdf/Timeline_06_09_2015.pdf
- [5] Neil E. Todreas and Mujid S. Kazimi. *Nuclear systems II: Elements of Thermal Hydraulic Design*. New York: Hemisphere Pub., c1990. ISBN 9781560320791.
- [6] *Computer Codes* [online]. NRC, 2015 [cit. 2020-02-06]. Available from: <https://www.nrc.gov/about-nrc/regulatory/research/safetycodes.html>
- [7] Erdal Özdemir, Kang Hoon Moon, Seung Jong Oh and Yongdeog Kim. *Comparison of THALES and VIPRE-01 Subchannel Codes for Loss of Flow and Single Reactor Coolant Pump Rotor Seizure Accidents using Lumped Channel APR1400 Geometry*. Korea, Republic of: N. p., 2014. Web.
- [8] Veronica Jauregui Chavez, Uwe Imke, Victor Sanchez-Espinoza, *TWOPORFLOW: A two-phase flow porous media code, main features and validation with BWR-relevant bundle experiments*, Nuclear Engineering and Design, Volume 338, 2018, Pages 181-188, ISSN 0029-5493, <https://doi.org/10.1016/j.nucengdes.2018.08.009>.
- [9] Wadim Jaeger, Jorge Perez Manes, Uwe Imke, Javier Jimenez Escalante, Victor Sanchez Espinoza, *Validation and comparison of two-phase flow modelling capabilities of CFD, sub channel and system codes by means of post-test calculations of*

- BFBT transient tests*, Nuclear Engineering and Design, Volume 263, 2013, Pages 313-326, ISSN 0029-5493, <https://doi.org/10.1016/j.nucengdes.2013.06.002>.
- [10] R. Henry, I. Tiselj, L. Snoj, *Transient CFD/Monte-Carlo Neutron Transport Coupling Scheme for simulation of a control rod extraction in TRIGA reactor*, Nuclear Engineering and Design, Volume 331, 2018, Pages 302-312, ISSN 0029-5493, <https://doi.org/10.1016/j.nucengdes.2018.03.015>.
- [11] Y. Alzaben, V. H. Sanchez-Espinoza, R. Stieglitz, *Analysis of a control rod ejection accident in a boron-free small modular reactor with coupled neutronics/thermal-hydraulics code*, Annals of Nuclear Energy, Volume 134, 2019, Pages 114-124, ISSN 0306-4549, <https://doi.org/10.1016/j.anucene.2019.06.009>.
- [12] M. Calleja, J. Jimenez, V. Sanchez, U. Imke, R. Stieglitz, R. Macián, *Investigations of boron transport in a PWR core with COBAYA3/SUBCHANFLOW inside the NURESIM platform*, Annals of Nuclear Energy, Volume 66, 2014, Pages 74-84, ISSN 0306-4549, <https://doi.org/10.1016/j.anucene.2013.11.034>.
- [13] M. Calleja, V. Sanchez, J. Jimenez, U. Imke, R. Stieglitz, R. Macián, *Coupling of COBAYA3/SUBCHANFLOW inside the NURESIM platform and validation using selected benchmarks*, Annals of Nuclear Energy, Volume 71, 2014, Pages 145-158, ISSN 0306-4549, <https://doi.org/10.1016/j.anucene.2014.03.036>.
- [14] Manuel García, Diego Ferraro, Ville Valtavirta, Riku Tuominen, Uwe Imke, Jaakko Leppänen, Victor Sanchez-Espinoza, *Serpent2-SUBCHANFLOW pin-by-pin modelling capabilities for VVER geometries*, Annals of Nuclear Energy, Volume 135, 2020, 106955, ISSN 0306-4549, <https://doi.org/10.1016/j.anucene.2019.106955>.
- [15] Kanglong Zhang, Victor Hugo Sanchez-Espinoza, *Optimization and verification of the coupled code TRACE/SubChanFlow using the VVER-1000 coolant mixing benchmark data*, Nuclear Engineering and Design, Volume 353, 2019, 110238, ISSN 0029-5493, <https://doi.org/10.1016/j.nucengdes.2019.110238>.
- [16] Armando Miguel Gomez-Torres, Victor Hugo Sanchez-Espinoza, Kostadin Ivanov, Rafael Macian-Juan, *DYNSUB: A high fidelity coupled code system for the evaluation of local safety parameters – Part I: Development, implementation and verification*, Annals of Nuclear Energy, Volume 48, 2012, Pages 108-122, ISSN 0306-4549, <https://doi.org/10.1016/j.anucene.2012.05.011>.
- [17] Armando Miguel Gomez-Torres, Victor Hugo Sanchez-Espinoza, Kostadin Ivanov, Rafael Macian-Juan, *DYNSUB: A high fidelity coupled code system for the evaluation of local safety parameters – Part II: Comparison of different temporal*

- schemes*, *Annals of Nuclear Energy*, Volume 48, 2012, Pages 123-129, ISSN 0306-4549, <https://doi.org/10.1016/j.anucene.2012.05.033>.
- [18] Miriam Knebel, Luigi Mercatali, Victor Sanchez, Robert Stieglitz, Rafael Macian-Juan, *Validation of the Serpent 2-DYNSUB code sequence using the Special Power Excursion Reactor Test III (SPERT III)*, *Annals of Nuclear Energy*, Volume 91, 2016, Pages 79-91, ISSN 0306-4549, <https://doi.org/10.1016/j.anucene.2016.01.005>.
- [19] Sándor Kiss, Sándor Lipcsei, *Measurement of average circulation period of temperature fluctuations in the coolant of VVER-440 reactors' primary circuit*, *Progress in Nuclear Energy*, Volume 71, 2014, Pages 188-194, ISSN 0149-1970, <https://doi.org/10.1016/j.pnucene.2013.12.003>.
- [20] *Design basis and design features of WWER-440 model 213 nuclear power plants* [online]. Vienna, Austria: IAEA, 1994 [cit. 2020-04-28]. Available from: https://inis.iaea.org/collection/NCLCollectionStore/_Public/25/047/25047648.pdf
- [21] ČEZ, *Final Safety Analysis Report Dukovany Nuclear Power Plant*, revision 2 v17, Prague, 2017.
- [22] D. A. Blokhin, V.M. Chernov, A.I. Blokhin et al. *Nuclear physical properties of zirconium alloys E110 and E635 under long-term neutron irradiation in VVER-1000 reactor*. *Inorg. Mater. Appl. Res.* 3, 124–128 (2012). <https://doi.org/10.1134/S2075113312020037>
- [23] František Hezoučský, Svatobor Štech. *Základy teorie normálních a abnormálních provozních režimů energetických bloků s tlakovodními reaktory*. Pilsen: University of West Bohemia, 2015. ISBN 978-80-261-0548-0.
- [24] Jan Štěpánek. *Dynamics of Heat Transfer During Cooling of Overheated Surfaces*. Prague, 2018. Dissertation. CTU in Prague. Supervisor Václav Dostál.
- [25] D. S. Rowe, *COBRA IIIC: A Digital Computer Program for Steady-State and Transient Thermal Analysis of Rod Bundle Nuclear Fuel Elements*, BNWL-1695, Pacific Northwest Laboratory (1973).
- [26] C. L. Wheeler, et al., *COBRA-IV-I: An Interim Version of COBRA for Thermal Hydraulic Analysis of Rod Bundle Nuclear Fuel Elements and Cores*, BNWL-1962, Pacific Northwest Laboratory (1976).

- [27] C. W. Stewart, J. M. Cuta, S. D. Montgomery, J. M. Kelly, K. L. Basehore, T. L. George and D. S. Rowe, (1989). VIPRE-01: A thermal-hydraulic code for reactor cores (EPRI-NP-2511-CCM-A-Vol1-Rev3). United States
- [28] D. Basile, R. Chierici, M. Beghi, E. Salina and E. Brega: *COBRA-EN, an Updated Version of the COBRA-3C/MIT Code for Thermal-Hydraulic Transient Analysis of Light Water Reactor Fuel Assemblies and Cores Report 1010/1 (revised 1.9.99)*, ENEL-CRTN Compartimento di Milano.
- [29] C. W. Hirt, B. D. Nichols and N. C. Romero, (1975). *SOLA-A numerical solution algorithm for transient fluid flows*. Rep. LA-5852, Los Alamos Scientific Lab., Los Alamos, NM.
- [30] Programming language Python, available from: <https://www.python.org/>.
- [31] M. Aghaie, A. Zolfaghari, M. Minucmehr, A. Norouzi, Enhancement of COBRA-EN capability for VVER reactors calculations, *Annals of Nuclear Energy*, Volume 46, 2012, Pages 234-243, ISSN 0306-4549.
- [32] I. Bell, CoolProp: *An Open-source Thermophysical Property Library*. 2017 <http://coolprop.sf.net> (accessed 15.4.2020).
- [33] F. Bowman, *Introduction to Bessel functions*. New York: Dover Publications, 1958.
- [34] J. Lorenzyk *Aplikace Besselových funkcí*. Brno University of Technology, Faculty of Mechanical Engineering, 2016. 28 s. Master's thesis supervisor: Mgr. Monika Dosoudilová, Ph.D.
- [35] MathWorks Inc. *Filtering and Smoothing Data*. <https://www.mathworks.com/help/curvefit/smoothing-data.htm>. Accessed: 2020-10-07. 2020.
- [36] KIT, U. Imke. *Subchannel software Subchanflow (Version 3.5)* [software], 2017.
- [37] J. T. Rogers and A. E. E. Tahir, *Turbulent Interchange Mixing in Rod Bundles and the Role of Secondary Flows*, ASME paper 75-HT-31, 1975.
- [38] O. S. Eiff and M. F. Lightstone. *On the Modelling of Single-Phase Turbulent Energy Transport in Subchannels*. Toronto, Ontario.
- [39] Nikolay Ivanov Kolev, *Multiphase flow dynamics*. New York: Springer, c2002-2007. ISBN 978-3-540-71442-2.

- [40] K. Rehme, *Pressure drop performance of rod bundles in hexagonal arrangements*, International Journal of Heat and Mass Transfer, Volume 15, Issue 12, 1972, Pages 2499-2517, ISSN 0017-9310, [https://doi.org/10.1016/0017-9310\(72\)90143-3](https://doi.org/10.1016/0017-9310(72)90143-3).
- [41] Klaus Maubach, *Reibungsgesetze Turbulenter Strömungen in Geschlossenen, Glatten Und Rauhen Kanälen Von Beliebiger Querschnitt*. Chem. Ing. Techn. 42,995-1004 (1970).
- [42] Neil E. Todreas and Mujid S. Kazimi. *Nuclear systems I: Thermal Hydraulic Fundamentals*. 2nd ed. Boca Raton, 2012. ISBN 978-143-9808-870.
- [43] Hiroshige Kumamaru, Yasuo Koizumi and Kanji Tasaka. *Critical Heat Flux for Uniformly Heated Rod Bundle under High-Pressure, Low-Flow and Mixed Inlet Conditions*. Journal of Nuclear Science and Technology [online]. 1989, 26(5), 544-557 [cit. 2020-06-01]. DOI: 10.1080/18811248.1989.9734345. ISSN 0022-3131. Available from: <http://www.tandfonline.com/doi/abs/10.1080/18811248.1989.9734345>
- [44] V.I. Astakhov, Y.A. Bezrukov, S.A. Logvinov and V.G. Brantov, *Analysis of the effect of the longitudinal heat release profile on burnout in rod bundles*, Proceedings of Seminar on Thermophysical studies for ensuring reliability and safety of water-moderated water-cooled nuclear reactors, Budapest, Hungary (1978).
- [45] Armando Gomez-Torres, Wadim Jäger, Victor Sanchez Espinoza. *On the Influence of Shape Factors for CHF Predictions with SUBCHANFLOW During a Rod Ejection Transient.*, Conference: International Topical Meeting on Nuclear Thermal-Hydraulics, Operation and Safety (NUTHOS-9), 2012.
- [46] V. V. Bol'shakov, S. M. Bashkirtsev, L. L. Kobzar' and A. G. Morozov. *Experimental study of burnout in channels with twisted fuel rods*. Thermal Engineering [online]. 2007, 54(5), 386-389 [cit. 2020-06-01]. DOI: 10.1134/S0040601507050096. ISSN 0040-6015. Available from: <http://link.springer.com/10.1134/S0040601507050096>.
- [47] L. L. Levitan and F. P. Lantsman, *Critical Heat Fluxes in Internally Heated Annular Channels*, Teploenergetica 24(4), 15-21 (1972).
- [48] D. G. Reddy, C. F. Fighetti, 1983. *Parametric study of CHF data, vol. 2: a generalized subchannel CHF correlation for PWR and BWR fuel assemblies*. EPRI report, EPRI, NP2609, January.
- [49] V. E. Doroshchuk, L. L. Levitan and F. P. Lantsman, 1975. *Recommendations for calculating burnout in a round tube with uniform heat release*. Thermal Engineering 22(12) 77-80.

Author's References Not Related to the Study

1. J. Syblík, L. Veselý, S. Entler, V. Dostál, J. Štěpánek, *Advanced s-CO₂ Brayton Power Cycles in Nuclear and Fusion Energy*. Proceedings of the ASME TURBO EXPO: Turbomachinery Technical Conference and Exposition. New York: American Society of Mechanical Engineers - ASME, 2019. 2019. vol. 9. ISBN 978-0-7918-5872-1.
2. J. Syblík, L. Veselý, S. Entler, J. Štěpánek, V. Dostál, *Analysis of s-CO₂ Brayton Power Cycles in Nuclear and Fusion Energy*. Fusion Engineering and Design. 2019, 2019(146), 1520-1523. ISSN 0920-3796.
3. L. Veselý, J. Syblík, S. Entler, J. Štěpánek, P. Záchá, V. Dostál, *Optimization of s-CO₂ Power Conversion System with an Integrated Energy Storage for the Pulsed DEMO*. IEEE Transactions on Plasma Science, 2020, PP(99):1-6, DOI: 10.1109/TPS.2020.2971718

Chapter 10

Appendix

10.1 Mixing Coefficients in SCF

10.1.1 Constant Mixing Coefficient

In SCF, if the case "Constant mixing coefficient" is chosen, then the constant is called c_{mix} for all j [36]. The equation for channel gap mixing flow parameter is

$$w_{psp}(k, j) = \frac{2 \cdot c_{mix}(ii) \cdot c_{mix}(jj)}{c_{mix}(ii) + c_{mix}(jj) + sm_r} q_{avg}(k, j). \quad (10.1)$$

Number sm_r is a very small number in order not to divide by zero.

The average flux is

$$G_{av} = \frac{|\dot{m}(ii, j) + \dot{m}(ii, l) + \dot{m}(jj, j) + \dot{m}(jj, l)|}{2 \cdot A_{sum}} \quad (10.2)$$

and the maximum hydraulic diameter

$$d_{h_{max}} = \frac{4 \cdot A(ii, j)}{[r(ii, j) + r(ii, l)]0.5}. \quad (10.3)$$

10.1.2 Rogers & Tahir (Triangulars)

Another possibility how to calculate mixing coefficients in SCF [36] is by Rogers & Tahir correlation. It is defined in SCF as

$$w_{psp}(k, j) = 0.0018 \cdot Re_{min}^{-0.1} \left[\frac{g(k, j)}{d_{av}} \right]^{-0.4} \frac{d_{h_{max}}}{g(k, j)} G_{av} g(k, j), \quad (10.4)$$

where

$$Re_{min} = \frac{|4[\dot{m}(jj, j) + \dot{m}(jj, l)]|}{[r(jj, j) + r(jj, l)]\mu(jj, j)}. \quad (10.5)$$

This correlation was first published by Roger's & Tahir in the publication from 1975 [37]. Another possible reproduction of this correlation is

$$\frac{w'_{ij}}{\mu} = 0.0018 \cdot Re_i^{0.9} \left(\frac{c}{d} \right)^{-0.4}, \quad (10.6)$$

where w'_{ij} is turbulent mixing rate and c is the gap width [m] [38].

Another option of this correlation is described by the following equation

$$\frac{u'_{c,ij} S_{gap}}{\nu_c} = 0.0058 \cdot Re_c^{0.9} \left(\frac{d_{rod}}{\Delta S_{ij}} \right)^{0.46} \quad \text{for bundle geometry,} \quad (10.7)$$

$$\frac{u'_{c,ij} S_{gap}}{\nu_c} = 0.0018 \cdot Re_c^{0.9} \left(\frac{d_{rod}}{\Delta S_{ij}} \right)^{0.4} \quad \text{for simple geometry,} \quad (10.8)$$

where u' is fluctuation velocity component along the x-axis [m/s], ν molecular kinematic viscosity [m²/s], d diameter [m] and ΔS is a distance between the channel axis [39].

10.2 Friction Factors in SCF

10.2.1 Armand

The two-phase friction factor φ is calculated the same way as in COBRA-IV-I [26] in three possible options depending on vapour void fraction α

1. $\alpha(i, k) \in (0; 0.6)$:

$$\varphi = \frac{(1 - x_p)^2}{[1 - \alpha(i, k)]^{1.42}} \quad (10.9)$$

2. $\alpha(i, k) \in (0.6; 0.9)$:

$$\varphi = 0.478 \frac{(1 - x_p)^2}{[1 - \alpha(i, k)]^{2.2}} \quad (10.10)$$

3. $\alpha(i, k) \in (0.9; 1)$:

$$\varphi = 1.73 \frac{(1 - x_p)^2}{[1 - \alpha(i, k)]^{1.64}} \quad (10.11)$$

On the other hand the COBRA-IV-I handbook [26] presents equation 10.9 without exponent in the numerator as

$$\varphi = \frac{(1 - x_p)}{[1 - \alpha(i, k)]^{1.42}}, \quad (10.12)$$

same as in the COBRA IIIC handbook [25].

10.2.2 Lockhart-Martinelli

This correlation is based on the different Reynolds number for vapour and for liquid

$$Re_v = |\dot{m}(i, j)| \frac{x_p}{A(i, j)} \cdot \frac{d_h(i, j)}{\mu_v(i, k)} \quad (10.13)$$

$$Re_l = |\dot{m}(i, j)| \frac{1 - x_p}{A(i, j)} \cdot \frac{d_h(i, j)}{\mu_l(i, k)}. \quad (10.14)$$

The Chisholm parameter C is then defined by one of the four possible flow regime:

Re_v	Re_l	C
Turbulent	Turbulent	20
Turbulent	Laminar	12
Laminar	Turbulent	10
Laminar	Laminar	5

Then the Lockhart-Martinelli parameter is set as

$$x_{tt}^2 = \left[\frac{\mu_l(i, k)}{\mu_v(i, k)} \right]^{0.25} \cdot \left(\frac{1 - x_p}{x_p} \right)^{1.75} \cdot \left[\frac{\rho_v(i, k)}{\rho_l(i, k)} \right] \quad (10.15)$$

and from this parameter the two-phase flow friction multiplier is calculated as

$$\varphi = (1 - x_p)^{1.75} \left(1 + \frac{C}{x_{tt}} + \frac{1}{x_{tt}^2} \right). \quad (10.16)$$

10.2.3 Blasius

The Reynolds number is taken as a maximum of two values defined by following equation

$$Re = \max \left\{ 1; \left| \frac{\dot{m}(i, j)}{A(i, j)} \cdot \frac{d_h(i, j)}{\mu(i, k)} \right| \right\}. \quad (10.17)$$

In SCF the maximum K of laminar and turbulent friction is taken for the Blasius and the Rehme correlations [2]

$$K = \max \{ b_{Tp} \cdot Re^{b_{Tr}} + b_{Tc}; b_{Lp} \cdot Re^{b_{Lr}} + b_{Lc} \} \quad (10.18)$$

The friction factor f_f is then calculated as

$$f_f(i) = K \cdot \left\{ 1 + \frac{r_h(i, j)}{r(i, j)} \cdot \left[\left(\frac{\mu_w(i, k)}{\mu(i, k)} \right)^{0.6} - 1 \right] \right\}, \quad (10.19)$$

where constants b_{Lp} , b_{Lr} , b_{Lc} , b_{Tp} , b_{Tr} and b_{Tc} may be changed in the input text file. The most classic approach for these constants is visible in a specification of equation 10.20

$$K = \max \{ 0.316 \cdot Re^{-0.25}; 64 \cdot Re^{-1} \}. \quad (10.20)$$

10.2.4 Rehme

Rehme correlation has its own subroutine in SCF. The task of this subroutine is to calculate an important *term in the friction calculation* Rh_t . In the beginning is calculated Reynolds number for this correlation Re_{Rh} which was already mentioned in section 10.2.3

$$Re_{Rh} = \max \left\{ 1; \left| \frac{\dot{m}(i, j)}{A(i, j)} \cdot \frac{d_h(i, j)}{\mu(i, k)} \right| \right\}. \quad (10.21)$$

For grid spacers are available these equations, which were validated with literature [40]

$$X_m = \left(2 \cdot \frac{\sqrt{3}}{\pi} \right)^{0.5} \cdot \frac{r_{av}}{d_{av}} \quad (10.22)$$

$$Rh_t = 5.5 - \frac{3.966 + 1.25X_m}{1 + X_m} - 2.5 \cdot \log [2(1 + X_m)]. \quad (10.23)$$

The *Rehme term* Rh_t is then used in subroutine *rehme_root*. The root finding method (finding of friction factor f_f) may be bisection, Newton-Raphson or combination of Newton-Raphson/bisection.

The Rehme correlation was confirmed with experimental results for $Re = 6 \cdot 10^2 - 2 \cdot 10^5$ with the rod distance ratio $PP/d = 1.025 - 2.324$ [40]. The study was done for incompressible, isothermal and fully developed turbulent flow and enlarges the study of Maubach [41].

10.2.5 Churchill

Churchill correlation needs the fuel rods surface roughness as an additional input which is used in the Churchill correlation only [2]. The first part of the calculation defines three parameters

$$a_{ch} = \left\{ 2.457 \log \left[\left(\frac{7}{Re} \right)^{0.9} + 0.27 \left(\frac{ra}{d_h(i, j)} \right) \right]^{-1} \right\}^{16} \quad (10.24)$$

$$b_{ch} = \left(\frac{37530}{Re} \right)^{16} \quad (10.25)$$

$$c_{ch} = \left(\frac{8}{Re} \right)^{12} \quad (10.26)$$

The last equation shows dependency of friction factor on the parameters

$$f_f(i) = 8[c_{ch} + (a_{ch} + b_{ch})^{-1.5}]^{1/12}. \quad (10.27)$$

10.3 Critical Heat Flux in SCF

10.3.1 Biasi

Biasi correlation is capable of predicting dryout CHF conditions and DNB [42].

$$q_{cr} = \max \left[\frac{2.764 \cdot 10^7}{d^a G^{1/6}} \left(\frac{1.468 \cdot f_1}{G^{1/6}} - x_e \right), \frac{7.086 \cdot 10^7 f_2}{d^a G^{0.6}} (1.0 - x_e) \right] \quad (10.28)$$

In this equation d refers to the diameter in centimetres, $a = 0.4$ if $d \geq 1$, $a = 0.6$ if $d \leq 1$, x_e is dry out quality and two functions f_1 and f_2 are

$$f_1 = 0.7249 + 0.099 \cdot p \cdot \exp(-0.032p), \quad (10.29)$$

$$f_2 = -1.159 + 0.149p \cdot \exp(-0.019p) + \frac{8.99p}{10.0 + p^2}, \quad (10.30)$$

where p is pressure in bars [2], [43].

10.3.2 OKB

OKB correlation was derived by OKB Gidropress [44]. This correlation is one of the most used for the CHF calculation in the russian types of the PWRs [45], [46].

$$q_{cr} = 0.795(1 - x)^{-0.5+0.105p} G^{-0.127+0.311(1-x)} \cdot (1 - 0.0185p) 10^6 \quad (10.31)$$

In this equation q_{cr} is the critical heat flux, x is relative enthalpy (equilibrium steam quality), G is the mass flux and p is pressure in MPa [2].

10.3.3 W-3

W-3 correlation is the most used correlation for the PWRs [42]. Inasmuch as SCF uses metric units, the W-3 correlation is:

$$\begin{aligned} q_{cr} = & 3.1546 \cdot 10^6 \{ (2.022 - 0.0624p) + (0.1722 - 0.01427p) \exp[(18.177 - 0.5987p)x_e] \} \cdot \\ & \cdot [(0.109 - 1.173x_e + 0.127x_e|x_e|) 10^{-3} G + 1.037] (1.157 - 0.869x_e) \cdot \\ & \cdot [0.2664 + 0.8357 \exp(-124.1d_h)] \{ 0.8258 + 0.3413 \cdot 10^{-6} [h(i, j) - h(i, 1)] \}, \end{aligned} \quad (10.32)$$

where p is pressure in MPa [2], $h(i, j)$ is saturated liquid specific enthalpy and $h(i, 1)$ is inlet specific enthalpy [42].

10.3.4 Levitan

The CHF correlation suggested by Levitan nad Lantsman [47] is

$$q_{cr} = (10.3 - 17.5p_r + 8.0p_r^2)G^{0.68p_r - 1.2q_e - 0.3} \cdot \exp(-1.5q_e) \sqrt{\frac{8.0 \cdot 10^{-3}}{d_h} 10^6}. \quad (10.33)$$

In this equation $p_r = p_t/p_{cr}$ stands for pressure ratio, p_t is total pressure used for coolant properties and $p_{cr} = 221,2 \cdot 10^5$ Pa is critical pressure of water. The mass flux $G = \left| \frac{\dot{m}_{av}}{A_{av}1000} \right|$, where \dot{m}_{av} is average axial mass flow rate and A_{av} is average actual channel area (at axial cell boundary) [2].

10.3.5 EPRI with Shape Function

The EPRI-1 CHF correlation was first published in 1983 [48]. It is obtained by assumption that the critical heat flux is linearly dependent on the local quality and the equation in SCF is

$$q_{cr} = \frac{B - x_{in}}{C + D}. \quad (10.34)$$

where x_{in} is equilibrium vapour quality at the CHF location. Coefficients B and C are functions of pressure ratio p_r and modified mass flux G . Coefficient D is a function of heat flux released to the rod related to the rod surface, rod perimeter fraction faced to a channel and coolant enthalpy.

10.3.6 Doroshchuk

Doroshchuk correlation is presented by simple equation due to the dependency on the tabulated data. Doroshchuk proposed a single equation, which was less reliable at high quantities and large tube diameters [49]. In SCF the equation for the CHF is following:

$$q_{cr} = \{A[q_d(kk) - q_d(kk - 1)] + q_d(kk - 1)\}k_1k_210^6, \quad (10.35)$$

where A is a function of equilibrium quality and tabulated Doroshchuk CHF data. Value q_d is a function of tabulated Doroshchuk CHF data, pressure and average mass flux, k_1 is a function of heated diameter, k_2 is a function of geometry and equilibrium quality.